TECHNISCHE UNIVERSITÄT DARMSTADT

Droplet Production and Handling in Microchannels Using Electric Fields

M.Sc. Mostafa Shojaeian

Center of Smart Interfaces

Nano- and Microfluidics

Droplet Production and Handling in Microchannels Using Electric Fields

Vom Fachbereich Maschinenbau

an der Technische Universität Darmstadt

zur Erlangung des akademischen Grades eines

Doktor-Ingenieurs (Dr.-Ing.)

genehmigte

Dissertation

von

M.Sc. Mostafa Shojaeian

Erstgutachter: Prof. Dr. rer. nat. Steffen Hardt

Zweitgutachter: Prof. Dr.-Ing. Jeanette Hussong

Tag der Einreichung: 11.08.2020

Tag der mündlichen Prüfung: 28.10.2020

Darmstadt, 2020

D17

Shojaeian, Mostafa: Droplet production and handling in microchannels using electric fields
Darmstadt, Technische Universität Darmstadt,
Jahr der Veröffentlichung der Dissertation auf TUprints 2022
Tag der mündlichen Prüfung: 28.10.2020

Abstract

Droplet-based protocols in microfluidic devices have found numerous applications in such different areas as bioanalytics, chemical synthesis, drug delivery etc. Droplets can either be produced in a continuous stream or on-demand. Employing an active technique via applying external sources such as temperature, acoustic, magnetic or electric fields, potentially in combination with a passive technique, could enhance the utility and controllability of droplet generation. Among these approaches, probably the most versatile and flexible one is based on the application of electric fields, because electric actuation tends to be faster and requires less complex components than mechanical actuation. This thesis addresses electrically manipulation of droplets inside microchannels generated both on-stream and on-demand along with some particular applications such as using the droplets as biological reaction compartments or as carriers to transfer tiny amounts of dissolved species.

For the on-stream case, the effect of DC electric fields on the generation of droplets of water and xanthan gum solutions in sunflower oil at a microfluidic T-junction is experimentally studied. The electric field leads to a significant reduction of the droplet diameter, by about a factor of 2 in the case of water droplets. The droplet size is tuned by varying the electric field strength, an effect that can be employed to produce a stream of droplets with a tailor-made size sequence. Compared to the case of purely hydrodynamic droplet production without electric fields, the electric control has about the same effect on the droplet size if the electric stress at the liquid/liquid interface is the same as the hydrodynamic stress.

The focus of the thesis, however, is the manipulation of droplets generated on-demand via electric fields. In the first scenario for droplets being utilized in the context of artificial genetic circuits in biological systems as outlined by the LOEWE CompuGene project (managed by TU Darmstadt), a method is presented allowing to produce monodisperse droplets with volumes in the femtoliter range in a microchannel on demand. The method utilizes pulsed electric fields deforming the interface between an aqueous and an oil phase and pinching off droplets. Water and xanthan gum solutions are considered as disperse-phase liquids, and it is shown that the method can be applied even to solutions with a zero-shear rate viscosity more than 10^4-times higher than that of water. The droplet formation regimes are explored by systematically varying the pulse amplitude and duration as well as the salt concentration. The dependence of the process on the pulse amplitude can be utilized to tune the droplet size. To demonstrate the applicability of the electric-field-driven droplet generator, it is shown that the droplets can be used as versatile biological reaction compartments. It is proven that droplets containing a cell-free transcription–translation system execute gene transcription and protein biosynthesis in a timely and programmable fashion. Moreover, it is verified that biomolecules inside the aqueous droplets such as small RNAs can be diffusionally activated from the outside to induce a ligand-driven biochemical switch.

In another scenario of using droplets as carrier, adding and subtracting the smallest amounts of liquid in a well-controlled manner is a key step. A principle is demonstrated allowing the transfer of tiny amounts of dissolved species to an aqueous femtoliter droplet reciprocating between two aqueous reservoirs (or interfaces) under the influence of a DC electric field. Mass transfer is shown to be size selective and adaptive, for example, via tuning the viscosity of the surrounding oil phase or the electric-field strength. A map of the dynamic regimes is provided, indicating under which conditions the reciprocating droplet motion occurs. A model based on diffusive mass transfer is formulated that describes the amount of species taken up and transferred by the droplet. Interestingly, in some cases, the droplets reciprocating between two aqueous interfaces show simultaneously volume losses (at most contacts with the reservoirs) under certain conditions, a phenomenon called ‘partial coalescence’.

Accordingly, a scaling model is provided allowing the prediction of daughter droplet size during partial coalescence. Overall, the results significantly help to facilitate the handling, production and manipulation of femtoliter droplets.

Kurzfassung

Tropfenbasierte Verfahren in mikrofluidischen Systemen haben zahlreiche Anwendungen in so unterschiedlichen Bereichen wie der Bioanalytik, chemischen Synthese oder Medikamentenverabreichung gefunden. Tropfen können entweder kontinuierlich oder (on-demand) erzeugt werden. Der Einsatz einer aktiven Technik durch die Verwendung externer Quellen wie Temperatur, akustischer, magnetischer oder elektrischer Felder, die unabhängig oder in Kombination mit einer passiven Technik eingesetzt werden können, könnte den Nutzen sowie die Kontrollierbarkeit der Tropfenerzeugung verbessern. Unter all diesen verschiedenen Ansätzen basiert die wahrscheinlich vielseitigste und flexibelste Technik auf der Anwendung elektrischer Felder, da die elektrische Steuerung tendenziell schneller ist und weniger komplexe Komponenten erfordert als eine mechanische Aktivierung. Die vorliegende Arbeit befasst sich mit der elektrischen Manipulation von Tropfen innerhalb von Mikrokanälen, die sowohl kontinuierlich als auch on-demand erzeugt werden, sowie mit einigen speziellen Anwendungen wie dem Nutzen der Tropfen als biologische Reaktionskompartimente oder als Träger zur Übertragung geringer Mengen einer gelösten Spezies.

Im Fall einer kontinuierlichen Tropfenerzeugung wird die Wirkung einer elektrischen Gleichspannung auf die Erzeugung von Wassertropfen und Tropfen aus Xanthan gum-Lösung in Sonnenblumenöl in einen mikrofluidischen T-Übergang experimentell untersucht. Das elektrische Feld führt zu einer signifikanten Verringerung des Tropfendurchmessers, im Falle von Wassertropfen um etwa den Faktor zwei. Die Tropfengröße wird durch Variation der elektrischen Feldstärke eingestellt, ein Effekt, der genutzt werden kann, um eine Sequenz von Tropfen mit einer kontrollierbaren Größe zu erzeugen. Verglichen mit dem Fall der rein hydrodynamischen Tropfenerzeugung ohne die Anwendung elektrischer Felder hat die elektrische Aktuation etwa den gleichen Effekt auf die Größe der Tropfen, wenn die Maxwell Spannung an der Grenzfläche zwischen beiden Flüssigkeiten der hydrodynamischen Spannung gleicht.

Im Fokus dieser Arbeit steht jedoch die Manipulation von Tropfen, die bei Bedarf durch elektrische Felder erzeugt werden. Im ersten Szenario in dem Tropfen in biologischen Systemen eingesetzt werden, wie es im Projekt LOEWE CompuGene (Leitung TU Darmstadt) skizziert wurde, wird eine Methode vorgestellt, die es erlaubt, monodisperse Tropfen mit Volumina im Femtoliterbereich in einem Mikrokanal on-demand zu erzeugen. Die Methode nutzt gepulste elektrische Felder, die die Grenzfläche zwischen einer wässrigen und einer Ölphase verformen und Tropfen abschnüren. Wasser und gum-Lösungen werden als Flüssigkeiten in disperser Phase betrachtet, und es wird gezeigt, dass die Methode sogar auf Lösungen mit einer Viskosität angewendet werden kann, die bei verschwindender Scherrate mehr als 10^4-mal höher ist als die von Wasser. Die Regimes zur Tropfenbildung werden durch systematische Variation der Pulsamplitude und –dauer sowie der Salzkonzentration untersucht. Die Abhängigkeit des Prozesses von der Pulsamplitude kann zur Einstellung der Tropfengröße genutzt werden. Um die Anwendung des durch ein elektrisches Feld angetriebenen Tropfengenerators zu veranschaulichen, wird gezeigt, dass die Tropfen als vielseitige biologische Reaktionskompartimente verwendet werden können. Es wird nachgewiesen, dass Tropfen, die ein zellfreies Transkriptions-Translationssystem enthalten, die Gentranskription und Proteinbiosynthese zeitnah und kontrollierbar ausführen. Darüber hinaus wird verifiziert, dass Biomoleküle innerhalb der wässrigen Tropfen, wie z.B. kleine RNAs, von außen diffusionsgetrieben aktiviert werden können, um einen ligandenbasierten Schalter zu aktivieren.

In einem anderen Szenario, bei dem Tropfen als Träger verwendet werden, ist die kontrollierte Addition und Subtraktion kleinster Flüssigkeitsmengen ein entscheidender Schritt. Es wird ein Prinzip vorgestellt, das die

Übertragung kleinster Mengen gelöster Spezies auf einen wässrigen Femtoliter-Tropfen ermöglicht, der sich unter dem Einfluss eines elektrischen Gleichspannungsfeldes zwischen zwei Reservoiren (oder Grenzflächen) hin- und herbewegt. Es wird gezeigt, dass der Massentransfer größenselektiv und adaptiv ist, z.B. durch Abstimmung der Viskosität der umgebenden Ölphase oder der elektrischen Feldstärke. Es wird ein Phasendiagramm der dynamischen Regime erstellt, aus dem hervorgeht, unter welchen Bedingungen die hin- und hergehende Tropfenbewegung stattfindet. Es wird ein auf diffusivem Massentransfer basierendes Modell formuliert, das die Menge der vom Tropfen aufgenommenen und übertragenden Spezies beschreibt. Interessanterweise treten bei den zwischen den zwei Grenzflächen hin- und herbewegten Tropfen in einigen Fällen Volumenverluste auf (bei der Mehrzahl der Kontakte mit den Reservoiren), ein Phänomen, das als partielle Koaleszenz bezeichnet wird. Hierfür wird ein Skalierungsmodell präsentiert, das die Vorhersage der Produkttropfengröße während des partiellen Koaleszenzprozesses ermöglicht. Insgesamt tragen die Ergebnisse wesentlich dazu bei, die Handhabung, Erzeugung und Manipulation von Femtoliter-Tropfen zu erleichtern.

Übersetzung: Michael Eigenbrod

Acknowledgement

First and foremost, I would like to sincerely express my appreciation to Prof. Dr. rer. nat. Steffen Hardt for offering me the opportunity to join his dynamic research group. Without his guidance and continuous supports in giving valuable suggestions and enlightening scientific concepts, the doctoral journey was hard to navigate. I would like to thank Pro. Dr.-Ing Jeanette Hussong for her consent to examine my PhD dissertation. I kindly acknowledge the support from the LOEWE CompuGene Project, funded by the Hessian Ministry of Science and Art. I am grateful to Mr. Klaus-Dieter for silicon wafer fabrication. I am thankful to Prof. Dr. H. Ulrich Göringer and François-Xavier Lehr for useful discussions and collaborative work in context of the CompuGene project.

I am very much grateful to Ms. Corinna Neumann for her assistance whenever asked. I express my sincere gratitude to Dr. Michael Eigenbrod for translation of the abstract section from English to German as well as his kindness. I am so much thankful to Dr. Tobias Baier for his kind supports and cooperation. I very kindly thank my officemates Dr. Tamal Roy for useful discussions and Mr. Florian Gebhard for his kindness and supports. I thank Mr. Jörg Bültemann, Mr. Frank Plückebaum, Mr. Sebastian Dehe, Mr. Johannes Hartmann, Mr. Maximilian Hartmann, Mr. Maximilian Schür and all past group members for creating supportive and excellent working environment in the group. I also acknowledge supports of IT members and all university staff who have contributed to deliver assets.

I wholeheartedly express my gratitude to my wife for her continuous supports, patience and encouragements during this PhD journey as well as for taking care of my lovely daughter. I also heartily express my profound regards to my parents for their blessings and cordial supports in my whole life. I am also very grateful to all teachers from whom I learned.

On top of all, I should never forget to wholeheartedly and humbly express my deepest thanks to Allah whose guidance, blessings and assets is always sending to not only humankind but also to all creatures from the origin of universe until eternity.

Contents

1 Introduction

1.1 Motivation and objective of the thesis

Microfluidics dealing with very small fluid volumes behaves differently from conventionally sized systems. Microfluidic devices take advantage of unique properties of liquids and gases in a scale of micrometer. The merits of working with microfluidic dePvices are vast. Among others, one may count less cost of fabrication and easy follow-up the protocol of microfluidic chip fabrication, requirements of less volume of samples (chemicals and reagents etc.), faster and cheaper analyses, shorter reaction time, easier automation and parallelization, higher portability and functionality of integration of several lab elements in one compact space. Droplet as a prominent partner has constructed a descent team-up with microfluidic devices, known as droplet-based microfluidics, with capability of investigating behaviors of biological entities, reagents and species inside droplets functioning as space reaction compartments or carrier fellows, apart from their inherent fluidic characteristics and applications. Droplet-based microfluidics has been host of many scientific subjects due to its versatility and functionality in both fundamental and application areas. In the recent decades, the rapid progress in microfluidics in all aspects spanned from fabrication to experimental methods has tremendously enhanced emergence of promising applications, and it has enabled researchers from diverse disciplines to gather and explore microfluidics-related projects that can pursue a specific target. Likewise, LOEWE CompuGene managed by TU Darmstadt aimed at design of complex genetic circuits in biological systems in a highly interdisciplinary approach. In that context, the current thesis, as a sub-project of LOEWE CompuGene, has addressed providing a microfluidic system with the potential of being used for the in-vitro characterization of genetic circuits. For that purpose, a microfluidic device with a system allowing to produce cell-sized droplets, as a representative for biological reaction compartments, is required to design such that adding and subtracting the smallest amounts of liquid volumes (with dissolved species) to or from droplets in a well-controlled manner become additionally possible, which could mimic the cell metabolism. To do so, use of pulsed and continuous electric fields acting on an appropriate two-phase system can fulfill the envisioned goal. Accordingly, the electric fields were used to produce pico-to femtoliter droplets inside microfluidic devices, where the appropriate system designs allowed the droplets containing a cell-free transcription–translation system execute gene transcription and protein biosynthesis, and also transfer tiny amount of liquid containing nano-beads or dissolved species between two aqueous reservoirs. These are applications beside the fundamental physics that run the experimental set-up and systems.

1.2 Structure of the thesis

In this dissertation, femto to-picoliter droplets are produced inside microchannels both on-stream and on-demand with/without pulsed electric fields and then are manipulated via electric fields. In addition to that, some (biological) applications are provided taking advantage of the electrical actuation. In chapter 2, a general overview on the droplet-based microfluidics is given. It includes the most commonly used geometries and the practical methods being as passive and active for generation and manipulation of droplets. This chapter indeed presents the employed geometries and methods in context of this work among others.

Chapter 3 demonstrates some concepts of electrohydrodynamically transport phenomena that constitutes the underlying physics related to the experimental observations in this work. As such, the basics of the electrohydrodynamics like modeling, instability and cone-jet mode (as the closest feature to the on-demand droplet generation process) are introduced as well as the relevant mechanisms such as electrophoresis and dielectrophoresis that typically exist in manipulation of droplets. In addition, some applications pertinent to the elctrohydrodynamics are briefly given.

The experimental results are presented in the following chapters. As known, droplets can be produced either on-stream where a large quantity of droplets are desired or produced on-demand where the focus will be on a single droplet. Chapter 4 concerns the experimental study of droplet production on-stream while the size of droplets is tuned by either varying flow rate ratios or electric fields. In addition to water as the standard working fluid, the xanthan gum solutions having zero-shear viscosities up to several order magnitude larger than that of water are investigated.

In chapter 5, femtoliter droplets of water and xanthan gum solutions are produced on-demand from a feature much larger than the size of droplets using pulsed electric fields through varying the voltage amplitude and pulse duration. This method is then used for production of droplets containing biomolecular species as an application proving that the droplets can be used as versatile biological reaction compartments.

In chapter 6, a method is reported with which the femtoliter droplets not only are produced on-demand between two aqueous interfaces but also show different dynamic regimes when electric fields are applied. Depending on oil viscosity, salinity of aqueous phase and electric field strength (or applied voltage), different regimes are identified: (full) coalescence, non-coalescence, partial coalescence and failure regimes. Defined as the non-coalescence regime, droplets are shown to reciprocate between two aqueous interfaces (or reservoirs) without merging to them. As an application, it is proven that this method allows the transfer of tiny amounts of dissolved species to an aqueous femtoliter droplet reciprocating between two aqueous reservoirs upon applying DC electric fields. Following that, a diffusive mass transfer model is described that are fitted with experimental data. It is described that under certain conditions, droplets reciprocating between two reservoirs could result in generation of submicron droplets. This dissertation ends with concluding remarks on the work.

2 Droplet based microfluidics

2.1 Introduction

Droplet-based microfluidics, as a multi-functional tool, offers numerous applications because of its merit being as lower consumption of reagents, ability to produce a large number of monodisperse droplets with their control independency, and fast reaction rate due to small scale. Droplets can serve as frameworks in material science used for pharmaceutical, food and industrial applications such as synthesizing microcapsules, microparticles and microfibers. The other significant realm of droplets can be found in lab-on-a-chip, where they are well-suitable compartments to function chemical and biochemical reactions. In that context, it is desirable to produce uniform droplets in a wide range of volumes for the sake of achieving reliable and comparable results in a well-controlled manner. This defines the droplet production on stream, where formation of a large number of droplets is explored for the above-mentioned applications. Nevertheless, some other applications may require and prefer a tunable sequence of droplets with different volumes, for instance, for detecting genetic targets precisely and quantitatively in multi-volume droplet digital polymerase-chain-reaction (PCR)[1]. Notably, when the task is to produce a droplet at a certain time at a specific location, or when samples that are only available in smallest amounts need to be processed, the on-demand production of droplets is favored over the continuous process[2], besides the promising specific applications that may favor the droplet production on-demand, for example, to encapsulate cells with deterministic cell numbers[3]. As mentioned, droplet production offers many applications for which device geometry design and/or fabrication method are basic steps and scheme of production, and accordingly is highly important and sometimes challenging. A brief overview is presented in the following.

2.2 Device Geometry

The droplet generation is greatly affected by the geometry of channels because they bound the boundary of fluid flows. The most widely used geometries are cross-flow, co-flow and flow-focusing in which viscous shear and/or pressure forces are responsible for droplets pinch-off. Other geometry configurations that facilitate or drive droplet production work based on variations in channel confinement such as step, microchannel, and membrane emulsifications. The latter techniques (i.e. cross-flow etc.) could be found in combination with the former ones (i.e. step emulsification etc.). Herein, we briefly introduce some of these geometries.

2.2.1 Cross-flow

The cross-flow geometry (see Fig. 2.1a) refers to the case when dispersed and continuous phase fluids meet at an angle larger than 0. The most frequently used feature is when the fluids meet at the angle of 90^{o} referred to as T-junction, providing a simple and facile mode of monodisperse droplet generation. Thorsen et al.[4] pioneered the use of T-junctions for production of water droplets in oil. Typically, the continuous phase enters from main channel and dispersed phase from side channel. However, the opposite can be feasible provided by modification of channel walls wettability [5]. Aside from being used as a droplet generator, T-junctions can be employed for designing microvalves [6] and microctuators [7]. Although the change in angle between the main and side

channels creates new configurations, for example Y-shaped junction [8] influencing droplet breakup process and resultant droplets [9], a different design of T-junctions can be drastic in droplet production and its application. In this regards, making use of multiple T-junctions, for example for formation of stable alternating droplet pairs [10], or combining with confinement steps, for example for on-demand droplet production [11], enhance their applicability.

2.2.2 Co-flow

The co-flow geometry (see Fig. 2.1b) refers to the case where the dispersed and continuous phase fluids meet in parallel streams. Umbanhowar et al. [12] initiates this geometry for use in microfluidic devices. It appears in two configurations; one is quasi-two-dimensional (2D) planer, which is doable by standard soft lithographic methods, and another is three-dimensional (3D) coaxial for which a glass capillary is inserted into a microchannel. The degree of dispersity of resulting droplets generated by this geometry is dependent on the flow condition [12,13].

2.2.3 Flow-focusing

In flow-focusing geometry (see Fig. 2.1c), the dispersed fluid is hyrodynamically focused by (typically two streams of) continuous phase fluids, passing through a contraction. Similar to co-flow geometries, it can be designed in the two configurations. This geometry can be a good candidate for production of droplets in smaller size. In addition, the 3D version of flow-focusing devices eliminates problems such as wetting of channel walls by disperse phase [14], introducing a robust high-throughput droplet generator.

2.2.4 Step-emulsification

On contrary to the abovementioned microfluidic geometries which work basically on shear/pressure forces to pinch off droplets, in step-emulsification (see Fig. 1d) the tendency to minimize interfacial energy is the mechanism responsible for droplet pinch-off. In this regard, when a dispersed phase fluid reaches to a contraction or expansion, its interface is destabilized due to a sharp change in capillary pressure and, as a result, droplets are produced so as to minimize the interfacial energy.
Several advantages of step emulsification were reported [15]; less sensitivity of droplet production to flow rate or pressure fluctuation, a wider range of flow rates if flow rate ratio is kept constant and easier for parallelization in high-throughput droplet generation. Microchannel and membrane emulsifications are also other techniques used for droplet generation, which are less popular compared with other techniques mentioned earlier.

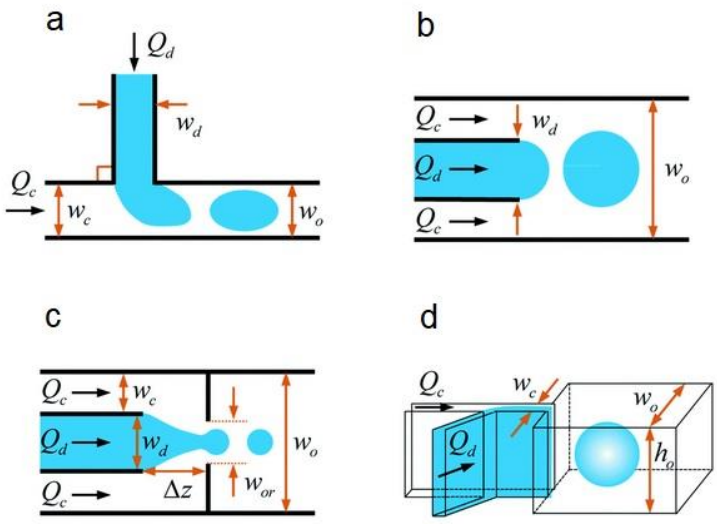

Fig. 2.1 The commonly used geometries in microfluidics devices: a) Cross-flow b) Co-flow c) Flow-focusing d) Step-emulsification. Reproduced with permission from [15]

2.3 Passive and active methods for droplet generation

When droplet generation is concerned, microfluidics devices become a decent and best host for it. This is because their peculiar ability to produce droplet volumes down to very small scales like cell-sized used in pharmaceutical and biological applications (drug delivery, diagnostic and so on), in addition to merits such as low consumption of fluids, easy implementation, high capability in integration with different techniques, high controllability and etc. However, microfluidic devices also offer an attractive platform for industrial applications and for research. In that context, methods used to generate droplets within microfluidic devices become highly important. Zhu and Wang [15] reviewed this subject in a well-manner way. Herein, these methods are briefly presented, which are classified in two major categories: passive and active methods.

2.3.1 Passive method

In passive method, syringe pumps, supplying constant flow rates, or pressure controllers and gravity-based units, providing stable and tunable pressures, typically lead to formation of two-phase fluid flows. The principle based on which the droplets are produced is the partial conversion of energy induced by the syringe pumps or pressure controllers into interfacial energy. This makes the destabilization of liquid-liquid or the gas-liquid interface easier and tendency to minimization of the interfacial energy is the driving mechanism for decaying the tip of dispersed fluid stream into droplets. As a result, droplets appear in various breakup modes (see Fig. 2.2), depending on the involved processes and underlying physics.

For the commonly used geometries, i.e. cross-flow, co-flow and flow-focusing geometries, there are different modes observed for droplet production in terms of breakup and formation, which are squeezing, dripping, jetting, tip-streaming and tip-multi-breaking. However, tip-streaming and tip-multi-breaking have not been reported in

cross-flow yet that might be because of the failure in formation of cone. The transitions between different modes are viable through tuning the flow characteristics by changing dispersed and/or continuous phase capillary numbers, defined as $Ca=\mu U/\gamma$ where μ is the dynamic viscosity, U is the flow velocity and γ is the interfacial tension. Since fewer studies have been devoted to identify different modes of droplet production in step-emulsification, which are shear-induced generation, step-regime and jet-regime, the main focus is put on those in cross-flow, co-flow and flow-focusing geometries.

2.3.1.1 Squeezing

In squeezing mode that typically happens at low capillary numbers (e.g. $Ca<<1$), a segment of dispersed fluid flow is squeezed inside the channel where the droplets form. As a result, the size of pinched-off droplet is larger than the width of the channel. In such a case, the dispersed flow tip occupies the entire cross-section area of the channel and thereby a pressure gradient in the continuous fluid across the tip is built-up. Nevertheless, the continuous phase may not completely block the entire cross-section, as confirmed by the microscopic particle image velocimetry (μ-PIV) [16], in particular for rectangular microchannels where the dispersed fluid possibly does not wet the wall around the corners. When the pressure gradient exceeds the pressure inside the dispersed fluid at the tip at the interface of dispersed-continuous fluids, the interface is narrowed down and necks, shedding into discrete droplets in a plug-like shape. The droplet formation process in this mode is divided in two stages being as filling and necking. Squeezing is the only mode for which the interfacial instability drives the pinch-off. Garstecki et al. [17] stated that the breakup in squeezing regime occurs in two stages: a necking stage and a following nonlinear rapid collapse. Their observations inferred to the independency of collapse from surface tension, and thereby discussed the collapse occurrence through a series of equilibria of minimal surface energy, in contrast to the non-equilibrium capillary instability.

2.3.1.2 Dripping

The increase of capillary number (of the continuous phase) causes the transition of mode from squeezing to dripping. This transition were reported to occur at continuous phase capillary numbers in the order of $Ca\sim O(10^{-2})$ [18], where both shear stress and squeezing pressure take a part in determination of droplet size. The capillary instability (also known as Rayleigh-plateau instability) is the dominant mechanism acting during breakup. In dripping mode, viscous force, which tends to rupture the fluid-fluid interface, overcomes interfacial tension that resists against the destabilization of the forming droplet during pinch-off event. Corresponding pinch-off takes place at junctions, where the dispersed and continuous phases immediately meet, sufficiently before the growing droplet block the major portion of the channel. Consequently, size of the resulting droplets is smaller than the channel dimension, so droplets maintain their spherical shapes. Highly monodisperse droplets can be achieved for a fixed viscous force.

2.3.1.3 Jetting

When flow rate of the continuous or dispersed phase is increased, transition from dripping to jetting happens. As a result, the liquid-liquid interface is elongated, forming the dispersed liquid jet. Tip of the liquid jet become eventually destabilized due to Rayleigh-plateau instability (or capillary instability), breaking up into droplets. Compared with squeezing and dripping, droplets produced in jetting regime are more polydisperse. In co-flow geometry, the common geometry producing jetting, the jetting takes place when viscous force (by taking the contributions of both dispersed-fluid inertia and continuous fluid into account) exceeds the interfacial tension force, with the condition reading as $Ca_c+We_d \geq O(1)$ [13]. *We* is the Weber number, defined as $We=\rho U^2 L/\gamma$ where ρ is the mass density and *L* is a characteristic length, where subscribes *c* and *d* denotes the continuous and dispersed phases, respectively. Accordingly, jetting in co-flow configuration exhibits two different behaviors. One is narrowing jet, occurring at $Ca_c \geq O(1)$ where the viscous force is dominant over capillary force. Another one is widening jet, occurring at $We_d \geq O(1)$ where the opposite holds true, that is, the deceleration of jet at downstream due to the larger velocity of dispersed phase with respect to that of continuous phase induces a shear force at the interface rendering the shape of jet widening.

2.3.1.4 Tip-streaming

Tip-streaming is the reminiscent of Taylor cone in electrified charged liquid seen during electrosprying process or electrohydrodynamic phenomenon. Two different mechanisms have been reported that causes tip-streaming. One is that surfactant drives the tip-streaming occurrence, which was initially proposed by De Bruijn [19] consistent with later experimental works [20]. Another is surfactant-free tip streaming, predicted by Zhang [21] almost a decade after the study of De Bruijn [19]. The tip-streaming is characterized by the steady cone-jet structure. When the flow rate ratio (flow rate of continuous phase over that of dispersed phase) is sufficiently large, a recirculating flow pattern forms within the cone region due to exertion of viscous shear stress from outer fluid. But when it exceeds a critical value [22], followed by a cone formation, a thin jet in a few order of magnitude smaller that the radius of nozzle is formed at the tip of conical shape and consequently droplets are generated from the jet tip during breakup process due to the capillary instability. However, several criteria have to meet in order that the tip-streaming triggers [23]. For instance, the device geometry is a significant one; the tip-streaming has not been reported for cross-flow possibly because of failure in local streamlines convergence near the interface [24]. Furthermore, no separation should exist between continuous phase and the growing droplet that requires $Re_c \ll 1$ where *Re* denotes the Reynolds number defined as $Re=\rho UL/\mu$. The viscous stress induced by the continuous phase must dominate over the capillary pressure at the nozzle injection. Besides, the Reynolds number of the dispersed flow in the thin jet region must be sufficiently small such that the average velocity of the dispersed flow equals that of the continuous phase, which brings about a cylindrical shaped jet at downstream of the cone.

2.3.1.5 Tip-multi-breaking

In contrast to the other mode of breakup in which droplets are produced continuously, tip-multi-breaking produces intermittent droplets in periodic sequences. The process is similar to that in tip-streaming mode, nevertheless, the conical structure of the dispersed phase from which the droplets are ejected in non-uniform sizes is unsteady. The capillary instability is responsible for the droplet ejection and apparently the jet formation stage is suppressed. The fluidic conditions of dispersed and continuous fluids are important in unsteadiness of the

fluid-fluid interface. For example, Gordillo et al. [25], for a liquid-liquid system in co-flow geometry, specified a critical capillary number of the continuous phase as a function of viscosity ratio by which the upper limit for the existence of the unsteady conical tip can be set.

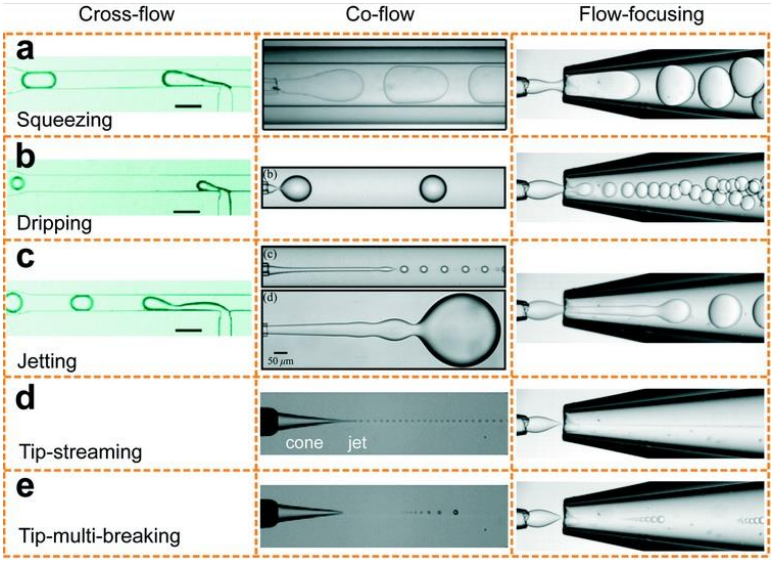

Fig. 2.2 Droplet generation images for different break-up modes in cross-flow, co-flow and flow-focusing geometries. Reprinted with permission from [15]

2.3.2 Active method

Active controls can modulate droplet generation through the aid of an additional energy input, offering several merits over the conventional passive methods. Active control can be used independently or in combination with passive methods. Making use of active method exhibits higher flexibility in control of both droplet size and frequency of generation, and it also allows the droplet generation on-demand in a case if characterizing a single droplet is concerned [2]. Furthermore, the response time in employing active control is much shorter than that in passive method, down to few milliseconds. Not all these advantages may be possible in passive droplet generation method, so using active method, independently or in combined with the passive one, remarkably facilitates and enables the practical applications of droplet-based microfluidics.

In active droplet generation, the fluid-fluid interface is targeted by disrupting the force balance temporarily or permanently. The force balance disturbance is viable through either exerting additional external forces or modifying intrinsic forces. In the former, the additional energy input can be by applying external electric, magnetic, centrifugal fields or even by laser light and so on. In the latter, modification of intrinsic inertial, viscous and capillary forces (scaled as $\rho_s u_s^2$, $\eta_s u_s/L$, and γ/L, respectively) is envisioned through a change in the dynamic velocity and material properties, including viscosity, interfacial tension, channel wettability, and fluid density. A brief description is given for some of abovementioned tools.

2.3.2.1 Magnetic control

The best candidate for magnetic control in droplet-based microfluidics is ferrofluid, a nanofluid containing magnetic nanoparticles. Ferrofluids magnetize when subjected to a magnetic field and demagnetize when the magnetic field is off. Magnetic force per unit volume, f_m, is expressed as $f_m=\mu_0 M\nabla H$, where μ_0 is the magnetic permeability of free space, M is the magnetism and ∇H is the gradient of magnetic field strength. In droplet microfluidics, ferrofluid is basically used as the dispersion phase and thus altering M and/or ∇H would affect the droplet generation characteristics. In that context, magnetic field can be manipulated in different points of view such as type of magnet, location, uniformity, direction, and polarity of magnetic field, where both permanent magnets and electromagnets cab be implemented. Magnetic field presence can play a significant role in the process of ferrofluid droplet production, affecting the droplet size (see Fig 2.3).

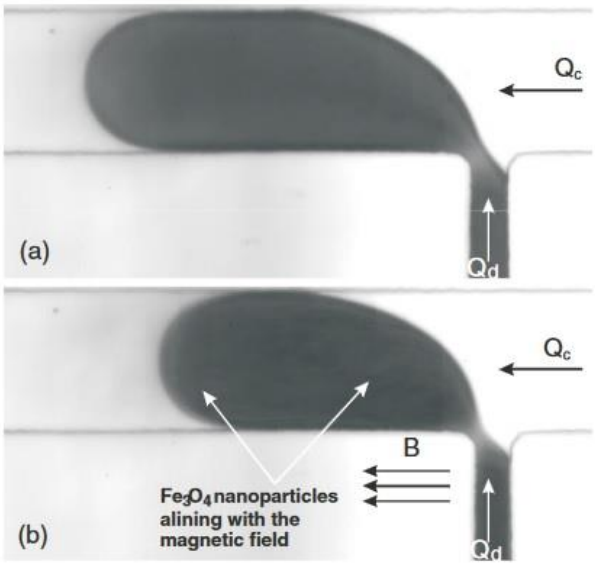

Fig 2.3 Ferrofluid droplet generation in a) absence and b) presence of a magnetic field. Reprinted with permission from [26]

2.3.2.2 Centrifugal control

Offering many fluidics functionalities such as mixing, separation, detection and pharmaceutical and biological applications, centrifugal microfluidics has been used for droplet generation as well. Rotation, as a prerequisite and pillar element for centrifugal force acting radially outward due to rotary motion of microchannel, is typically accompanied with Coriolis force acting perpendicular to the motion direction due to relative motion of the object and Euler force proportional to the rotational acceleration. During droplet generation process, these forces, if any, compete with interfacial tension force, where their interplay determines droplet size. Bond numbers, defined for both centrifugal force ($Bo_\Omega = \rho\Omega^2 rL^2/\gamma$) and Coriolis force ($Bo_{Co}=\rho^2\Omega^3 rL^4/\mu\gamma$), represent the ratio of these forces to

that of the interfacial tension. *L* is the characteristic length, *r* is the radial position, ρ is the dispersed phase density, μ is dynamic viscosity, Ω is the angular velocity, and γ is the interfacial tension.

2.3.2.3 Electrical control

The most commonly used external force among active methods is the electrical control in which electric field is employed to manipulate production of droplets [27] offering potential applications [11]. Its effect is similar to what seen in electrospray and electrohydrodynamic phenomena. Integrated electrodes into microfluidic devices at different features such as IOT or aqueous electrodes provide drastic tools to induce electric fields, which can exist in direct current (DC fields) and alternating current (AC fields). The DC electric field (i.e. voltage) can be applied at constant and pulsation modes, whereas the AC electric field can be employed in low- and high-frequency (in Hz). Due to presence of electric field the electric Maxwell stress comes into play and as a significant key parameter it must compete with other forces such as interfacial tension force and so on. Notably, as the current thesis is centered on the electrical control, which is the active control with electric fields, it is reviewed comprehensively in detail in appropriate sections in the text.

2.3.2.4 Material properties modification: Viscosity

Change in material properties is able to serve as an active mechanism to affect droplet generation. Viscosity, a main fluid characteristic, behaves differently subject to external forces such as electrical, magnetic and thermal stimuli if consists of some special agents. For example, in electrorheological fluids, which are comprised of non-conducting but electrically active particles dispersed in an insulating base fluid, their particles are aligned along electric field lines along with viscosity changed when subjected to an electric field. Accordingly, the fluid motion perpendicular to the field lines is suppressed. As a result, the continuous electrorheological fluid is stopped flowing when exposed to a sufficiently large electric field and only the dispersed fluid moves forward. Following decrease in electric field below a critical value allows the movement of the continuous flow, leading to pinching off the dispersed fluid and producing of droplets [28].
Similarly, viscosity of magnetorheological fluids, like ferrofluids, varies when subjected to a magnetic field and the magnetic particles inside this type of fluids align along the magnetic field direction, forming chains or columns. In droplet generation with ferrofluids, magnetic field clearly plays the key role in the control of droplet size [29].
Thermal control of droplets generated in microchannel is performed by considering the fact that temperature would influence the fluid viscosity and interfacial tension. Since the variation in viscosity with temperature is faster than in interfacial tension, while both decrease with the increase of temperature, the droplets would increase in size [30] predicted by

$$\mathrm{D(T)} \propto Ca_c^{-1} = \frac{\gamma(T)}{\mu_c(T)U_c} \tag{2.1}$$

Where γ is the interfacial tension, μ is the (dynamic) viscosity, and *U* is the fluid velocity. Subscript *c* denotes the continuous phase.

2.3.2.5 Material properties modification - Interfacial tension

In view of material property modification, the interfacial tension can play a significant role observed from different approaches such as thermal, optical and electrical controls. Owing to dependency of interfacial tension to temperature, control of droplet generation is thermally possible that exists in two categories in terms of heating being as uniform and non-uniform. In the uniform case, the entire liquid-liquid interface is heated and consequently the interfacial tension is adjusted homogeneously affecting the droplet generation [31]. In case of non-uniform heating, only a part of the interface is locally heated and thereby the resulting thermal gradient causes an interfacial gradient that induce the Marangoni stress (a stress tangential to the liquid-liquid interface). In Optical control, including laser-heating, a laser beam locally generate heat at the focused beam area and therefore, similar to non-uniform heating in thermal control, the Marangoni effect mediates droplet generation [32]. The droplet generation could also be altered by modulating the interfacial tension through electrical control in a way that Maxwell stress is absent but electrochemical and electrocapillary effects get into play if both disperse and continuous phases are electrically conductive and immiscible [33].

3 Electro-hydrodynamics

Transport phenomena in electrohydrodynamic construct foundation of many applications such as electrokinetic, electrospray, electrospinning, electroprinting, electromixing and electro-coalescence etc. Despite that stable flow is commonly desirable in most cases, however, unstable flows become favorable in certain applications (e.g. in mixing). Understanding concept of electrohydrodynamics is essentially significant, which constitutes the underlying physics of the investigations given in the thesis as well. Here in this section, the basics of electrohydrodynamics - including modeling, electrohydrodynamic instability and cone-jet mode – electrophoresis, dielectrophoresis and eventually some applications are briefly introduced.

3.1 Basics of Electro-hydrodynamics

The interaction of electric and flow fields is the central pillar of electrohydrodynamics (EHD) for which the ohmic model, also so-called leaky dielectric model, is an excellent approximation [34]. Here, the commonly used model for electrohydrodynamic analysis and cone-jet, the most frequent mode of electrohydrodynamics, are briefly introduced.

3.1.1 Leaky dielectric model

When transport process characteristic time, τ_p, that comes from viscous relaxation, diffusion, oscillation of an imposed field, or motion of a boundary is larger than characteristic time of electric phenomena, also known as charge relaxation time defined as $\tau_t=\varepsilon\varepsilon_o/\sigma$, the electro-quasi-static approximation would be appropriate and leaky dielectric model can be used [34]. In such a case, even for leaky dielectric liquids (i.e. not perfectly conducting liquids), the liquid bulk is quasineutral and charges tend to stay at the interface. Therefore, the slow processes are defined when $\tau_p \geq \tau_t >> \tau_M$ in which τ_M is the characteristic time for magnetic phenomena. In the absence of magnetic field, the magnetic effect can be ignored and therefore, the electrostatic field is irrotational, that is

$$\nabla \times \boldsymbol{E} = 0 \tag{3.1}$$

and the Gauss's law for electrically linear medium yields the following equation

$$\nabla \cdot \varepsilon \boldsymbol{E} = \rho_f \tag{3.2}$$

where $\boldsymbol{E}$ is the electric field, ε is the permittivity, and ρ_f is the free charge density. The charge conservation for the ohmic regime is as

$$\frac{\partial \rho_f}{\partial t} + \nabla \cdot \left(\rho_f \mathbf{v} + \sigma \boldsymbol{E}\right) = 0 \tag{3.3}$$

Here, $\boldsymbol{V}$ is the fluid velocity, σ is the electrical conductivity.

The above equations together with continuity equation and momentum equation with included electric body forces constitute the governing equations for Leaky Dielectric Model used for analysis of electrohydrodynamic phenomena.

Korteweg-Helmholtz force density is more appropriate for prediction of electromechanical coupling compared to Kelvin approach. For an electrically linear medium with polarization dependent on mass density and temperature alone, the electrical force density can be represented as

$$f_{KH}^{e} = \rho_f \boldsymbol{E} - \frac{1}{2}E^2\nabla\varepsilon + \nabla\left[\frac{1}{2}\rho\left(\frac{\partial\varepsilon}{\partial\rho}\right)_T E^2\right] = \nabla\cdot\left[\varepsilon\boldsymbol{E}\boldsymbol{E} - \frac{1}{2}\varepsilon E^2\mathbf{I} + \frac{1}{2}\rho\left(\frac{\partial\varepsilon}{\partial\rho}\right)_T E^2\mathbf{I}\right] = \nabla\cdot\mathbf{T}_{KH}^{e} \tag{3.4}$$

where, on the left-hand-side, the first term is the contribution of Columbic force exerted on free charges, the second term is related to the polarization force due to the polarization charge at the interface between fluid phases with different dielectric properties acting normal to the interface, and the last term stands for the electrostriction force density associated with volumetric change in the material. $\mathbf{T}_{KH}^{e}$ is the Maxwell stress tensor corresponding to the Korteweg-Helmholtz force density. For the case of electrically linear, incompressible dielectric medium, the last term disappears. The continuity and momentum equations including the electric body force are given by

$$\nabla\cdot\mathbf{v} = 0 \tag{3.5}$$

$$\rho\frac{\partial\mathbf{v}}{\partial t} + \rho\mathbf{v}\cdot\nabla\mathbf{v} = -\nabla p + \mu\nabla^2\mathbf{v} + \rho_f\boldsymbol{E} - \frac{1}{2}E^2\nabla\varepsilon \tag{3.6}$$

where *p* is the pressure and the two last terms on the right-hand-side of Eq. (3.6) are Coulombic and polarization electric body forces.

Two models can be employed for systems having non-uniform properties. One is bulk-coupled model in which a bulk region is considered at the interface with continuously varying properties. Therefore, the jumps in physical properties across the interface is handled using smoothing. In the bulk-coupled model for a diffusive interface, the electromechanical coupling fulfills via volumetric forces distributed across the diffusive interface and material properties are incorporated in solution through addition of further equations. Furthermore, it is worth noting that the surface force is a local surface phenomenon whose implementation requires considering jump condition for force balance. In the bulk-coupled model, it is commonly transformed into an equivalent volumetric force as introduced by Brackbill et al. [35] who proposed the Continuum Surface Force (CSF) method. Accordingly, the sharp interface between two fluids is replaced by a transition region of a finite thickness, known as diffuse interface. The alternative volumetric surface force then is included in the momentum equation. Consequently, a diffuse interface approach based on the Volume of Fluid (VoF) method is usually used to track the interface between fluid phases [36] with smoothing fluid properties on the interface. A diffuse electric interface at the phase boundary between fluids can be also considered as the harmonic averages [37,38] .

Another model is surface-coupled model by which adjoining regions with piecewise uniform properties are assumed and the electromechanical coupling is through interfacial stresses. Nevertheless, in this model for a sharp interface, jump conditions, obtainable by integrating the differential equations across the interface, are required to relate the interfacial and bulk properties [39] as follows

$$\mathbf{n} \times \|\boldsymbol{E}\| = 0 \tag{3.7}$$

$$\mathbf{n} \cdot \|\varepsilon \boldsymbol{E}\| = q_s \tag{3.8}$$

$$\frac{\partial q_s}{\partial t} + \nabla_s \cdot (q_s \mathbf{v}) = -\mathbf{n} \cdot \|\sigma \boldsymbol{E}\| \tag{3.9}$$

$$\mathbf{n} \cdot \|\mathbf{v}\| = 0 \tag{3.10}$$

$$\mathbf{n} \times \|\mathbf{v}\| = 0 \tag{3.11}$$

$$\mathbf{n}\|p\| = \mathbf{n} \cdot \left\| \mu\left(\nabla \mathbf{v} + \nabla \mathbf{v}^{\boldsymbol{T}}\right) + \varepsilon \boldsymbol{E}\boldsymbol{E} - \frac{1}{2}\varepsilon E^2 \mathbf{I} \right\| + \nabla_s \gamma - \gamma \mathbf{n}(\nabla_s \cdot \mathbf{n}) \tag{3.12}$$

where the notation $\|x\|$ denotes the jump in a quantity x across the interface, $\mathbf{n}$ denotes the outward normal vector, subscript s denotes surface quantities, q_s is the surface charge density, $\nabla_s = (\mathbf{I} - \mathbf{nn}) \cdot \nabla$ is the surface gradient operator, and γ is the surface tension.

The motions of EHD are electrically driven forces applied on boundaries or in the fluid bulk. Corresponding forces given by net Maxwell stress in normal and tangential components are

$$\mathbf{n} \cdot \left\| \left(\varepsilon \boldsymbol{E}\boldsymbol{E} - \frac{1}{2}\varepsilon E^2 \mathbf{I} \right) \cdot \mathbf{n} \right\| = \frac{1}{2} \|\varepsilon (\boldsymbol{E} \cdot \mathbf{n})^2 - \varepsilon (\boldsymbol{E} \cdot \mathbf{t_1})^2 - \varepsilon (\boldsymbol{E} \cdot \mathbf{t_2})^2\| \tag{3.13}$$

$$\mathbf{t_i} \cdot \left\| \left(\varepsilon \boldsymbol{E}\boldsymbol{E} - \frac{1}{2}\varepsilon E^2 \mathbf{I} \right) \cdot \mathbf{n} \right\| = \|\varepsilon \boldsymbol{E} \cdot \mathbf{n}\| (\boldsymbol{E} \cdot \mathbf{t_i}) \tag{3.14}$$

where $\mathbf{t_1}$ and $\mathbf{t_2}$ are orthogonal tangential vectors on a surface. Eq. (3.14) demonstrates that a tangential Maxwell stress vanishes either for a perfect dielectric ($q_s = 0$) or a perfect conductor ($\boldsymbol{E_t} = 0$).

In case of droplet generation, the process of detachment is a strong function of wettability of capillary surface or channel wall. The contact angle at contact line, the meeting points of two fluid phases with solid wall, could contribute to the process of droplet generation to some degree. The contact line is typically represented by a contact angle. In contrast to the static equilibrium where the contact angle is defined by its minimal advancing (θ_{adv}) and maximal receding (θ_{rec}) values, the contact angle for the dynamic state is dependent on the local contact line velocity (u_{cl}). Kistler [40], for example, suggested the following correlation to model dynamic contact angle

$$\theta = f_H \left(C_a + f_H^{-1} \left(\theta_{adv/rec} \right) \right) \tag{3.15}$$

with $$f_H(x) = \arccos\left(1 - 2\tanh\left[5.16\left(\frac{x}{1+1.31x^{0.99}}\right)^{0.706}\right]\right) \tag{3.16}$$

where C_a is capillary number (defined as $\mu U_{cl}/\gamma$). The capillary number is a signed quantity being positive for advancing contact angle and negative for receding contact angle.

3.1.2 Electro-hydrodynamic instability and cone-jet phenomenon

In fluid mechanic and related subjects, the effect of electric fields on shape and stability of drops has drawn the attention of many researchers. The electrohydrohynamic cone-jet is particularly relevant as it puts forth many applications such as electrospray, electrospinning, electroprinting etc. Having stable and controllable liquid cones formed through applying an electric field on an interface between a conducting liquid and a non-conductive fluid is of great importance required for emission of electrified liquid jets and thereby droplets. For example, generation of fine droplets and/or liquid fibers observed in electrospraying and electrospinning rely on downstream destabilization of a steady cone-jet [41] or on-demand drops in electroprinting on the transient cone-jets [42].
In electrohydrodynamics a transition from cone to jet (cone-jet mode) is achieved when a conical meniscus liquid is formed at the expense of an amount of electric potentials applying on a capillary needle or a fluid-fluid interface. As a result, beyond a threshold electric potential difference, a thin but robust jet is emerged from the tip of the conical meniscus liquid with typical diameter in several orders of magnitude smaller than the cone itself, which remains steady until termination of the stimuli (the electric potential difference).
In absence of jet, i.e. when the only conical meniscus liquid exists, in a hydrostatic state, which is known as pure Taylor cone, the surface/interfacial tension is balanced with electric Maxwell stress, assuming an equipotential cone and an insulating medium free of charge. In such a case, the balance and the electrical potential φ (in spherical coordinates (r, θ)) in terms of the Legendre function of order ½ (regular at θ=0) are given in Eqs. (3.17) and (3.18), respectively.

$$\gamma\nabla\cdot\mathbf{n}-\frac{1}{2}\varepsilon(\nabla\varphi)^2=\Delta p \tag{3.17}$$

$$\varphi=\mathrm{a}_o\mathrm{r}^{1/2}\mathrm{P}_{1/2}(\cos\theta) \tag{3.18}$$

$$\mathrm{a}_o{}^{-2}={}^1\!/_2\,\gamma^{-1}\varepsilon\mathrm{P}'_{1/2}{}^2(\cos\alpha_T)\tan\alpha_T=0.552\left(\frac{\varepsilon}{\gamma}\right)^2 \tag{3.19}$$

$$\mathrm{P}_{1/2}(\cos\alpha_T)=0 \tag{3.20}$$

where $\nabla.\mathbf{n}$ is the curvature, Δp is the pressure jump across the fluid-fluid interface. If Eq. (3.18) is substituted in Eq. (3.17) and compute $\nabla.\mathbf{n}$ for a cone angle α_T, the constant a_o (in Eq. 3.19) is fixed, also yielding ΔP=0 [43].
The conical equipotential surface requires that $P_{1/2}(\cos\theta)$=0, which results a cone angle of $\theta_0=\pi$-49.29° in the range $0<\theta<\pi$. Since $P_{1/2}(\cos\theta)$ is finite and positive in the range $0<\theta<\theta_0$ but is infinite at $\theta=\pi$ the only possible electric field in equilibrium with equipotential fluid surface yields a semi vertical angle (Taylor angle) α_T=49.3°[44].
Although being simple, there are some missing facts in the above solution. The following briefly touches these missing elements but to see more details one may refer to Ref. [43]. The most significant missing factor is that Eq. (3.18) corresponds to the special case when Δp=0, and therefore finite range of possible values of Δp has been ignored, which are related to the stability of a Tylor cone and existence of multiple solutions and hysteresis. Another point is that this equation is valid only locally due to the singularity of φ at semiaxis $\theta=\pi$ while growing with no bound in all directions when the distance r increases toward the apex.

To see the effect of pressure jump Δp, De La Mora [43] reported that by leaving out possible eigenfunctions noted by F. Higuera (in a private communication) [43], for an axisymmetric pointed tip with its apex located at r=0, the following expansion in half-integer powers of the rescaled polar coordinate $\rho = r a_1$ satisfies Laplace's equation:

$$\varphi(\rho,\theta) = \mathrm{a_0 r}^{1/2}\begin{Bmatrix} \mathrm{P}_{1/2}(\cos\theta) + \alpha_1\rho\mathrm{P}_{3/2}(\cos\theta) + \alpha_2\rho^2\mathrm{P}_{5/2}(\cos\theta) \\ + \cdots + \alpha_n\rho^n\mathrm{P}_{n+1/2}(\cos\theta) + \cdots \end{Bmatrix} \tag{3.21}$$

If a perturbed Taylor cone geometry of the form is postulated such that

$$\theta(r) = \alpha_T + \beta_1\rho + \beta_2\rho^2 + \beta_3\rho^3 + \beta_4\rho^4 + \cdots \tag{3.22}$$

The criteria of equipotential surface and mechanical equilibrium of the surface meet, and the pressure jump Δp can be fixed through $\Delta p/\gamma$=-0.524826 a_1.
The expansion coefficients given in α_n and β_n are given in Table 3.1 [43].

Table 3.1 Initial a_n and s_n coefficients calculated for the series Eq. (3.21) and Eq. (3.22) [43]

n	1	2	3	4	5	6	7	8	9
α_n	1	1.34872	2.15378	3.28424	4.82025	6.71530	8.37544	8.12630	1.96622
β_n	−0.5053	0.2718	−0.2090	−0.2114	0.27853	0.40655	−0.5829	0.82082	−1.1725

As a_1 is related to the dimensionless pressure jump, it can completely determine the potential and meniscus shape itself, whereas the case a_1=0 (and thereby Δp=0) corresponds to the pure Taylor cone, characterized by a strictly conical shape.
As mentioned, the meniscus shapes are dependent on the value of Δp. Δp=0 is associated to a conical shape. Δp<0 belongs to a family of short pointed menisci curved away from the axis [43], indicating that the pressure in the cone is less that its outside due to electrostatic suction [45] as a consequence of electric force (i.e. Maxwell stress) exceeding the surface tension force. In contrast, Δp>0 corresponds to a family of long acorn-shaped pointed menisci curved toward the axis [46,47] in which pressure inside droplets are larger than their surrounding and exposed to an electric field above a critical amount they emit jets and progeny droplets.
Although there are some studies controlling the Taylor cone (or cone-jet) directly via Δp and voltage V [48,49], however, most studies control it through voltage V and flow rate Q. Steady cone-jet offering many applications is an important mode of an electrified meniscus that can be nicely characterized by the stability island in the electric field-flow rate (E-Q) operating diagram. As a typical E-Q diagram shown in Fig 2.5 [39], at the minimum flow rate Q_m, the electric field must be E_m to form a steady cone-jet. When $Q>Q_m$, a steady cone-jet formation is possible but within a limited range of electric field around E_m. For $Q<Q_m$, a steady cone-jet cannot be produced, however pulsating cone-jet may occur around E_m, which is resemble to the case of intermediate flow rate ($Q \geq Q_m$) at $E \leq E_m$. One may consult with literature for more details [50–52]. The pulsating cone-jet, which is further doable by applying pulsed electric fields, constitutes foundation of the current thesis in which droplets on-demand can be produced [2,53] along with their electrical manipulation [11,27].

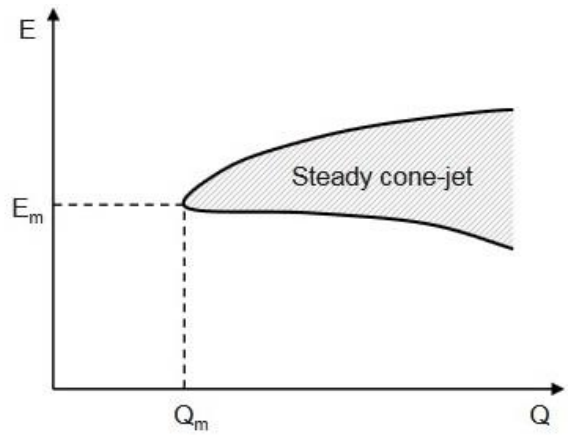

Fig. 2.5 Operating regime of steady cone: *Q* denotes the flow rate. Reprinted with permission from [50].

3.2 Electrophoresis

Electrophoresis is associated to the relative motion of dispersed charged particles inside a fluid when exposing a spatially uniform electric field. Its principle is used for size-based separation of nanoparticles and macromolecules, and comes especially with wide spectrum of use in analyzing DNA, RNA and proteins. In electrophoresis only charged particles can move, regardless of uniformity of the electric field, which their direction of motion are determined by the particle charges.
Electrophoretic force is obtained by the action of the electric field strength on a particle with a certain amount of net charge given by

$$\mathrm{f}_e = qE \tag{3.23}$$

where *q* is the net charge associated with the particle and *E* is the electric field strength. This force is the same as the electric force term in the Lorentz force. When electric field is constant and homogeneous, a charged particle accelerates until the drag force compensates the electrophoretic force. As a result, an equilibrium is reached between the two opposing forces and the particles move with constant velocity. For a moving particle in a viscous medium, in the case of low Reynolds number and moderate electric field strength, a corresponding drift velocity *v* is proportional to the electric field strength through which electrophoretic mobility is defined as:

$$\mu_e = \frac{v}{E} \tag{3.24}$$

the electrophoretic mobility can be also expressed in terms of the zeta (ζ) potential (developed by Smoluchowski in 1903 [54]) as:

$$\mu_e = \frac{\varepsilon_0 \varepsilon_r \zeta}{\mu} \tag{3.25}$$

where ε_r is the dielectric constant of the dispersion medium, ε_o is the permittivity of free space, μ is dynamic viscosity of the dispersion medium, and ζ is zeta potential. From these two different electrophoretic mobility definitions, one can further notice that the velocity of particles depends on some parameters like electric field strength, the dielectric constant and the viscosity of the medium, and the zeta potential of the particles. However, the Smoluchowski theory is valid only for sufficiently thin double layer, where the Debye length is much smaller than the particle radius.

As an application of electrophoresis, charged particles when placed in a uniform electric field, created by a pair of electrodes, can show a cyclic motion in a way that the charged particle initially moves to the electrode with opposite charge. Upon contact, its charge sign switches and it becomes oppositely charged and thus reverses its direction of motion towards the other electrode. Performing this process, the particle continues indefinitely cyclic motion between the electrodes. This was first observed by Cho [55] who found the acquired charge (due to contact with electrode) depends on the DC field and the size of particle. The cyclic motion of metallic sphere between two electrodes has been observed earlier [56,57]. However, electrophoresis is not only limited to rigid particles; it also applies to deformable and flexible drops containing some amount of charge, that is, the charged drops move electrophoretically as known from long time ago [58]. Charged aqueous droplets in oil move by electrophoretic driving force for which more complex charge transfer mechanisms may be present. Similar to rigid particles, the electrophoretically motion of aqueous droplets in oil mediums have shown bouncing of droplets back and force between aqueous/non-aqueous electrodes upon which the charge transfer occurs [11,59]. Nevertheless, droplets exhibit different modes of cyclic motion, perhaps in contrast to rigid particles. These modes of cyclic motion are stationary drop, small and large amplitudes [60], which could be due to the loss of charge drop to the surrounding oil medium while moving away from an electrode. The charge dissipation rate depends on the conductivity of the medium, σ_m, and the local electric field, E_z, written as [61]

$$\frac{dq''}{dt} = \sigma_m E_z \tag{3.26}$$

where q'' is the surface charge density given by q/A with A being as the surface area. If a droplet loses its charge to its surrounding medium during a motion between two electrodes, there must be another force or mechanism by which the droplet could reset the motion after being discharged such as gravity or electrophoresis force. In this regard, a different design of electrodes in terms of orientation or structure can be drastic. For example, a combination of pin and plate electrodes that causes generation of non-uniform electric field is a good choice [61], in particularly for microfluidic devices [11] where the gravitational force is absent.

The amount of aqueous droplet charge acquired upon contact with an electrode during the electrophoretically cyclic motion in oil between two planar electrodes was reported to be less than the one theoretically predicted for a perfectly conductive sphere [62]. It was also found that charging process accomplishes in three steps [63]. In the first step, the charge of droplet induces the charge accumulation on the opposite electrode when closely approaches. In the second step, the droplet gets discharged by the accumulated charge on the electrode when are in contact, and in the last step at the same time, the neutralized droplet acquires a certain charge that is the opposite charge before contact.

3.3 Dielectrophoresis

The electric field in practice is rarely uniform. An uncharged droplet when placed in a non-uniform electric field undergoes a net force by which it may move towards either large or low electric field strength. Upon applying electric field, polarizable particle gets polarized and induces a dipole. Because of the non-uniform distribution of the electric field, and thereby non-uniform electric force, acting on the polarized particle, a net force exerts on the particle moving it in one direction depending on relative polarizability of dispersed particle and dispersion medium. When polarizability of particle is greater than the medium, the particle moves to the region of large electric field strength (called positive dielectrophoresis) and when polarizability of particle is less than the medium the opposite occurs (called negative dielectrophoresis). In contrast to electrophoresis, uncharged particles can experience dielectrophoretic force but only in non-uniform electric field. Pohl [64] initially suggested the dielectrophoretic force for an uncharged dielectric particle (or droplet) inside another dielectric medium exposed to a non-uniform DC electric field as

$$F_{DEP} = 2\pi a^3 \varepsilon_m \varepsilon_0 CM \nabla \boldsymbol{E}^2 \tag{3.27}$$

where *r* is radius of particle and ***E*** is electric field acting on the particle, ε_m is the dielectric constant or permittivity of medium, ε_o is the dielectric constant or permittivity of space, and *CM* is called Clausius Mossotti factor defined as

$$CM = \frac{\varepsilon_d - \varepsilon_m}{\varepsilon_d + 2\varepsilon_m} \tag{3.28}$$

Here, ε_d is the dielectric constant of the droplet (or particle). Sign of Clausius Mossotti factor determines the direction of particle motion to or from the region of strong electric field intensity.

Dielectrophoresis can occur in AC electric field as well as DC electric field because the corresponding force is dependent on the gradient of the field instead of the direction of the field. Furthermore, the relative polarizabilities of the particle and medium are frequency-dependent. In such a case (i.e. AC field) the DEP force is similar but with few changes as given below

$$F_{DEP} = 2\pi a^3 \varepsilon_m \mathrm{Re}\left\{\frac{\varepsilon_d^* - \varepsilon_m^*}{\varepsilon_d^* + 2\varepsilon_m^*}\right\} \nabla |\boldsymbol{E}|^2 \tag{3.29}$$

Here the asterisk superscripts denote the complex permittivity given as $\varepsilon^* = \varepsilon + i\,\sigma/\omega$, where ε is the dielectric constant, σ is the electrical conductivity, ω is the frequency of the electric field, and *i* is the imaginary unit.

Similar to rigid particles, a drop can also experience dielectrophoresis, but at the same time can bear deformation. Furthermore, when placed in a non-uniform electric field, the drop can exhibit a cyclic motion by a combination of electrophoresis and dielectrophoresis forces. The systematic experimental study on this was carried out by Mhatre and Thaokar [61] who observed two distinct cyclic motions for a water droplet in an oil medium subjected to a non-uniform electric field produced by a pin-plate configuration; pin-plate and near-electrode cyclic motions. Mhatre and Thaokar found that in the pin-plate system, a droplet alternatively moves back and forth between two electrodes in which the electrophoretic dominates over the dielectrophoretic force. In such a case, the charge

relaxation time was larger than the time scale of motion. The charge relaxation time and the time scale of motion are $\varepsilon_r\varepsilon_o/\sigma$ and $6\pi a\mu L/qE$, respectively, wherein a is drop radius, L is the distance traveled. By contrast, in the near electrode system, the charge relaxation time was smaller than the time scale of motion and therefore the droplet after contacting the pin electrode traveled some distance up to a certain point without reaching to the plate electrode. At that point, the droplet reversed its direction of motion because of the charge loss to the surrounding oil. Indeed, the droplet became uncharged followed by reversal of motion by the dielectrophoretic force towards the region of large electric field (i.e. towards the pin electrode) and thus the dielectrophoresis is the driving mechanism for assisting the cyclic motion when droplet gets uncharged.

Aside from the fact that dielectrophoresis can play a role during cyclic motions at some points together with the electrophoresis, it is basically used for transporting liquid volumes, dispensing droplets, manipulating droplets and sorting purposes which are briefly introduced in the following application section.

3.4 Applications

Dielectrophoresis has become a tremendous tool for separation of rigid particles and, in particular, nanobio-particles [65]. In that context, dielectrophoresis, which has a nondestructive electrokinetic mechanism and is based on polarization effects, has been used for manipulation, concentration and separation of DNAs, proteins, viruses and spores and etc., which find significant applications in genetics, microbiology, medicine, biochemistry and so on. For example, a non-uniform electric field, which dielectrophoresis stands on that basis, can stretch DNA molecules into a line up to several times larger than its coiled form structure [66] that is especially useful for determination of size of DNA molecules. The DNA molecules when stretched were prone to be treated in different ways such as cutting by employing high intensity UV light [66], a laser beam [67] or even mechanically through microscale cantilever with a sharp tip [68].

Strong dependency of dielectrophoretic force on size of particles and nanobioparticles allows the dielectrophoresis technique be impetus for separation purposes. For instance, separation of λ-DNA and oligonucleotide in a microchannel containing a large number of corrugated electrodes was achieved by applying an electric field which demonstrated the application of dielectrophoresis chromatography [69]. As a result, the biomolecules were trapped transiently depending on the dielectrophoretic force based on size such that larger molecules with a higher polarization (λ-DNA) took much longer passing through microchannel compared to smaller molecules with less polarization (oligonucleotide). There are abundant similar studies focusing on manipulation, concentration and separation of proteins, viruses and spores as well as DNA (see the review [65]). More recently, Viefhues and Eichhorn [70] reported a review on the theory and applications of DNA dielectrophoresis, presenting dielectrophoresis with abilities in trapping and immobilization, separation and purification of DNA molecules. Furthermore, capability of implementing in microdevices [71,72] and construction of material in nanoscales such as carbon nanotube as an electrode [73] have added advantage of using dielectrophoresis for manipulation of nanobioparticle like DNAs.

Electrophoresis, likewise, has numerous applications in biological and medical sciences. It is used for separation of proteins based on their mobilities in an electric field. One of the main methodologies in that context is capillary gel electrophoresis (CGE) [74]. Proteins in biological fluids due to complexity of their media are challenging to analyze and CGE provides a drastic tool for analysis [75]. In food industry for monitoring food safety and quality, analysis of proteins becomes essential and it can be implemented by applying CGE technique [76]. In

pharmaceutical industry, a CEG technique can be developed to analyze the quality and purity of recombinant monoclonal antibodies that are increasing in therapeutic use [77]. Similarly, DNA separation has been speeded up through using capillary electrophoresis, which has more advantages over the classical slab-gel electrophoresis. Typical applications of capillary electrophoresis can be found in DNA sequencing [78], fragment sizing [79], SSCP [80] or RFLP [81] analysis.

Dielectrophoresis and electrophoresis, aside from being widely used for biomolecular and biochemical applications, are used for manipulation of drops that may or may not contain other (bio) entities. As already pointed out, dielectrophoresis phenomenon is being remarkably used to transport liquid volumes, dispense and manipulate droplets. As few examples, a parent droplet siting on an insulating substrate coated with a dielectric when exposed to an electric potential on co-planar electrodes emerges a finger of liquid all the way down to the location where the electrode structures end. By removing the applied voltage, capillary instability caused the liquid finger decays into discrete droplets [82]. For drop transportation, in contrast to uniform electric field in which an uncharged droplet only shows deformation without any translational movement, in a non-uniform electric field an uncharged droplet dielectrophoretically transports in both DC [61] and AC [83] fields before acquiring some charge upon touching the target electrode and thereby moving electrophoretically. Water droplets can be moved, split and merged in an oil medium in a dielectrophoresis manipulator chip by means of electric fields [84].

4 Generation of droplets in-series in microfluidics devices and their electrical manipulation

4.1 Introduction

Microfluidic droplet generation systems are being widely used for producing water or oil droplets in a counterpart immiscible phase, mainly by passive technique. To apply this technique, the simplest way is to bring two immiscible fluids in contact at a T-junction channel (T-junction geometry) or bring two streams of the same fluid perpendicular to an immiscible phase (flow-focusing geometry), where these geometries are the commonly used geometries for generating monodisperse droplets. Droplet generation offer tremendous applications such as in analysis of biological assays [85], chemical reactors [86], drug delivery [87], food engineering [88] and pharmaceutical applications [89] and etc. Despite of emerging microfluidics with complex geometries [90,91], the T-junction and flow-focusing geometries are still fundamental and there are plenty of studies in the literature concerning droplet generation using them [15].

Employing active technique via applying external sources such as temperature [92], acoustic [93], magnetic [94] and electric fields, which can be either solely used or combined with passive technique, would enhance the utility of droplet generation for controlling droplet size. Among these approaches, the more achievable, fast-response and high flexible tool for tuning droplet size is applying electric field. In this regard, there are a number of efforts in the literature investigating the effect of electrical control on the droplet size in microfluidic droplet generation process basically in a flow-focusing geometry. For example, Link et al. [95] generated water droplets with size of several to several hundred picoliters in oil. To manipulate them, they employed a DC electric field by a voltage in the range of about 20-1000 V across the 500-micron separation of the nozzles, applied to indium tin oxide (ITO) electrodes on the glass. Tang et al. [33] applied a DC electrical potential to liquid metal stream of EGaIn in contact with a glycerol-NaOH solution while connecting each inlet tubes to both anode and cathode for electrochemical and electrocapillary control of EGaIn microdroplets size. They could reduce the size of the EGaIn droplets from 200 µm (in absence of electrical potential) to half by applying a positive voltage of 18 V, whereas the minimum droplet diameter (about 134 µm) was obtained in excess of applying a negative voltage of -5 V. Kim et al. [96] produced water droplet in mineral oil with Span 80 (6 wt. %) and controlled the size of droplets by DC electric field (the voltage was in the range of 0-2000 V over the 0.3645 mm distance between the electrodes). They found that the electric field can only be effective in tuning the droplet size only at small flow rate ratios with a low flow rate of water. They could decrease the size of droplets by one order of magnitude (to less than 1 µm), where the droplets were more polydisperse in form of conical spray. In a further study [97] with almost similar conditions, they investigated the effect of low-frequency AC electric field of triangular waveform on the control of droplets and obtained a continuously size-reducing droplet series at the voltage ramp-up stage. Tan et al. [98] performed a study on the effect of a sinusoidal voltage from 1 to 1 kV at frequencies from 1 kHz to 50 kHz on the droplet size of NaCl aqueous solutions at different electrical conductivities in mineral oil with 5w/w% Span 80. Their used microelectrodes were not in contact with the fluids and were patterned around the flow-focusing junction. They realized that droplet generation regimes are a function of connection of the chip, electrical parameters, and

electrical property of the dispersed fluid. The droplet size was between around 35-85 µm. At low voltages ($\lesssim$ 600 V), the droplet size was only a function of the AC electric field while dripping regime was prevailing. At high voltages ($\gtrsim$ 600 V), the droplet size was a function of AC electric field and the electrical conductivity of the fluid while jetting regime was prevailing. Gu et la. [99,100] exploited the electrowetting approach for producing highly monodisperse water droplets in mineral oil containing 5% (wt.) Span 80 in conical spray regime under an AC voltage with a frequency of 10 kHz, and variable root-mean-square (rms) voltages from 0 to 100 Vrms. In addition to dripping regime in which droplets can be manipulated under electric field, they found that in jetting regime, the formed jets can be handled in the same manner. Castro-Hernandez et al. [101,102] reported that jets of the NaCl aqueous solutions in mineral oil with 5 % (w/w) Span 80, with shedding droplets at their ends, can be produced by applying AC electric field while the emerging AC electrified jets are variable as a function of water electrical conductivity, signal frequency and voltage amplitude.

In all studies reported until now addressing the electric control of droplet formation, the flow-focusing configuration has been used. By contrast, in this chapter, we demonstrate the electric tuning of the droplet size in the T-junction configuration. Compared to the flow-focusing configuration, the T-junction configuration offers the option to integrate a larger number of droplet generators in a compact space. This is due to the fact that flow focusing is based on merging three fluid streams (compared to two for the T-junction configuration), which either requires three inlets or two inlets arranged in a special way to avoid the crossover of channels. The effect of electric fields on droplet production by flow-focusing can be qualitatively understood by referring to work on Taylor cones [44]. When an electric field acts on a liquid surface, the surface assumes the shape of the cone if the Maxwell stress is of comparable magnitude as the surface tension. Above a threshold field strength, the surface becomes unstable and ejects droplets. Compared to that, the physics underlying the electric tuning of the droplet size in the T-junction configuration is far less obvious. Among the most prominent samples being processed in microfluidic devices are blood as well as solutions containing DNA or proteins. The associated rheological behaviour is complex, and non-Newtonian models are required. To demonstrate the broad applicability of the present method, in this work droplets of highly viscous and/or nonNewtonian fluids are also considered. There exist some experimental studies on the behaviour of non-Newtonian fluids in microfluidics [103–107], but usually Newtonian fluids are considered. Up to now, microfluidic emulsion or droplet generators have been scarcely explored for non-Newtonian fluids [108–111], in particular in context with electric fields [112].

4.2 Experimental set-up

A schematic view of the microfluidic chip is displayed in Fig. 4.1. It consists of a T-junction configuration along with a U-shaped microchannel close to the junction. The U-channel serves as an electrode, exposing the T-junction to an electric field. The experimental set-up has two electrodes; one is the water-filled U-shaped microchannel with an electric connection through a needle, and the other is the side channel of the T-junction which is connected (via a needle) to the second outlet of the power supply. The T-junction has two inlets for the disperse and continuous phases and an outlet for the two-phase flow.

All microchannels have rectangular cross-sectional shape. The disperse-phase and continuous-phase channels are 51 µm and 65 µm in width, respectively. All microchannels have a depth of 30 µm. The distance between the U-shaped channel and the channel junction is 25 µm.

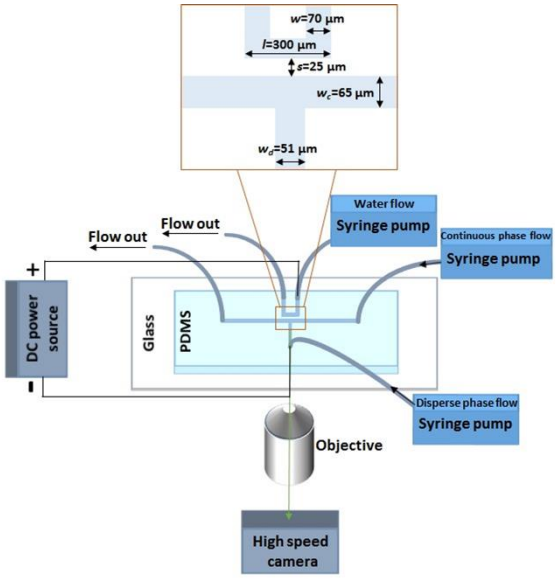

Fig 4.1 Schematic of the experimental setup. Reprinted with permission from [27].

The soft lithography protocol is utilized for fabrication of the microchannels. Briefly, a SU-8 photoresist structure on a silicon wafer, purchased from Microchem, is used as a mold for the device. First PDMS, purchased from Dow Corning (Sylgard 184 Silicone Elastomer), is mixed with a cross-linker in a 10:1 ratio and then cast onto a silicon wafer containing the master structure, followed by curing for 30 min at 100 °C. The surface of the obtained PDMS structure along with a glass slide is treated with oxygen plasma (Femto, Diener Electronic GmbH, Germany). After plasma treatment, the PDMS structure is attached to the glass slide, and the assembly is kept at 100 °C in an oven overnight to render the device hydrophobic.

PTFE tubing is used to connect the device to 1 ml syringes (B. Braun Medical Inc.). The tubing is connected to the PDMS inlets through metallic needles with which the connection to the power supply is made. The power supply is a function generator (Tektronix AFG 3102) combined with a voltage amplifier (A800DI, FLC electronics AB). For monitoring and recording the fluidic behaviour, a high-speed camera (Redlake Motion Pro Series Y) is connected to an inverted microscope (Nikon Eclipse Ti). Both the continuous and disperse phase are fed to the microchannels by syringe pumps (KD Scientific Inc.).

4.3 Materials

4.3.1 Non-Newtonian Xanthan gum solutions

Water, as a Newtonian fluid, and aqueous polymer solutions, as non-Newtonian fluids, are used as disperse phases, and sunflower oil served as the continuous phase. All disperse-phase liquids contain 0.017 mol/l NaCl salt. The polymer solutions are prepared by dissolving xanthan gum powder (xanthan gum from Xanthomonas campestris), purchased from Sigma-Aldrich, in water at 40 °C aided by a magnetic stirrer. Xanthan gum concentrations of 0.5 and 1 g/l are employed. No surfactant is added to any of the liquids.

4.3.2 Interfacial tension and viscosity measurements

The rheological behaviour of xanthan gum solution has already been reported in the literature. It has a shear-dependent viscosity that can be fitted by a number of well-known models [113] such as the non-Newtonian shear-thinning model [108,114]. The viscosities of the employed xanthan gum solutions at a zero shear rate are more than two orders of magnitude larger than the viscosity of water, i.e., 205 and 460 mPa.s for the concentrations of 0.5 and 1 g/l, respectively, as reported by Tam and Tiu [115].
The interfacial tensions between the aqueous phases and the oil phase are measured by a drop and bubble shape tensiometer (PAT-1, Sinterface Technologies, Germany). The measurements show that the interfacial tension between water and oil does not change upon addition of 0.5 and 1 g/l of xanthan gum into water.
The obtained value (23.5±60.6 mN/m) is consistent with literature values [116]. The viscosities of water and sunflower oil are measured with a rheometer (Brookfield LVDV-III), being about 1 and 53.5 mPa.s, respectively.

4.4 Experimental procedures: Fluidic and electric system set-up

The syringe pumps are set to provide a fixed flow rate of 50 µL/h for the oil and two flow rates of 20 and 50 µL/h for water and xanthan gum aqueous solutions. The size of the needles is a bit larger than the size of inlet holes and well press-fitted to the PDMS inlets to make sure there is no leakage for each phase. The combination of the function generator and the voltage amplifier is utilized to supply a DC voltage in the range between 0 and 500 V, corresponding to electric fields of up to about 11.6 $x10^6$ V/m, acting between the U-shaped channel and the aqueous phase entering the T-junction. The length of the water-filled U-shaped channel (i.e. the U-shaped electrode) in front of the junction is larger than the width of dispersed channel (i.e. the fluidic electrode), which thereby creates a non-uniform electric field with the largest electric field strength at the aqueous-oil interface at the junction.
Initially, the entire microchannel domain is filled with the oil phase. Once the aqueous phase reaches the junction, the flow of oil starts. After a few minutes, when the steady state condition for droplet generation is achieved, and a high-speed camera is employed at 1000 fps to record the dynamic behavior of droplet production with/without an applied electric field. For each case, after the electric field has been switched off, the next experiment is carried out after a delay of at least 5 to 10 minutes to make sure that capacitive effects are suppressed.

4.5 Results and discussion

In this study, the effect of a DC electric field on droplet production of water or xanthan gum solutions in sunflower oil at a T-junction is explored. Accordingly, the influence of DC electric field via applying DC voltages in the range of 0-500 V on the dynamic behavior of aqueous droplets produced in the oil are examined and discussed. In addition, for the sake of comparison between the effects of electrical and mechanical stresses on the droplet formation, some experiments are carried out for the case where the electric field is absent and only mechanical stress acts at the liquid-liquid interface. Corresponding results are compared with those performed at combination of the electrical and mechanical stresses.

4.5.1 Image analysis

To measure the size of the produced droplets, the equivalent diameter concept is adopted. Accordingly, the visible area of a droplet is calculated using the ImageJ software (National Institute of Health, USA), and the equivalent diameter is obtained using the equation $D_e = (4A/\pi)^{0.5}$, wherein A is the visible area of the droplet. To obtain statistical information about the droplet size, the average diameter and the corresponding standard deviation are obtained from a sample of at least 30 droplets for each set of operating parameters.

4.5.2 The effect of electric fields on water droplets

Figure 4.2 exhibits the production of water droplets in sunflower oil for different applied voltages and a flow rate ratio, φ, of 50/50. As seen, for all dispersed phase liquids, the droplet size decreases with application of electric field. Owing to the Maxwell stresses acting at the liquid-liquid interface, the interface protruding into the channel gets more and more deformed with increasing voltage. At around 200 V, the water phase forms a tongue with a relatively sharp tip. The droplets are produced from the decay of this liquid tongue. The tip is reminiscent of a Taylor cone [44]. As reported by Fernandez de la Mora and Loscertales [117], for liquids with relatively large conductivities, when the diameter of the jet emerging from the Taylor cone is smaller than the capillary tube diameter, the geometry of the jet becomes independent of the electric field strength. It may be speculated that in an analogous manner, the shape of the liquid tongue becomes largely independent of the electric field strength, resulting in droplets whose diameter cannot be reduced upon further increase in the field strength.

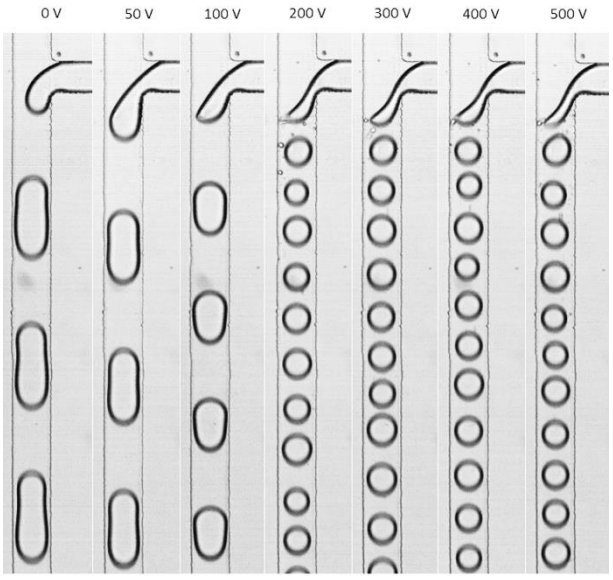

Fig 4.2 High-speed video microscopy images showing the influence of the electric field on the production of water-in-oil droplets at a flow-rate ratio of 50/50. Reprinted with permission from [27].

It is known that droplet production at T-junctions may either occur in the squeezing, dripping or jetting regime. The squeezing regime is characterized by the buildup of a pressure gradient across the droplet blocking major portions of the main channel [118]. By contrast, in the dripping regime, the viscous shear stress and not the pressure is the main influence that drives droplet pinch-off. Figure 1(b) and related image sequences reveal that in the absence of electric fields, the droplets are produced somewhere in between the squeezing and the dripping regime. The figure also reveals that the droplet generation process accelerates and the number of droplets increases by applying electric field.

Furthermore, the application of the electric field (i.e. Maxwell stress) not only decreases the size of droplets, but it also causes the transition in regime happens from (almost) squeezing to dripping. The Maxwell (electric) stress indeed suppresses the interfacial instability prevailing in the squeezing regime. At sufficiently large electric field strength, it remarkably manipulates the formation of droplets in such a way that the capillary instability runs the physics, accompanied by the transition to the dripping regime. In dripping regime, the size of the droplets is typically smaller than the channel width and therefore droplets keep their spherical shape when they are sufficiently away from the junction. Tan et al. [98] similarly reported regime transition from dripping-to-jetting with the increase of the voltage for a flow-focusing device. Therefore, in the active method, it becomes possible to change the flow regime by an electric actuation over the interface through exposing it to an electric field. It has been also observed that similar to water, the electric field has qualitatively almost the same effect on the non-Newtonian xanthan gum solutions.

Figure 4.3 shows a close-up of the channel junction, exposing some details of the droplet production mechanism. In a similar manner as for a Taylor cone, the electric field is strong enough to let the liquid tongue become unstable, letting it decay in a number of small droplets. Shortly thereafter, the liquid tongue pinches off from the liquid volume filling the side channel, producing a droplet much larger than those originating from the decay of the Taylor-cone like structure. Subsequently, the larger droplet merges with the smaller ones, leaving virtually no smaller droplets behind. The production of the small droplets is quite erratic, which could be the reason that the final product droplets are somewhat less uniform in size than the droplets produced without the electric field.

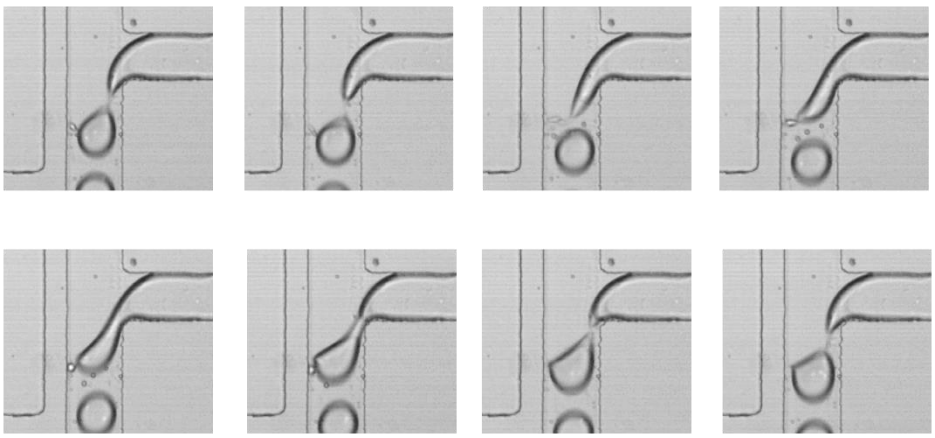

Fig. 4.3 Time lapse of the production of water droplets at a flow-rate ratio of 50/50 and a voltage of 200 V. The increment between the different frames is 1 ms. Reprinted with permission from [27].

4.5.3 The combined effects of electric field and fluid property

Figure 4.4 (a) shows the variation of the size of droplets of water and Xanthan gum solutions with concentration of 0.5 and 1 gr/l versus the applied voltage magnitude at a flow rate ratio, φ, of 20/50 (dispersed phase to continuous phase). This figure demonstrates that the droplet size considerably decreases up to a voltage of 200 V. An increase in the voltage beyond that value only has a comparatively small effect on the droplet size. This can be explained as follows. At very small voltages, the deformation of the liquid/liquid interface is mainly due to hydrodynamic stresses. When increasing the voltage, the Maxwell stresses become dominant. The deformation mode of the liquid/liquid interface remains more or less the same for voltages between 200 V and 500 V, leading to a droplet size which is largely independent of the applied voltage. At the highest voltage, the equivalent diameter of water droplets is almost a factor of two smaller than for the case without the electric field, while the size reduction is somewhat less pronounced for xanthan gum solution droplets. It is surprising that the data points show a non-monotonic trend with the viscosity of the disperse phase, i.e., the solution of intermediate viscosity (xanthan gum solution with a concentration of 0.5 g/l) exhibits the strongest deviation from the case of water as the disperse phase.

The variation of the droplet sizes of water and xanthan gum solutions with a concentration of 0.5 and 1 g/l with voltage at a flow rate ratio of 50/50 is presented in Fig. 4.4(b). Overall, the trends observed in this figure are similar to those of Fig. 4.4(a), but some differences exist. Most notably, a steady decrease in the droplet size of xanthan gum solutions up to voltages of 500 V is observed, in contrast to the behavior of water at the same flow rate ratio and to the behavior of xanthan gum solutions at the 20/50 flow rate ratio. A possible explanation of this effect is due to the viscous stresses building up in the xanthan gum solutions. While viscous stresses in water are negligible throughout most of the parameter range considered here, this is no longer true in xanthan gum solutions. The importance of viscous stresses in the aqueous phase is expected to increase as the relative flow rate of this phase increases.

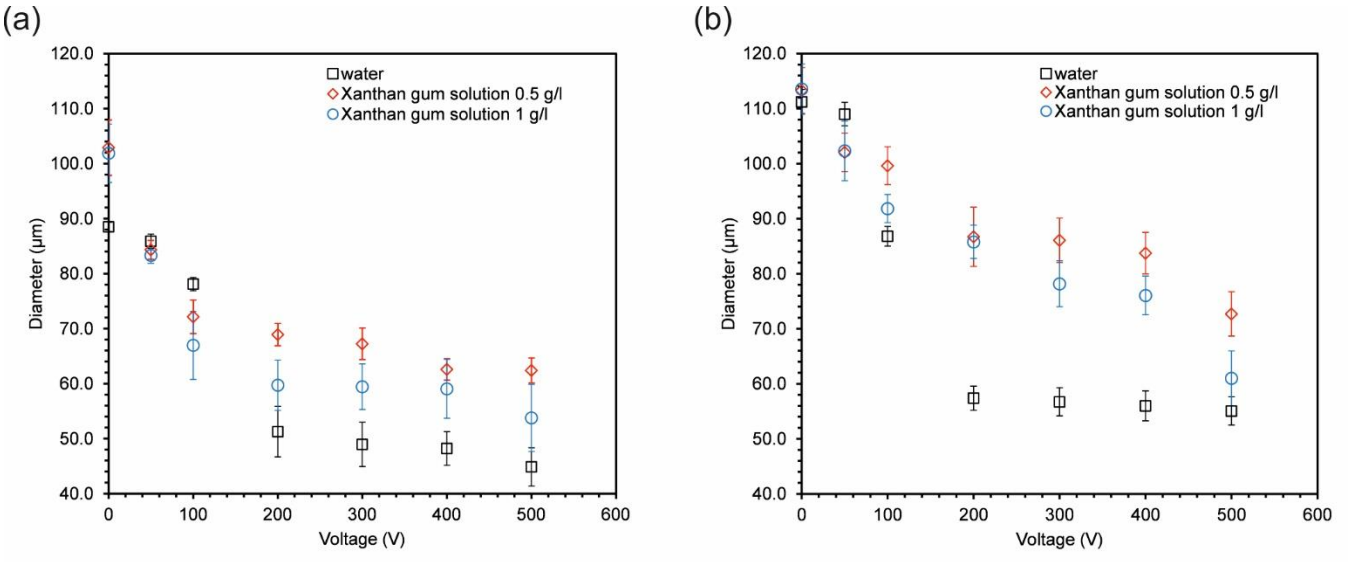

Fig. 4.4 (a) Variation of the droplet diameter with the voltage for different disperse phase liquids at a flow rate ratio of 20/50. The error bars represent the standard deviation of the droplet diameter. (b) The same for a flow rate ratio of 50/50. Reprinted with permission from [27].

4.5.4 2D non-uniformity analysis of electric field

The average electric field strength at the fluid interface corresponding to the smaller (aqueous) electrode is estimated based on the assumption that the field builds up between two parallel isopotential surfaces of lateral extension *l* (corresponding to the U-shaped channel) and w_d+*b* (corresponding to the fluid interface), where w_d is the width of the side channel. The average electric field strength at the fluid interface then follows from the compression of the electric field lines, and the voltage *U* is computed by assuming a linear variation of the field strength between the isopotential surfaces. The separation between the isopotential surfaces is given by w_c+*s*-*b*. The resulting electric field strength at the fluid interface is

$$E = \frac{2l}{(l+w_d+b)} \frac{U}{(w_c+s-b)} \tag{4.1}$$

As the water-filled U-shaped channel and the aqueous electrodes are different in width, the resulting electric field between them is non-uniform. The strength of the electric field varies from one electrode toward another one, where the largest strength forms at the fluid interface with smaller surface area upon applying a potential difference (i.e. voltage).

4.5.5 Force analysis

It is known that the passive method is a typical way of producing aqueous droplets in oil for which syringe pumps are the most widely used tools in that sense. For changing size of droplets, it is sufficient to increase/decrease the relative flow rate ratio of continuous to disperse phase. On the contrary, in the active method, such as electrical control, as mentioned earlier, the electrical stress comes into play that in most cases counteracts with mechanical stress.

To compare the effects of the Maxwell stress and the hydrodynamic stress in the droplet formation process, additional experiments without the electric field with water as the disperse phase are performed, where the flow rate of water is kept fixed at 50 μl/h and the flow rate of oil was varied from 50 to 550 μl/h. The corresponding results were compared with the case where the flow rate ratio is kept fixed at 50/50 and voltage is varied between 0 to 500 V.

For the calculation of the hydrodynamic stress acting on the liquid-liquid interface (in an order-of-magnitude sense), the sum of the shear stress σ_τ and the squeezing pressure σ_p due to the obstruction of the channel by the forming droplet are used [119] with

$$\sigma_\tau = \frac{\mu_c Q_c}{(w_c-b)h^2} \tag{4.2}$$

$$\sigma_p = \frac{12\mu_c Q_c b}{(w_c-b)^2 h^2} \tag{4.3}$$

where μ_c is the viscosity of the continuous phase, Q_c is the flow rate of the continuous phase, w_c is the width of the main channel, and *h* is its depth. For simplicity, it is assumed that the length of the forming droplet as measured from the downstream corner of the T-junction and the extent of the droplet across the width of the

channel are equal, denoted by b. The value of b is obtained from the high-speed images. It is worth noting that the value of b changes with the oil flow rate. The Maxwell stress is given as $0.5\ \varepsilon_r\varepsilon_0 E^2$, where ε_r is the relative dielectric permittivity of the oil phase ($\varepsilon_r \approx 3.3$ for sunflower oil [120]).

In Fig. 4.5, the droplet size as a function of the applied stress obtained in the two cases described above is displayed. In the case of purely hydrodynamic droplet formation, the stress is given by the hydrodynamic stress, whereas in the mixed hydrodynamic/electric mode, the stress is the sum of the hydrodynamic and the electric stress. However, note that in the mixed mode, at a voltage of 500 V, the electric stress is by a factor of 18 larger than the hydrodynamic stress, so in most of the parameter range, the electric effects dominate over the hydrodynamic ones. Figure 4.5 shows that also in the case of purely hydrodynamic droplet formation, the droplet diameter decreases with increasing stress. When comparing the two different modes, roughly equivalent relationships are obtained when plotting the droplet diameter as a function of the total stress. This leads to the conclusion that, as far as the diameters of the produced droplets are concerned, the electric stress has roughly the same effect as the hydrodynamic stress.

In the absence of electric field, the interfacial tension force interacts with the hydrodynamic forces, which are the shear force and the force caused by squeezing pressure due to the obstruction of the channel during the forming droplet [121]. When the interfacial tension force dominates the hydrodynamic force, the droplet is willing to stick to the source fluid (i.e. dispersed phase liquid) and thereby more dispersed liquid protrudes in the continuous liquid at the junction, resulting in the squeezing regime. In the squeezing regime, the size of the droplets is larger than the width of continuous phase channel and thus the droplet is squeezed and occupies the whole channel cross-section separated by a very thin layer of oil. In the presence of electric field, the Maxwell (electric) stress would suppress the interfacial instability in the squeezing regime and at sufficiently large electric field strength contributes to the formation of finer droplets.

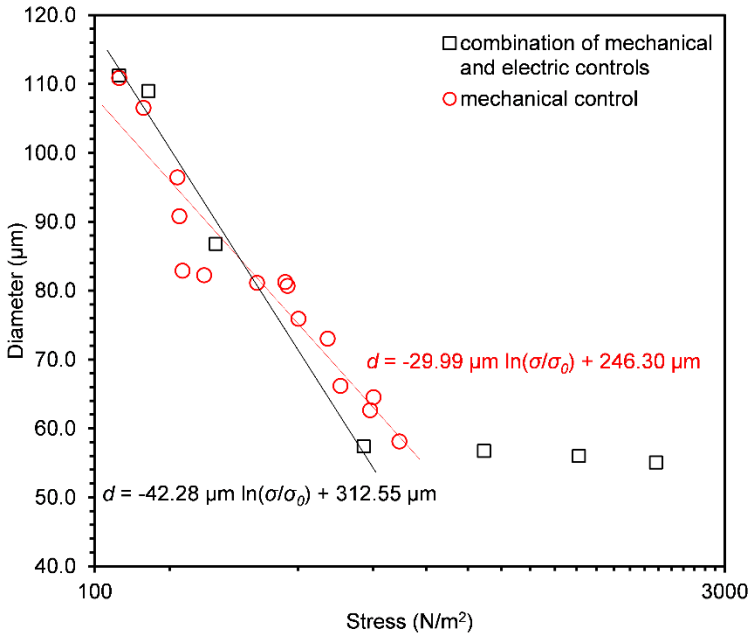

Fig. 4.5 Comparison between the effects of pure mechanical stress and a combination of mechanical and electric stresses on the droplet diameter for water as the disperse phase. The lines represent logarithmic fits to the data corresponding

to mechanical stress (red line) and the first four data points corresponding to mechanical/electric stress (black line). The data points represented by the square symbols are the same as in Fig. 4.4 (b), which allows the identification of the voltage corresponding to a specific stress value. σ_0=1 N/m^2. Reprinted with permission from [27].

4.5.6 Manipulation of water droplets by irregular electric field pulses

Figure 4.6 demonstrates the size control of individual water droplets via the applied electric field for the 50/50 flow rate ratio. By applying electric field pulses of specific duration, the size of successive droplets can be tuned in a desired manner. It thereby becomes possible to encode arbitrary sequences of large (*l*) and small (*s*) droplets. The examples shown in Fig. 4.6 demonstrate the sequences *lsls*, *lsslss*, and *lssslsss*, corresponding to the application of zero voltage for 20 ms, followed by a rectangular voltage pulse with an amplitude of 300 V and a duration of 15 ms, 30 ms, and 40 ms, respectively. Up to now, similar results appear to have been achieved only with drop-on-demand systems [122,123].

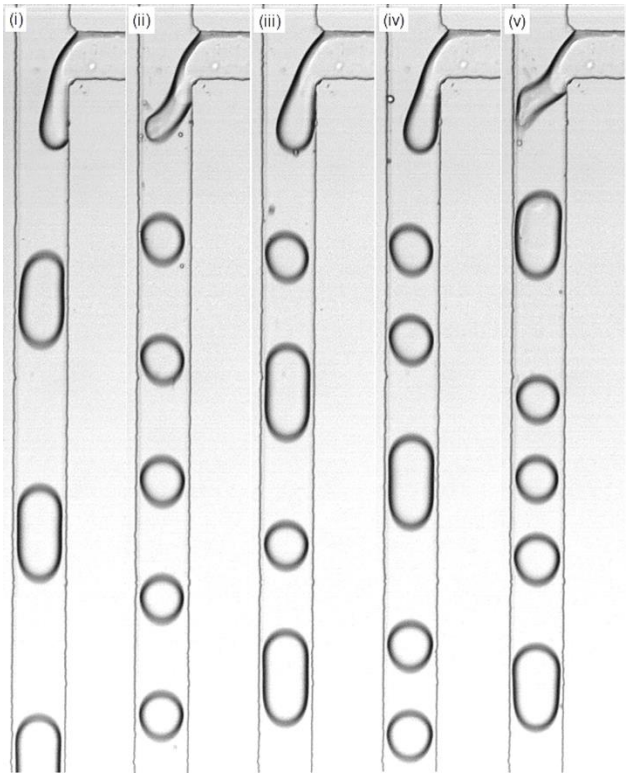

Fig. 4.6 High-speed images showing the size control of individual water droplets at a flow-rate ratio of 50/50: (i) 0 V, (ii) 300 V, (iii) 300 V pulse, duration 15 ms, (iv) 300 V pulse, duration 30 ms, and (v) 300 V pulse, duration 40 ms. For the time-periodic pulsed signals, the off-time between the pulses is always 20 ms. Reprinted with permission from [27].

4.6 Summary

The effect of DC electric field on the generation of droplets of water and xanthan gum solutions (dispersed phase liquids) in sunflower oil (continuous phase) at a microfluidic T-junction configuration is experimentally studied. Two flow rate ratios, φ, of 20/50 and 50/50 (dispersed to continuous)-flow rate in µl/h unit- and DC voltages in the range between 0 to 500 V are considered. The xanthan gum solutions show a shear-thinning behavior, with a zero-shear viscosity of about 460 mPa.s for the highest concentration employed. In each case, the average equivalent droplet diameter is determined based on high-speed video microscopy, using a sample of at least 30 droplets. The results can be summarized as follows:

In absence of electric field, for both flow rate ratios, droplets form in somewhere between squeezing and dripping regime and the size of droplets of xanthan gum solutions are larger than that of water, especially for the flow rate ratio, φ, of 20/50. Also, there is not much difference in size of droplets of the xanthan gum solutions when concentration increases.

The electric field leads to a significant reduction of the droplet diameter. A reduction by about a factor of 2 is achieved for water droplets. At sufficiently large electric field, the transition from almost squeezing to dripping regime occurs.

For water or for the case of comparative small ratios of the disperse and the continuous phase flow rate, the droplet size shows a rapid decrease at small electric fields, whereas it only shows a weak dependence on the electric field strength at larger fields. In the dynamic range considered, the electric stress has about the same effect on the droplet size as the hydrodynamic stress in the absence of electric fields. The electric field may be used to actively control the size of individual droplets, allowing to produce a stream of droplets with a tailor-made size sequence.

5 On-demand generation of droplets and their use in biological applications

5.1 Introduction

Droplet-based microfluidics has attracted many researchers from different research backgrounds since its applications spread over a wide spectrum of research disciplines such as engineering, chemistry, physics and biology. It is basically concerned production of droplets in small scales using either independently passive and active techniques or their combination. T-junction and flow-focusing are two most popular schemes used for droplet generation in the continuous mode [118]. A part from such passive droplet production schemes, often temperature [92], acoustic, magnetic [94] or electric fields [27,95,124] are used to control the droplet production. Droplets can either be produced in a continuous stream or on-demand.

When the task is to produce a droplet at a certain time at a specific location, or when samples that are only available in smallest amounts need to be processed, the on-demand production of droplets is favoured over the continuous process. In this case, the primary goal is not to perform a highthroughput screening operation, which means that the droplet production rate is only of secondary importance. Typical applications in that context require outcomes of sample preparation steps to be wrapped into droplets. One example is the processing of droplets containing the products of an electrophoretic separation step [125]. Another example is transferring the product of a fluorescence-activated cell sorting step into droplets [126].

Drop on-demand droplet generation, which implies to production of a single droplet within an immiscible phase, has been meagerly explored. The most widespread scheme for the on-demand production of droplets in microfluidic devices is based on pressure pulses. In that context, a number of systems have been presented that differ in the microchannel architecture and the method by which the pressure pulse is applied. That way, production of droplets with volumes ranging from femtoliters to nanoliters has been demonstrated. In this regards, to generate femtoliter droplets on demand in a microfluidic and optical system, Lorentz et al. [127] used a microinjector to withdraw the aqueous hemidroplet growing at the opening of a very narrow inlet channel connected to a chamber filled with continuous phase where the sudden pressure drop (i.e. pressure pulse) caused the formation of the droplets. In their earlier work [128], the same approach was utilized to form femtoliter-volume droplets by optically polystyrene beads encapsulated. Jung et al. [129] employed a pressure regulator to induce a pressure pulse on a water/oil interface at the junction of a 1×1 μm^2 (width×height) aqueous channel with a 200×18 μm^2 (width×height) oil channel. With a pressure pulse of 134.5 kPa at 10 ms (4.4 kPa higher than the backing pressure for filling the aqueous channel and positioning the interface at the vicinity of the junction) they produced femtoliter droplets on demand. Zhou and Yao [130] took advantage of a modified T-junction by a nozzle, serving as a capillary stop, for positioning water/oil interface at the junction. They applied pulsed pressures (generated by a solenoid valve) in the range of ~5 to 22 kPa with different pulse durations up to 100 ms to generate nanoliter volume single droplets. This method was later used by them for encapsulation of the preconcentrated sample into droplets to eliminate diffusion and dispersion of conventionally sample preconcentration taking place

in continuous flow [131]. To produce droplets on-demand through pneumatically actuation, Lin and Su [132] used a membrane valve sandwiched between the control and flow channel at a T-junction. The membrane valve could block the flow channel under a constant pressure and open for a certain short time via electromagnetic actuator, resulting in production of the droplet volumes from 458.8 to 0.55 pL corresponding to decreasing the valve open time from 2.8 to 0.05 s. The same approach was also utilized for generation of droplets on-demand in some other studies [122,123,133]. Xu and Attinger [134] introduced a droplet generator system based on actuation of a piezoelectric bimorph mounted on top of a disperse channel with a nozzle of different sizes at designed a T-junction channel. Water droplets in hexadecane were produced down to 40 picoliter in volume by varying the voltage pulse shape and geometry of the chip.

The on-demand production of droplets by electric fields is especially appealing because corresponding systems often do not require any moving parts. The electric actuation can be accomplished in different ways such as by electrowetting on dielectric (EWD) and electric field pulse etc. For instance, the principle of electrowetting on dieletric (EWOD) can be utilized for producing droplets on demand by employing the local contact angle variation of an aqueous liquid wetting an array of microelectrodes [135,136]. Cho et al. [135] built a digital microfluidic circuit working based on electrowetting principle, which was able to create, transport, cut and merge liquid droplets in contact with air. To do so, they evaporated the control electrodes of chromium and platinum on a glass substrate covered with Oxide and Teflon (a dielectric) layers and deposited IOT on another glass slide covered with Teflon. The aqueous liquid was then confined between these two glass parallel plates. Making use of 7 discrete control electrodes, a liquid droplet of 270 nL in volume was pinched off from a large reservoir droplet (2~3 L in volume) by activating the electrodes in sequence. Using the same technique, Srinivasan et al. [136] produced KCl droplets of ~ 20 nL in 1 cSt silicone oil from an on-chip reservoir at 50 V by tuning an array of electrodes. Gu et al. [137] combined EWOD with the hydrodynamic control of a flow-focusing device to produce droplets on demand through applying AC Pulse.

Droplet production from Taylor cones forms the foundation of the work reported in this chapter. When an electric field is applied to the interface of an aqueous liquid and a dielectric fluid, above a threshold field strength, the interfacial tension forces are no longer strong enough to balance the Maxwell stress, which results in the ejection of a jet of the aqueous phase decaying into droplets. Taking advantage of this technique, He et al. [138,139] used electric field pulses to generate femtoliter droplets on demand based on that principle. Recently, Chen et al. [140] produced subfemtoliter droplets on demand by combining flow focusing with droplet ejection from Taylor cones.

Apart from that, a few rather exotic principles have been applied to produce droplets on demand in microfluidic devices. Park et al. [141] applied a pulse laser of 100 μJ at various pulse durations to a phosphate-buffered saline buffer as a disperse phase, which injected droplets with volume in the range of picoliters into a channel filled with corn oil. Demirci [142] designed an acoustic-based 2-D micromachined microdroplet ejector array that enabled the generation of droplets in air in on-demand and continuous modes of operation (for example, 28 μm in diameter isopropanol droplet was ejected upward into the air at 1 kHz). Collins et al. [143] integrated an interdigital transducer producing surface acoustic waves in a T-junction microfluidic device and were able to eject water droplets of picoliter volumes into an olive oil medium within the time scale of several to hundreds milliseconds.

The miniaturization of biological assays has become a desired feature in many biological research areas [144]. Especially attractive in this context is the generation of droplets, which when produced in a high-throughput format allows the screening of very large parameter spaces, which represents inherent characteristics of biological

systems. Droplet-based systems have enabled a plethora of new applications ranging from medical diagnostics tests [145] to systems and synthetic biology [146]. Microfluidic-based, monodisperse droplet generators allow the formation of femto- to picoliter droplets [147,148], which can be used to compartmentalize in vitro reactions. This represents a cell-like biological quality and, as a consequence, has been used to study biomolecular binding reactions [149], enzyme reactions [150] and other real-time scenarios. Individual droplets containing single molecules have successfully been used in emulsion polymerase chain reactions [151] and have been tested in single cell sequencing experiments [152]. The reduction the reaction volume down to nanoliters not only reduces reagent costs, but also avoids amplification and recombination artifacts [153], in addition to simplifying the integration with other on chip"-devices. Droplet systems have also been used in directed in vitro evolution experiments [154] and have been applied analyze protein/protein [155] and protein/nucleic acid interactions. Because of the efficient mixing of reactants in the droplets, these reactions proceed in a precise and quantifiable fashion, which can be used to extract high quality time-resolved kinetic data [156]. Finally, water-in-oil droplets have recently been used as a promising tool to investigate cell/cell-communication in three-dimensional tissue-like materials [157].

In this chapter, the principle of drop on-demand production from Taylor cones is further explored. Through extensive parameter studies, it is demonstrated that this principle may not only be applied to liquids with viscosities close to that of water, but also to highly viscous solutions with a zero-shear-rate viscosity roughly 14 000-times higher than that of water. This is especially relevant for biological fluids, which invariably contain high concentrations of cosolutes including biopolymers such as proteins and nucleic acids. Further, the parameter space in which monodisperse droplets can be produced on-demand in terms of the electric pulse amplitude, pulse duration, and the salinity of the solution is explored. By deliberately choosing a specific parameter combination, droplets of a specific size can be produced. Finally, their use as biochemical reaction compartments is demonstrated.

5.2 Experimental set-up

Figure 5.1 depicts the schematic of the microfluidic device. As shown, a T-junction microchannel with a constriction at the junction which controls the position of liquid-liquid interface and a separate U-shaped microchannel in front of the junction comprise the microfluidic device. The water-filled U-channel, a part of which is directed parallel to the main channel of the T-junction, is served as an electrode through connction to one of the power supply port. The other port of the power supply is connected to the inlet of the disperse channel, served as another electrode. The disperse-phase liquid is introduced into the T-channel from one inlet where it partially displaces the continuous phase that is filled into the channel from the other inlet. The channels have a height of 20 µm, and the other dimensions are specified in Figure 5.1.

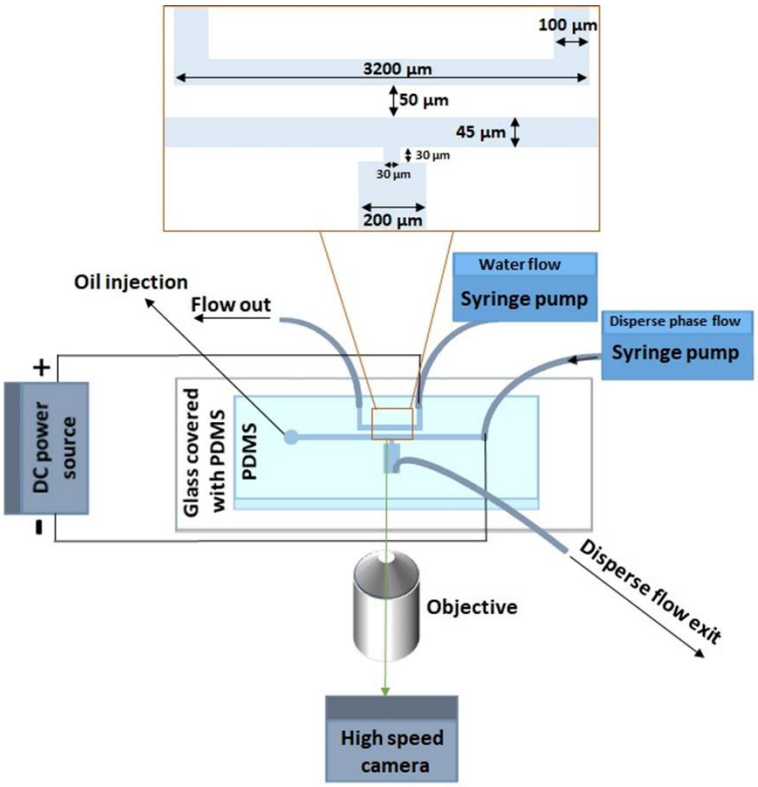

Fig 5.1 Schematic of the experimental setup. Reprinted with permission from [158].

To fabricate the microfluidic device, the soft lithography protocol is used. A SU-8 photoresist structure on a silicon wafer, purchased from Microchem, is used as a mold for the device. First, polydimethylsiloxane (PDMS), purchased from Dow Corning (Sylgard 184 Silicone Elastomer), is mixed with the cross-linker in two different ratios of 10:1 and 20:1. Then the 10:1 PDMS/cross-linker mixture is poured onto the master structure and cured at 75 °C for 40 min, which results in a thick layer of PDMS containing the microchannels. The 20:1 PDMS/cross-linker mixture is spin coated on a glass slide at 2000 rpm for 30 s and cured for 10 min at 75 °C to form a sticky thin layer of PDMS. After the holes are punched for inlets and outlets into the thick PDMS layer, it is gently brought in contact with the glass slide covered by the thin PDMS layer. The assembly is cured overnight at 75 °C, which results in a microfluidic chip with channel walls fully made of PDMS. This fully PDMS structure would render the microchannel hydrophobic whose resulting low wettability facilitate the generation of droplets.

Polytetrafluoroethylene (PTFE) tubing is used for connecting the microfluidic chip to 1 mL syringes (B. Braun Medical Inc.) filled with the disperse- and the continuous phase liquids. The tubing is connected to the PDMS inlets using metallic needles, which are connected to the power supply. A high voltage sequencer (LabSmith HVS448) is employed as the power supply to provide the desired voltage pulse. A high-speed camera (Redlake Motion Pro Series Y) is mounted on an inverted microscope (Nikon Eclipse Ti) to image the fluid dynamics inside the channels. After the microchannels have been filled with the continuous phase using capillary suction, the disperse phase is introduced using a syringe pump (KD Scientific Inc.).

To quantify the products of the biomolecular reactions, fluorescence microscopy is employed. For this purpose, a Nikon Ti Eclipse microscope with a Lumencor SPECTRAX light source is used.

5.3 Materials

5.3.1 Materials used for non-biological experiments

The working fluids in the experiments are water and aqueous polysaccharid solutions (xanthan gum solution) as the disperse phase and 1000 cSt Silicone oil AP (purchased from Sigma-Aldrich) as continuous phase. If not stated otherwise, all disperse-phase liquids contain 17 mM (0.1% wt/v) of NaCl salt. To prepare polymer solutions, the xanthan gum powder (from Xanthomonas campestris), purchased from Sigma-Aldrich, in different amounts are dissolved in water at 40 °C by aid of a magnetic stirrer for some hours, resulting in xanthan gum solutions with concentrations of 0.5, 1, 2 and 3 g/l. The rheological behaviours of xanthan gum solutions has been reported in the literature and can be fitted by a number of well-known models [113]. The dissolution of xanthan gum powder in water not only makes the viscosity shear-rate dependent but also significantly increases the viscosity of the solutions at zero shear rate [159]. For example, at zero-shear, the 3 g/l solution has a viscosity of about 13.9 Pa.s. The interfacial tensions between the aqueous phases and the oil phase are measured by a drop and bubble shape tensiometer (PAT-1, Sinterface Technologies, Germany). The measurements show that the interfacial tension does not significantly change upon addition up to 3 g/L of xanthan gum into water. The obtained value (~35 mN/m) is consistent with literature values [116]. The viscosities of water and the 1000 cSt Silicone oil AP are about 1 and 1000 mPa·s, respectively.

5.3.2 Materials used for biological experiments[1]

Plasmid-DNA (pBESTOR2-OR1-Pr-UTR1-deGFP-T500; Addgene #40019) for the cell-free transcription/translation (TX/TL) reactions inside the droplets is isolated by anion-exchange chromatography on silica NucleoBond Xtra columns (Macherey-Nagel). DNA concentrations are determined by UV-absorbance measurements at 260 nm. Cell-free TX/TL-reactions are performed using an E. coli-based TX-TL-competent protein extract (myTXTL, Arbor Bioscience). In vitro transcription experiments inside the droplets are conducted using PCRassembled DNA-fragments containing the sequence of the T7 promoter and the coding sequence of the iSpinach aptamer. All DNA-primer sequences are listed in Appendix Table A1. PCR fragments (50 nM) are purified (Monarch NA purification, NEB) and added to a transcription mix containing 2 mM of each NTP, 25 mM MgCl , 40 mM Tris-HCl pH 8.0, 5 mM DTT, 1 mM spermidine, 20 nM of DFHBI, and 70 µg/mL T7 RNA-polymerase. Reactions are incubated and microscopically monitored at 37 °C (TX-reactions) and at 29 °C (TX/TL reactions).

[1] This part has been performed by François X. Lehr and Prof. Ulrich Göringer in context of a collaborative research project managed by the CompuGene project.

5.4 Experimental procedures

Seeing as the oil wets the channel wall better than aqueous phase, if pumping the disperse-phase liquids is stopped, the aqueous liquids recedes toward the inlet accompanying with a significant distortion of interface shape, leading to failure in performing experiments. On the other hand, as repeatability and maintaining the identical initial experimental conditions are concerned, it is important to perform the experiments when the position and shape of the meniscus for all disperse phases are the same. Accordingly, during the droplet-formation experiments, the syringe pump providing the disperse-phase fluid was running. The corresponding backpressure together with constriction at the junction, which was acting similar an exit valve, enabled keeping the aqueous liquid/oil interface at a desired location where it becomes exposed to the electric field originating from the U-shaped channel. The equilibrium contact angle of all aqueous solutions without electric field were the same (at around θ_0~150), indicating the same meniscus curvature (or radius) for all disperse liquids and an evidence to setting the same initial conditions.

The high voltage sequencer device is used to create a voltage pulse of several hundred volts with a duration of some milliseconds. At the beginning of an experiment, the main channel is filled with silicone oil. Then, by switching on the disperse-phase pump, the oil in about half of the channel is displaced by aqueous solution, which results in a stationary liquid/liquid interface close to the junction. Subsequently, a voltage pulse is applied, and the jet formation and droplet pinch off are recorded by the high-speed camera at frame rates of 1000 fps or 4000 fps. The visible area of the generated droplets, A, is measured using the ImageJ software (National Institute of Health, USA), and the droplet diameter is calculated by the equation $D=(4A/\pi)^{1/2}$. For each case, the experiments are repeated several times to compute the average droplet diameter and its standard deviation.

5.5 Results and discussion

5.5.1 Electric field distribution

Before the experimental results on droplet production are analyzed, it is instructive to study the electric field distribution between the liquid/liquid meniscus and the U-shaped channel. For this purpose, the electrostatic potential is computed numerically using the commercial finite-element solver COMSOL Multiphysics. For simplicity, a two-dimensional model is set up, which treats the aqueous phases filling the U-shaped channel and partially filling the main channel as conductors. These are visible as white areas in Fig. 5.2. Consequently, the tangential component of the electric field vanishes at the surface of the white areas. The relative dielectric permitivities of the PDMS substrate and silicon oil are about 2.8 and 2.9, respectively. The inset of Fig. 5.2 shows a microscopy image of the liquid/liquid meniscus. The electric field distribution is obtained by solving the Laplace equation, that is, $\Delta\phi = 0$, with ϕ being the electric potential. The U-shaped channel is modeled as an isopotential surface with vanishing potential, and the electric potential at the surface of the water finger in the partially filled main channel is set to 400 V. At the other boundaries of the computational domain, a vanishing normal component of the electric field is imposed. An unstructured mesh of triangular elements with quadratic shape functions is employed. It is ensured that the results obtained are virtually grid independent.

The resulting electric field distribution is shown in Fig. 5.2. The color map indicates the magnitude of the electric field strength in V/m. The lines are the electric field lines, and the vectors indicate the electric field vectors at the surface of the conductors. It is clearly visible that the maximum electric field strength is found at the circular-arc shaped liquid meniscus close to the lower channel wall (adjacent to the U-shaped channel). This is the position where it is expected the liquid-liquid interface to break down, that is, to form a Taylor cone from which droplets emerge.

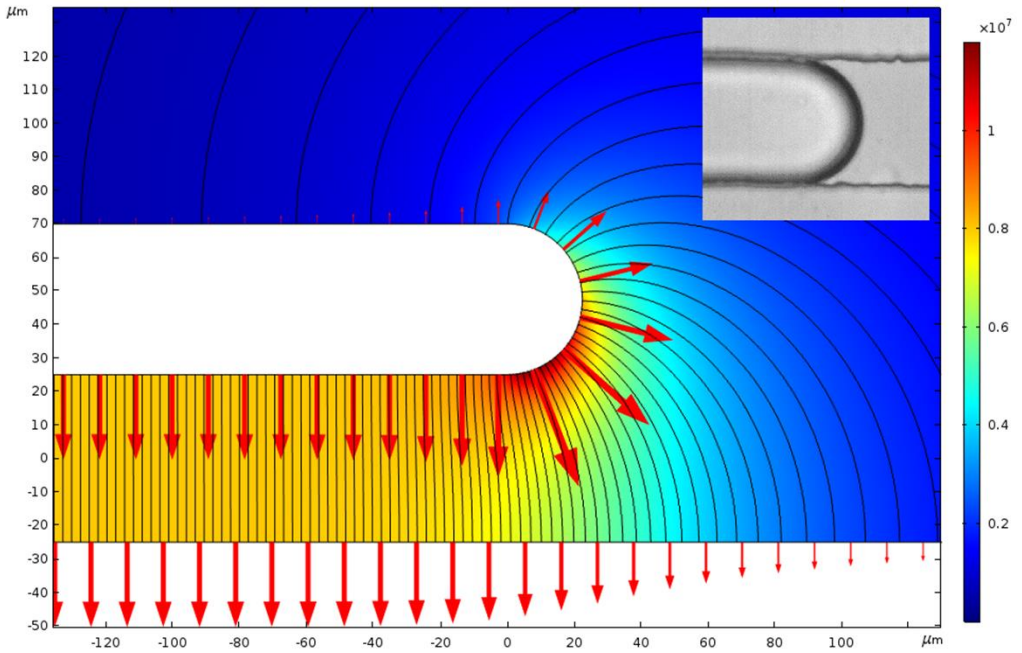

Fig. 5.2. Electric-field distribution around the water finger in the main channel. The color map indicates the electric field strength in V/m; the lines are electricfield lines. The inset shows a corresponding microscopy image of the water finger. Reprinted with permission from [158].

5.5.2 Dynamics of Droplet Formation

One of the major challenges related to droplet production in microchannels is the droplet size distribution. On the one hand, a uniform droplet size is desired. On the other hand, while the production of droplets with volumes in the pico- or nanoliter range is well established, producing femtoliter droplets still poses some challenges. The challenges are related to the fact that in most microfluidic droplet generators, the droplet size is larger than the scale of the geometric features of the microchannels, which translates to very small features in the case of femtoliter droplets. So far there are two major technologies allowing to generate droplets significantly smaller than the smallest geometric scale, flow-focusing, and electrospray technology.

In flow focusing, the diameter of the liquid jet from which droplets are produced is reduced by the sheath flow of a second immiscible fluid [160]. Electrospray technology relies on the formation of Taylor cones [44,161]. The effect of electric field on liquid interface was investigated in pioneering study of Zeleny [161]. It was later explained

by Taylor [44] who introduced the Taylor cone. A Taylor cone results from the deformation of the surface of a conducting liquid to which an external electric field is applied. Up to a critical value of the electric field strength, a static deformation of the liquid surface is observed, which results from the balance of Maxwell and capillary stresses. When the critical value of the field strength is exceeded, a jet emerges that decays into small droplets. The electrospray approach was reconsidered by the group of Daniel T. Chiu as a method to produce small droplets inside microfluidic channels [138]. Employing electric-field pulses, they demonstrated the on-demand generation of droplets significantly smaller than the channel dimensions.

Herein, a configuration inspired by their work to produce droplets by electric-field pulses has been used. Figure 5.3 shows time lapse images of the droplet production process taken at a frame rate of 4000 fps. Compared to Figure 5.1, the frames are rotated by 90°. Water is used as the liquid from which the droplets are produced, the second liquid is silicon oil. The pulse amplitude and duration are 400 V and 10 ms. When the voltage pulse starts, the liquid-liquid interface exhibits a Taylor-cone-like structure protruding quickly into the medium oil, forming a relatively short liquid jet. Once the pulse is terminated the liquid/liquid interface recedes to its initial position after some miliseconds, leaving behind a single droplet with a diameter of about 8 µm. The jet is much shorter than the one reported in the literature [138] at the instant when the droplet is produced. This is due to the special asymmetric structure of the electric field, shown in Figure 5.2. The electric field strength at the liquid/liquid interface is maximal in close vicinity of the channel wall. This is the position where the interface becomes unstable and the jet emerges. However, because of the proximity of the channel wall, the jet does not grow to a significant length before the droplet pinches off. This is presumably the reason why a much more uniform droplet size distribution than reported in [138] is obtained.

Apart from electric field effect on the droplet generation on-demand, the pressure difference in fluids can play a prominent role as reported by Chen et al. [140] and He et al. [138]. He et al. [138] furthermore pointed out that some other factors may come into play such as the displacement of the external silicone oil phase by the aqueous jet and wetting/dewetting interaction of wall with the working fluids, in addition to the backpressure, electric Maxwell and surface/interfacial tension force. It is again worthy note that the liquid-liquid interface is kept at the same position during all experiments to ensure the same initial conditions (besides the same meniscus shape) for all disperse-phase liquids. However, experiments show that there will be insignificant effect on the size of droplets if the interface moves fast forward, which could be due to the much faster process of the droplet production with respect to the interface motion. In addition, the electric fields should be the same for even moving interface case as the length of the U-shaped channel (U-shaped electrode) is long enough. The sequential images of droplet generation of xanthan gum solutions do not present any new insights compared to those of water and therefore, they are not displayed here to avoid repetitions.

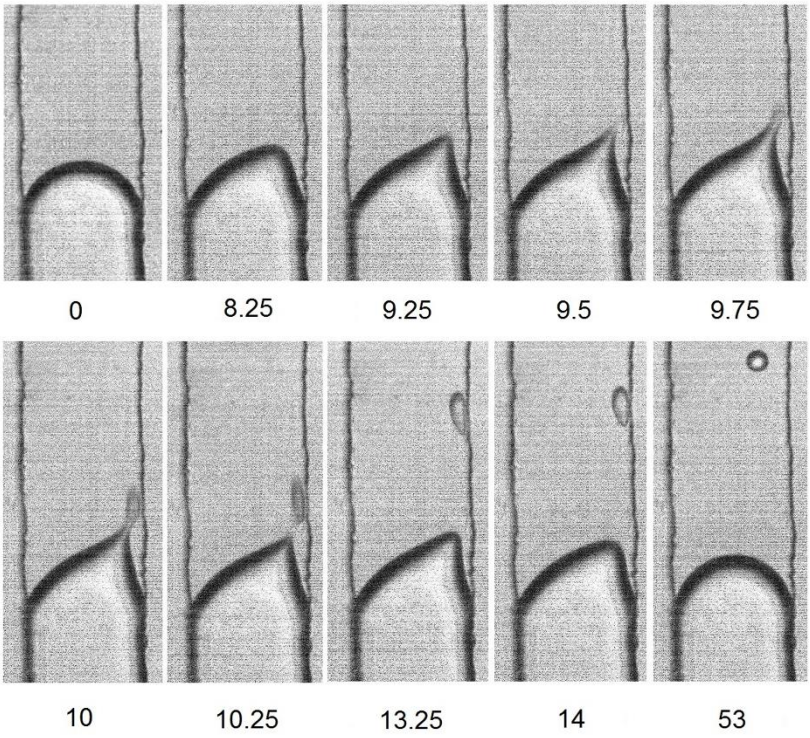

Fig 5.3 Time-lapse images of the on-demand production of a water droplet using a voltage of 400 V and pulse duration of 10 ms. The numbers below the individual frames denote the time in milliseconds. Reprinted with permission from [158].

5.5.3 Droplet Size Distribution

Since the uniformity of the droplet size distribution is a key feature of a microfluidic droplet generator, systematic studies with different liquids for the droplet phase is essential. Biological fluids often contain proteins, DNA, and other polymers, resulting in a significant increase of the viscosity. To study the influence of viscosity, experiments with aqueous solutions of xanthan gum are performed. Xanthan-gum solutions show a shear-thinning behavior, that is, the viscosity decreases as a function of the shear rate. Experiments with liquid/liquid systems in which one of the phases is a xanthan gum solution have the advantage that the dissolved polymer leaves the interfacial tension largely unaffected, such that the viscosity and the interfacial tension can be varied independently. The viscosity values given in Table 5.1 are the values at zero shear rate obtained from the literature [159], where, different from our experiments, desalinated water is used as a solvent. Since an indication of the order of magnitude of the aqueous-phase viscosity is intended, it is sufficient to refer to the literature results. The experiments with different aqueous phases are performed with a pulse amplitude of 400 V and a pulse duration of 10 ms. Table 5.1 displays the properties of the different aqueous-phase liquids and the corresponding average droplet diameters obtained, together with the standard deviations of the droplet diameter. The average is obtained from at least 25 independent measurements for water and at least 10 measurements for each xanthan-gum solution. Overall, the standard deviation of the droplet diameter is sufficiently small, that is, our method allows generating uniformly sized droplets. Increasing the viscosity of the aqueous phase slightly reduces the

average droplet diameter, where for viscosities above 6×10^2 mPa.s, hardly any change in the droplet diameter is observed. Remarkably, even for zero-shear rate viscosities 10^4-fold higher than that of water, still droplets with a size distribution comparable to that of water droplets are produced.

Table 5.1 Average droplet diameter and standard deviation of droplet diameter for aqueous-phase liquids containing different concentrations of xanthan gum. The viscosity values are the zero-shear literature values [159].

Xanthan gum concentration [g/l]	Zero shear rate viscosity [mPa·s]	Average droplet diameter [µm]	Standard deviation of droplet diameter [µm]
0	1.01	8.3	0.7
0.5	6.00×10^2	6.9	0.8
1	1.46×10^3	6.9	1
2	3.59×10^3	6.5	0.8
3	1.39×10^4	6.6	0.5

Notably that in electrostatic point of view, there is no difference between water and the other xanthan gum solutions when it comes to the critical voltage required to deform the interface. Because, firstly the interfacial tension between all the disperse phase liquids (i.e. water and xanthan gum solutions) and the silicone oil are more or less the same at about 35 mN/m. Secondly, the curvatures of the menisci of all xanthan gum solutions are almost the same as that of water before applying any electric fields. Therefore, it can be deduced that the voltage at which the liquid-liquid interface starts deformation should be identical for all disperse phase liquids. The experimental observations confirmed this hypothesis. It was observed that for all disperse liquids for a given voltage amplitude the same pulse duration (or vice versa) is required to start deformation onset of the interface, although the size of produced droplets of xanthan gum solutions are different from that of water due to their different dynamic behaviors.

For any microfluidic droplet generator, the question arises which parameters need to be varied to tailor the droplet size. One option would be to vary the height of the channel in which the droplets are produced. Some experiments were conducted with water in channels of half the height (10 µm) of the standard channels and found the average droplet size to be reduced by a factor of 2.4.

Comparing the present results on the droplet size distribution with the results reported in the literature [138], it does not observe a broad size distribution with a bimodal structure, but a largely monodisperse size distribution. Figure 5.4 shows the size distributions for water (blue filled bars) and for the xanthan gum solution at a concentration of 3 g/L (red open bars). Previously, the formation of satellite droplets was reported [138]. As already indicated, it is hypothesized that the proximity of the wall limits the extension of the liquid jet and has a positive effect on the droplet size distribution, whereas in previous studies [138] the jet grows to a significant length before it decays into droplets. However, obtaining a monodisperse size distribution requires working in the right domain of the parameter space spanned by pulse amplitude and pulse duration, as will be shown in the following chapter.

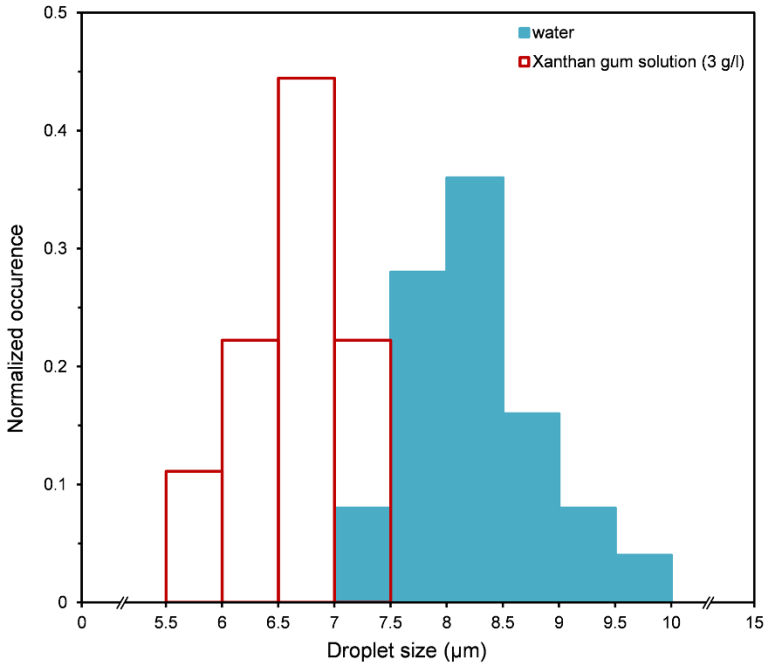

Fig 5.4 Droplet size distribution for water (blue filled bars) and 3g/L xanthan gum solution (red open bars). The data were normalized such that the integrals of the two histograms are the same. Reprinted with permission from [158].

5.5.4 Droplet Formation Regimes

The results reported so far are obtained in a domain of the parameter space in which single, virtually monodisperse droplets are produced. However, there are other domains in which different phenomena are observed. For applications of the method described in this chapter, it will be important to know how material and process parameters influence the results and in which domains one should work to obtain single droplets of uniform size.

For this purpose, parameter studies with water droplets containing different amounts of NaCl are performed. The pulse amplitude is kept fixed at 400 V, and the pulse duration is varied. The results are displayed in Figure 5.5(a), outlining the different dynamic regimes. While black filled circles indicate the absence of droplet formation, open circles show the formation of multiple ($\geq$2) droplets. Between these two regions lies an area where the on-demand production of single droplets is possible (colored circles). The different colors denote average droplet sizes. It can be seen that for the majority of NaCl concentrations, there is a pulse duration range that enables the formation of single droplets. Lower pulse durations result in no droplets, higher values in multiple droplets. At salt concentration $\geq$1 mol/L, the production of single droplets becomes impossible. Figure 5.5(b) captures the dynamic regimes in the case that the pulse amplitude and the pulse duration are varied. The higher the pulse amplitude, the narrower the regime in which single droplets are formed. However, there is a threshold below which droplet formation is no longer possible. This lies between 300 and 325 V. Of course, the voltage amplitudes are specific for the design and the dimensions of the system outlined in Figure 5.1. Rather than the voltage, it is the electric field strength that determines the physical response of the liquid-liquid interface. Figure 5.5(b) also indicates that

varying the pulse amplitude presents an option to tailor the droplet size. Achievable droplet diameters range from 3 µm (violet) to 9 µm (red). The significance of the yellow symbol at 450 V is limited, since at that voltage the range of pulse durations in which single droplets are produced is already very narrow. Discarding the yellow symbol, the trend is that as pulse amplitude increases, the droplet diameter increases.

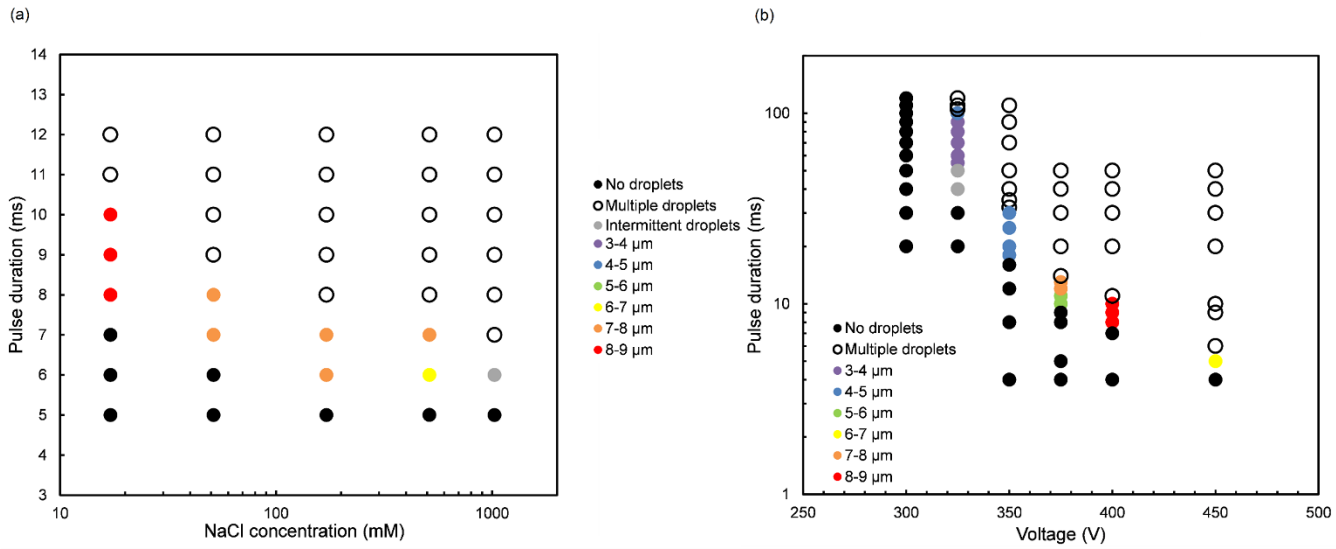

Fig. 5.5 Droplet formation regimes for water. (a) For varying pulse duration and NaCl concentration at a pulse amplitude of 400 V. (b) For varying pulse duration and amplitude with 17 mM NaCl. Black filled circles indicate cases where no droplets are produced, the open circles denote the formation of multiple droplets. Gray filled circles indicate situations in which only in a part of the experiments a droplet was formed. The different colors encode the droplet diameters. Reprinted with permission from [158].

Figure 5.6 shows the images of multiple droplets produced when the pulse duration is larger than the one required for producing a single droplet at a voltage of 400 V. It is vivid that when the pulse duration exceeds the limit for single droplet production (i.e. 10 ms for a voltage of 400 V), the multiple droplets (marked with red circles) produce such that the number of droplets expectedly increases with the pulse duration. For the voltage of 400 V with duration of 10 ms, a very tiny satellite droplet is rarely formed along with the main single droplet, defining the upper limit of the single droplet on-demand.

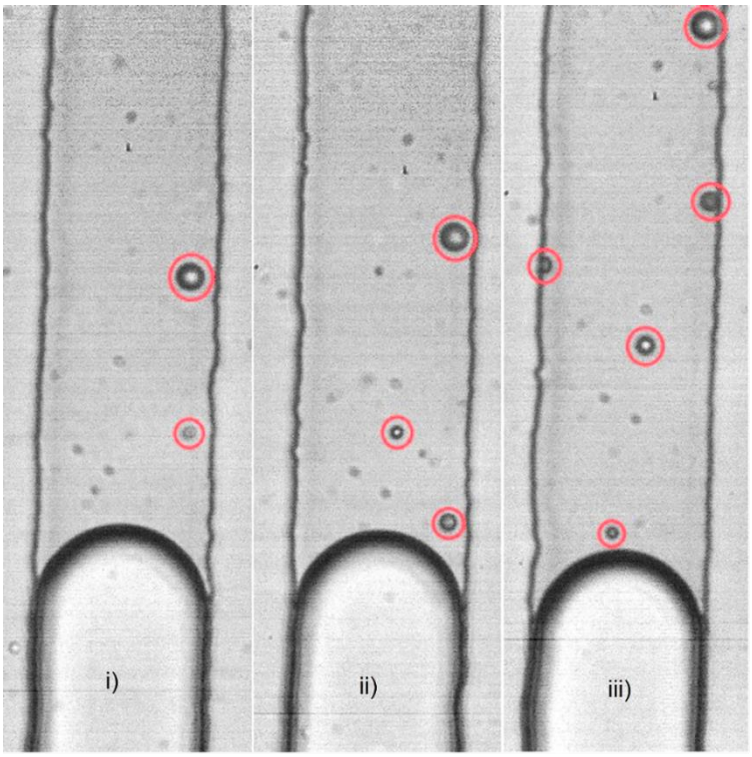

Fig. 5.6 Images of the droplets produced at 400 V for the case where the pulse durations are larger than required for single droplet production (at 10 ms here) for pulse duration being as i) 11 ms ii) 15 ms and iii) 100 ms.

5.5.5 Biological applications: Droplets as Biological Reaction Compartments[2]

5.5.5.1 Biological protocol and fluorescence Imaging and analysis

Cell-free TX/TL-reactions inside the droplets are started by adding the deGFP-gene containing plasmid (pBEST-OR2- OR1-Pr-UTR1-deGFP-T500) to a myTXTL master mix at a final concentration of 5 nM. The reagents are mixed and prewarmed to 29 °C before being injected into the microfluidic device. Microscopic imaging is conducted at a constant temperature of 29 °C. To quantify the reaction product inside the droplets, the autofluorescence of the synthesized deGFP (λex 485 nm, λem 520 nm) is measured using fluorescence microscopy. Measurements are performed in 15 min intervals over 2 h using an exposure time of 500 ms. For quantification of the same reaction in the bulk, clear-bottom 384-well plates containing cell-free myTXTL master mix (10 µL) and plasmid DNA (114 ng) are analyzed using a PHERAstar FSX microplate reader (BMG Biotech). Measurements are performed at 29 °C for 5 h to obtain a readout of the deGFP-fluorescence every 5 min.

[2] This part has been performed by François X. Lehr and Prof. Ulrich Göringer in context of a collaborative research project managed by the CompuGene project.

5.5.5.2 Biological results

Having demonstrated that the method described above allows the generation of single femtoliter-size droplets in a reproducible manner, it suggests itself to use the droplets as reaction compartments. An important potential application in the field of synthetic biology is seen. Synthetic biology utilizes artificial genetic circuits, that is, transcription-translation systems are key components in that context. An important challenge is to bridge the gap between in vivo implementations of artificial generic circuits (for example based on yeast cells) and their in vitro counterparts. Therefore, it is important to formulate in vitro implementations that mimic the implementations in biological cells. In that context, our drop-on demand generator brings along at least two key advantages. First, it allows creating biological reaction compartments with a size comparable to that of yeast cells, one of the most frequently used cell types in synthetic biology. The comparable size translates to a comparable number of biologically relevant molecules. That way, it becomes possible to mimic the stochastic behavior of biological cells. Second, it allows to mimic the crowding characteristic for biological cells. The interior of biological cells is densely packed with different molecular species, effectively providing a highly viscous environment. As apparent from Table 5.1, it is demonstrated the creation of droplets with a viscosity more than 10^4-fold higher than that of water.

To begin with, two of the most fundamental biochemical reactions inside the droplets are performed: gene transcription and mRNA-translation. For that an Escherichia colibased cell-free transcription-translation (TX-TL) system [162] is used in which a plasmid encoding a gene variant of the enhanced green fluorescent protein (deGFP) is first transcribed into mRNA and subsequently translated into protein. deGFP represents a start codon-optimized version of the enhanced (e)GFP, and its synthesis and bioactive folding can be monitored by the autofluorescence of the protein [163]. The synthesis of deGFP is analyzed in a time-dependent manner, and the product of the reaction when performed at standard (“bulk”)-conditions in a microliter volume (10 µL) is quantified in Fig. 5.7(a): eGFPfluorescence starts at roughly 30 min.

The protein concentration is a linear function of time up to 1 h and reaches a plateau roughly at 3 h. The TX-TL reaction mix is enclosed in aqueous droplets after 60 min of “bulk” reaction (arrow in Fig. 5.7(a)) using the method described in the previous sections. Droplets with diameters between 3 and 8 µm are tested, corresponding to droplet volumes between 20 fL and 300 fL. As an example, Fig. 5.7(b) shows micrographs of the fluorescence signal of a 5.1 µm diameter droplet at three different points in time. A representative fluorescence signal of deGFP averaged over 23 droplets is shown in Fig. 5.7(c). The individual fluorescent traces of all droplets from which the average fluorescence curve (figure 5.7) was obtained are presented in Appendix Fig. A1. While the negative control containing no DNA template shows no traceable signal over the entire time interval, the fluorescence signal in the droplets increases over 2 h. A fast increase within the first 15 min is followed by a slower increase thereafter. As expected and previously demonstrated [164,165], the data show a high statistical variance, likely due to the stochastic repartition of plasmid DNA and TX-TL-extract components [166] in the small reaction volumes. In that sense, the droplets perfectly mimic the stochastic behavior of single cells [167].

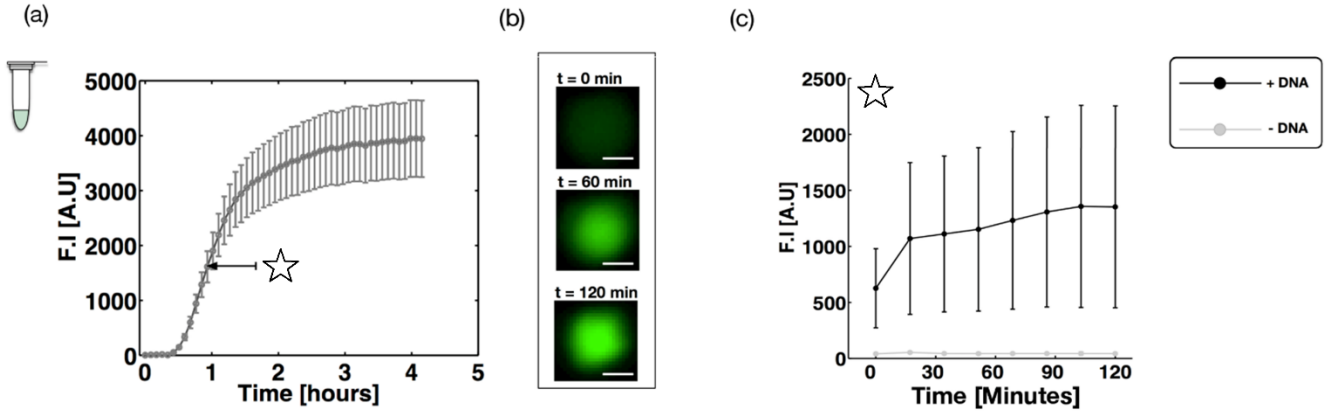

Fig. 5.7 On-demand droplets as biological reaction compartments.(a) Signal from the bulk TX-TL reaction generating autofluorescentdeGFP-protein. (b) Microscopic images of a single droplet containingthe cell-free TX-TL reaction mix at 0, 60, and 120 min of incubation.Scale bar: 2.5µm. (c) Plot of the time-dependent accumulation ofdeGFP. Data points in black represent the average obtained fromn=23 droplets. Gray curve: control experiment in the absence of plasmidDNA (*n*= 3). Error bars are standard deviations from the mean. Reprinted with permission from [158].

As an additional biologically relevant experiment, it is tested whether low-molecular mass ligands can diffuse across the oil-water interface to bind to a cognate receptor molecule and execute a biochemical switch. For this an in vitro transcription reaction within the droplets to synthesize the “light-up” RNA aptamer iSpinach [168] is set up. iSpinach is a synthetic, intricately folded small RNA-molecule that can bind to low molecular mass compounds such as 3,5-difluoro-4-hydrox-ybenzylidene imidazolinone (DFHBI). RNA-binding triggers DFHBI to fluoresce. The fluorophore is solubilized in the oil phase inside the microfluidic device. About 2-3 min after droplet formation, the droplets start to fluoresce, reaching a stable plateau after 30 min. Representative fluorescence micrographs of a 5.9 µm diameter droplet at different time points are shown in Fig. 5.8(a). Figure 5.8(b) displays the averaged fluorescence intensity as a function of time from a sample of nine droplets. As before, the strong electric field required for droplet formation does not adversely affect the bioactive structure of the biomolecules, in that case the polyanionic RNA molecules. Similar to the case of the TX-TL system, this reinforces the compatibility of the droplets produced using the method described above with biomolecular reactions.

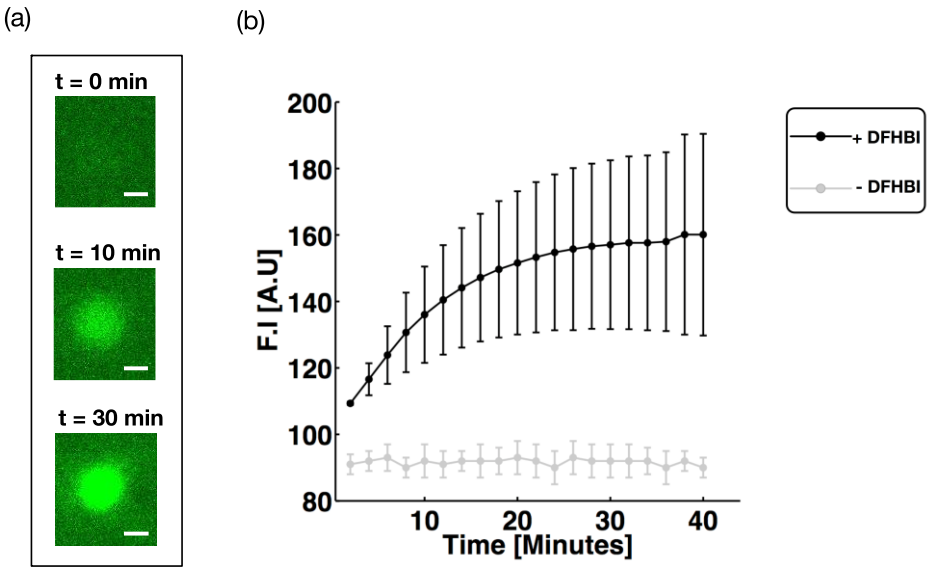

Fig 5.8 Droplet uptake experiment. In vitro transcription of iSpinach RNA-aptamers inside aqueous droplets. Diffusion of the fluorogenic DFHBI-ligand from the surrounding oil-phase into th edroplet results in the formation of iSpinach RNA-aptamer/DFHBI complexes, which can be detected by their green fluorescence (λ_{em}473 nm). (a) Time-lapse microscopic images (0, 10, 30 min) of a 108fL droplet expressing the iSpinach RNA-aptamer. Scale bar: 3µm. (b)Plot of the time-dependent formation of green fluorescent iSpinach RNA-aptamer/DFHBI complexes. Data points in black represent the average from *n*=9 droplets. Gray curve: control experiment in the absence of DFHBI (*n*=3). Error bars are standard deviations from the mean. Reprinted with permission from [158].

5.6 Summary

The effects of electrical and fluidic properties on the production of cell-sized droplets on-demand are experimentally investigated in this chapter. A principle that allows the on-demand formation of aqueous femtoliter-volume droplets in an oil phase is demonstrated. The xanthan gum solutions at different concentrations (from 0.5 to 3 g/l) with a zero-shear viscosity up to several orders of magnitude higher than that of water are examined. They prove the employed method based on electric field pulses deforming the aqueous-oil interface yields similar results as in the case of water. Production of droplets on-demand is performed by applying electric field pulses acting on the liquid-liquid interfaces. With carefully tuning the voltage magnitude and the pulse duration, production of droplets on-demand is achieved. In a space spanned by the salt concentration in the aqueous phase and the amplitude of the voltage pulse, the single droplet regime is delimited by regimes in which no droplets or multiple droplets are produced. The same is true in the space spanned by the pulse duration and the pulse amplitude. Varying the pulse amplitude allows tuning the droplet size.

To demonstrate the applicability of the electric-field-driven droplet generator, it is showed that the droplets can be used as versatile biological reaction compartments. First, it is demonstrated that droplets containing a cell-free transcription-translation system execute gene transcription and protein biosynthesis in a timely and programmable fashion. Second, it is verified that biomolecules inside the aqueous droplets such as small RNAs can be diffusionally activated from the outside to induce a ligand-

driven biochemical switch. As such, the droplets mimic defined cell-like characteristics, making the on-demand droplet generator a promising tool for a variety of (bio)molecular studies including high-throughput screening experiments.

6 Electrical manipulation of droplets generated on-demand: Coalescence, non-coalescence and partial coalescence

6.1 Introduction

In fluidic multiphase systems where immiscible fluids are in contact, electrically induced motion of a conducting phase through a non-conducting medium can produce intriguing phenomena spanning from liquid transport and patterning features [169] to droplet manipulations [170]. In a wide spectrum of applications, in particular for microfluidic applications, such as ink-jet printing [171], electrospray ionization [172], electrowetting [173] and microfluidic-based droplet manipulation [27], electric field evinces the realm of control and manipulation. Since long time ago, the electric field has been used as a driving force to bring a droplet in contact with a second droplet or an aqueous interface instigating coalescence, non-coalescence or partial coalescence. A briefly introduction is given in the following.

6.1.1 Coalescence and non-coalescence

A pair of uncharged aqueous droplets when subjected to an electric field, each droplet polarizes (and creates a dipole) and coalesces with the neighboring droplet by a dipolar interaction [174], which the process takes drop approach, film drainage, and film rupture and eventually coalescence steps [175]. Nevertheless, the repulsive interaction and thereby moving droplets away from each other has been observed in some cases where the line joining of the center of a pair of uncharged drops made a certain angles with respect to the electric field direction [176]. The failure in electro-coalescence was reported in application of alternating current (AC) field on a pair of uncharged drops inside a microchannel [177].

Initiating the electro-coalescence of droplets is a drastic technique used in microfluidics for mixing and merging encapsulated chemical and/or biological entities [178,179]. The charged droplets can be generated, particularly in microfluidic devices, by inserting electrodes either directly in contact with the fluid streams [178] or inside individual separated droplets [180]. The charged droplets inherently tend to coalescence due to attraction of oppositely charged droplets. However, violation from this natural tendency has been reported in the seminal study of Ristenpart et al. [59] who showed that the oppositely charged droplets show bouncing rather than coalescence.

Here, it is demonstrated the manipulation of femtoliter droplets using electric fields. The creation or manipulation of droplets using electric fields is proven to be a versatile scheme, for example, in electrospray technology [181] or in electrowetting-based devices [182]. The present version of droplet manipulation based on DC fields utilizes the reciprocating motion of droplets between two electrodes [60,62,63,183–185]. In this scheme, a droplet, electrostatically attracted by an electrode, comes into contact with the electrode surface, upon which it reverses its charge and direction of motion. A natural extension is to replace the solid electrode by an aqueous medium. The key experiment in this context was conducted by Ristenpart et al. [59]. They pipetted an aqueous microliter

droplet into an insulating liquid between a metallic pin electrode and an interface to an aqueous medium. Two different regimes are observed, depending on the parameters of the experiments (e.g., the electric field strength): either the droplet merges with the aqueous medium, or it bounces back, similar to that found on a solid electrode. Here, the scheme of droplets reciprocating between two electrodes to femtoliter droplets is extended, where both electrodes are liquid media. Unlike other methods for manipulating small-scale droplets, the present method does not require channels of a diameter similar to that of the droplet size. It is proving the controlled and selective addition and extraction of even smaller liquid volumes. Based on this, the handling of droplets with diameters as small as 2 μm becomes possible. Corresponding droplets with volumes in the femtoliter range may serve as tiny semibatch reactors, which is important in the context of synthetic cells. Alternatively, the method can be used to transfer tiny amounts of liquid in a controlled way, which represents an unconventional mode of mass transfer between two compartments.

The inherent coalescing tendency of a charged droplet with another charged droplet or planar surface with opposite charge could be failed in some conditions. Bird et al. [186] reported that this electro-coalescence tendency of oppositely charge droplets fails at sufficiently large electric field strength even though the two droplets are in direct contact. According to their results, the recoiling occurring between two micro-liter droplets was found to be a strong function of the electric field strength and cone angle between the two drops. In their further study [59], they showed that a droplet in a large scale (of micro-liter volume), pipetted into an insulating medium between a metallic pin electrode and a aqueous planar surface (aqueous electrode), exhibits either coalescence or bouncing (non-coalescence) behaviors onto the aqueous planar surface depending on the governing parameters. Their results demonstrated the charged droplet bounces from the planar surface at stronger electric fields and higher electrical conductivities, resulting in a drop cyclic motion. Inspired from that study, the cyclic motion of femto-liter droplets between two aqueous reservoirs inside microfluidic chips is implemented, wherein the droplets are produced from the reservoirs through applying appropriate voltage pulses. The dynamic behavior of droplets in terms of coalescence and non-coalescence (or bouncing) under different electrical and fluidic conditions are investigated. As the droplet in a cyclic motion between the two aqueous reservoirs requires apparent contact with them for switching net charge sign, it allows transport of nano-reagents embedded in reservoir(s) to/from droplets. Therefore, a part of the current study is focused on the transport and quantification of dye molecules, as a reminiscence of biological nano-reagents, to/from droplets that could mimic behavior of cells.

6.1.2 Partial coalescence

When a droplet/drop neither fully coalesces nor bounces from an interface or a droplet, there will be an intermediate phenomenon, called partial coalescence, at which a droplet partially coalesces with its partner. This could occur in both absence [187–190] and presence of an external force such as electric field [191–194]. This can be between two drops (drop-drop system) or a drop and an interface (drop-interface system). In absence of an external force, in the process, sometimes called cascade partial coalescence, the occurrence of partial coalescence is determined by a criterion that is Ohnesorge number (*Oh*), the ratio of the viscous to the inertial and surface tension forces. In such a case, large value of *Oh* displays full coalescence [192,195]. There are abundant studies concerning the partial coalescence without electric field, however, the partial coalescence in presence of electric field has been meagerly investigated in literature. Allan and Mason firstly reported the partial coalescence of a

drop at a flat liquid-liquid interface [192,196] in presence of electric field. They stated that the DC electric field intensifies the film perturbation between a drop and an interface, and the resulting daughter (or secondary) drop in the partial coalescence process is larger at a fixed *Oh*. At high *Oh*, the drops fully coalesced with the interface when there was no electric field, whereas the daughter drops emerged when a sufficiently strong electric field was applied. In a further study they showed that in the Stokes flow regime, a daughter droplet bears forming jet with fine droplets at its tip [192] if sufficiently large electric field is applied.

Mousavichoubeh et al. [193] experimentally investigated the coalescence of aqueous droplets onto a liquid-liquid interface to explore the conditions at which secondary droplets are observed. They found that the primary droplet size, the electric field strength and the height of droplet from the interface are significant factor affecting on the volume of secondary droplets. In their further study, it was found that the presence of ionic and non-ionic surfactants accompanied with the change in the interfacial tension increases the volume of secondary droplets [197]. Aside from the DC electric field, the pulsatile electric field can tremendously alter the coalescence behavior. Mousavi et al. [194] illustrated that the partial coalescence of drop-drop and drop-interface systems is suppressed by application of a pulsatile electric field where the type of waveforms can influence the effectiveness of the suppression. A frequency threshold was also found at which a transition from the partial coalescence to full coalescence observes. Yang et al. [198] reported critical electric field strength required for occurrence of partial coalescence of droplets on oil–water interface under DC electric field, which was dependent to various parameters like as droplet radius, conductivity, permittivity, viscosity, oil density and interfacial tension. They later investigated the effects of electric waveform, frequency and surfactants on the critical electric field strength [199,200]. More recently, Anand et al. [201] studied the electro-coalescence behavior of aqueous droplets at a water-oil interface. Their experimental results revealed that a critical electrocapillary number can determine the transition from full to partial coalescence, whereas the transition from partial to non-coalescence was further dependent on Ohnesorge number as well.

All the above-mentioned experimental studies concerned the partially coalescence of uncharged drop/droplets to a liquid-liquid interface. By contrast, coalescence of charged drops partially with a liquid-liquid interface has been rarely explored. The partial coalescence of oppositely charged drops was studied in the seminal study of Ristenpart et al. [59], followed by study of Hamlin et al. [202] extensively in detail. Hamlin et al. [202] reported that a critical ionic conductivity exists below which only a fraction of an oppositely charged drop coalesce with the interface. Surprisingly, the size and charge of the daughter droplets did not show any dependency to the ionic conductivity. Having provided explanation for the charge transfer mechanism, they stated that daughter droplet size is independent of the oil viscosity too.

To purify water from crude oils or water-in-oil emulsion in petroleum industry, using electric field to electrically coalesce water drops is a drastic technique, and therefore, generation of daughter (or secondary) drops in this context is basically undesirable [197,203]. By contrast, based on the current method, if generation of smaller droplets from mother droplets is concerned, the existence of daughter droplets after the partial coalescence process is beneficial, for example for generation of droplets in nanoscale. Here, the coalescing behavior of charged droplets in an oil channel moving back and forth between two aqueous reservoirs of different widths are explored in detail. The droplets impacting the small and large reservoirs can mimic the droplet-droplet and droplet-interface coalescence systems, respectively. The factors such as the salt concentration (i.e. ionic conductivity), the electric field strength and the initial droplet size are examined to see how large they affect the daughter droplet size. Since the droplets undergo reciprocating motions between the interfaces while simultaneously shrinking in

size, the number of cycles will be another factor, which is relatively hard to control. The employed system here allows the generation of submicron droplets whose sizes are challenging to measure.

6.2 Experimental set-up

Experiments are performed using the microfluidic device schematically shown in Fig. 6.1. The key part of the chip is a cross-junction configuration. The shallow main channel is placed between two side channels of larger depth, to form a pressure barrier that prevents liquid from the side channels from protruding into the main channel. The main channel contains the oil phase, and the side channels are filled with aqueous phase. The inlet sections of the side channels are connected to two ports of a power supply through needles, so that the aqueous phases filling the side channels serve as electrodes. The width of the two side channels is different, so that the electric field lines are concentrated at the side channel of smaller width. This asymmetry enables droplet production through electric-field pulses from the side channel of smaller width. The protocol to fabricate the microfluidics device is identical to the one given in the previous chapter and therefore it is not mentioned here to avoid repetition.

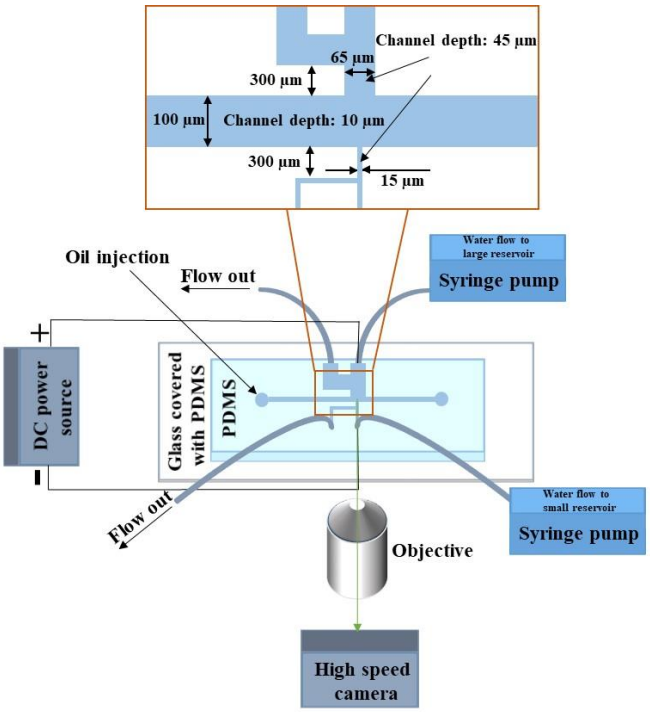

Fig. 6.1 Schematic of the microfluidic chip and its periphery. PDMS, polydimethylsiloxane. Reprinted with permission from [11].

6.3 Materials

The working fluids in the experiments of non-coalescence and partial coalescence are water as the aqueous phase at different salinities, through the addition of NaCl, and standard silicone oils with kinematic viscosities of 500,

1000, 2000, and 5500 mm^2/s. It should be noted that one centistokes (cSt) is equal to one milimeter^2/second (mm^2/s). Besides 1000 mm^2/s silicone oil AP is used, which is a modified version of standard silicone oils enhanced with phenyl groups. The silicone oil enriched with phenyl (i.e. silicone oil AP) has merits over the standard silicone oil, which will be discussed later. The silicone oils are purchased from Sigma Aldrich, Dow Corning, or HUDY.

6.4 Experimental procedures

During the experiments, the oil phase is filled into the main channel using capillary suction, i.e., the oil spontaneously fills the channel, since it wets the channel walls very well. By contrast, since PDMS is hydrophobic, aqueous liquids are introduced into the side channels via syringe pumps (KD Scientific Inc.). The pumps are kept running to build up a pressure head to fix the oil-aqueous interfaces at their desired positions. A high voltage sequencer (LabSmith HVS448) is employed as a power supply to provide pulsed and dc voltages. A high-speed camera (Redlake Motion Pro Series Y) is mounted on an inverted microscope (Nikon Eclipse Ti) to capture the behavior and motion of droplets. Fluorescence microscopy is utilized to visualize droplets containing rhodamine B. The same inverted microscope with a 50X objective (numerical aperture 0.8) is used to capture images of the fluorescent droplets in epifluorescence mode. An epifluorescence illuminator (Nikon Intensilight C-HGFI) is used for fluorescence excitation. An Andor iXion EM+ DU-897 EMCCD camera with 50-ms exposure time captures the emitted signals, and the NIS-elements software is employed for image acquisition.
To infer the dye concentration inside the droplets, a relationship between fluorescence intensity and concentration is needed. For this purpose, droplets are produced from a reservoir with a known dye concentration and their fluorescence intensity is measured. To determine the concentration inside the droplets studied in the mass-transfer experiments, a linear relationship between fluorescence intensity and concentration is assumed.

6.5 Results and discussion

6.5.1 Coalescence and non-coalescence

6.5.1.1 Time lapse images of droplet generation

Figure 6.2 displays time-lapse images showing the generation of a water droplet (containing 1M NaCl) using a voltage pulse. The droplet is generated in 1000 cSt silicone oil AP by application of a voltage pulse of 400 V with a duration of 10 ms. It can be seen that the oil/water interface starts deforming upon triggering the voltage pulse. At the end of pulse, the electrified liquid jet reaches its maximum length, and due to the Maxwell stress exceeding the capillary pressure at the tip, a droplet pinches off. This is followed by the retraction of the jet. The fact that the droplet is created from the small reservoir can be qualitatively explained by the converging electric field lines and the scaling of the Maxwell stress ($\sim E^2$). The droplet size can be tuned by varying the voltage pulse and amplitude, where the salt concentration and viscosity of the aqueous phase can play a significant role [2].

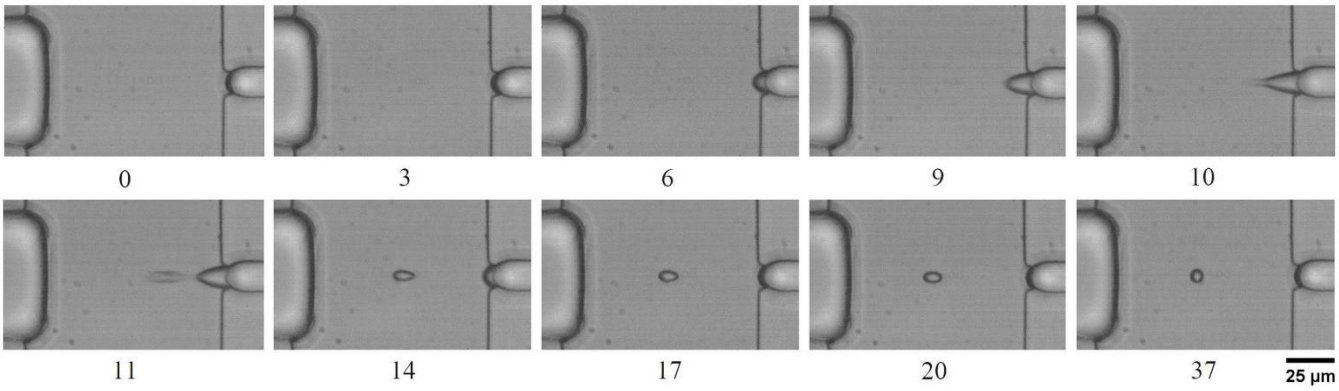

Fig. 6.2 Time-lapse images of the on-demand production of a water droplet using a voltage of 400 V and a pulse duration of 10 ms. The numbers below the individual frames denote the time in milliseconds. Reprinted with permission from [11].

6.5.1.2 Size distribution of the produced droplets

The size distribution of the droplets produced as described in the previous section is shown in Fig. 6.3. The distribution corresponds to the results obtained for 24 individual droplets produced in 1000 cSt silicone oil AP, applying a voltage amplitude of 400 V over 10 ms. If desired, the size distribution can be narrowed down by carefully tuning the electric and fluidic parameters. However, in the current study this is of secondary importance. Referring to Fig. 6.3, the average droplet diameter is ~ 8.7 µm with a standard deviation of 1.5 µm.

The type of silicone oil has an influence on the droplet size distribution and the reproducibility of droplet production. AP silicone oils have phenyl groups attached to the polymer chains. They have been reported to show a higher threshold with respect to dielectric breakdown as compared to standard silicone oils [204], probably because the generation and/or migration of charges is more efficiently suppressed. It is found that using AP silicone oils is important to render the droplet generation reproducible. In that case the droplet generation can always be achieved with the same parameters (in terms of voltage amplitude and pulse duration). However, when using standard silicone oils instead, memory effects are observed, i.e. the parameters needed to produce droplets are different for the first droplet compared to subsequent ones. Therefore, the droplets produced in standard silicone oils require some re-adjustment of the electric parameters. The corresponding droplets tend to be smaller than those produced in silicone oil AP, but because of the reproducibility issues mentioned above, their size distributions are not displayed.

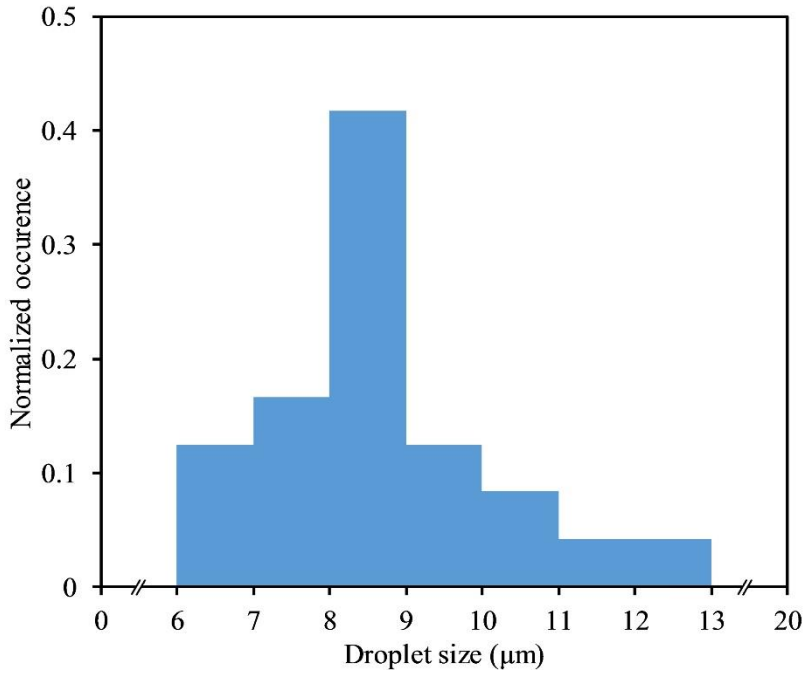

Fig. 6.3 Size distribution of water droplets in 1000 mm^2/s silicone oil AP, using a pulse amplitude of 400 V and a pulse duration of 10 ms. Reprinted with permission from [11].

6.5.1.3 Reciprocating droplet motion between two liquid-liquid interfaces

Figure 6.4 shows the key feature of the microfluidic design, i.e., the channel junction. Droplets performing the reciprocating motion between the two oil-aqueous interfaces are produced by applying a voltage pulse between the electrodes. The electro-hydrodynamic generation of droplets utilized here has been described before [2,138,139]. To unambiguously assign the liquid interface at which the droplets are generated, the side channels differ in widths. Via the concentration of electric-field lines, the liquid interface at the small reservoir experiences a higher electric-field strength than that at the other one, which guarantees that the droplets are produced from the small reservoir. In Fig. 6.4, a droplet produced that way (diameter approximately 8 µm) is visible at the center of the main channel.

In the following, the left-side channel in Fig. 6.4 will be denoted “large reservoir” whereas the right-side channel is the “small reservoir.” When a DC voltage is switched on between the electrodes, under suitable conditions, a reciprocating motion of droplets (in the following referred to as ping-pong mode) sets in between the liquid interfaces (see Video 1 within the Supplemental Material of Ref. [11]).

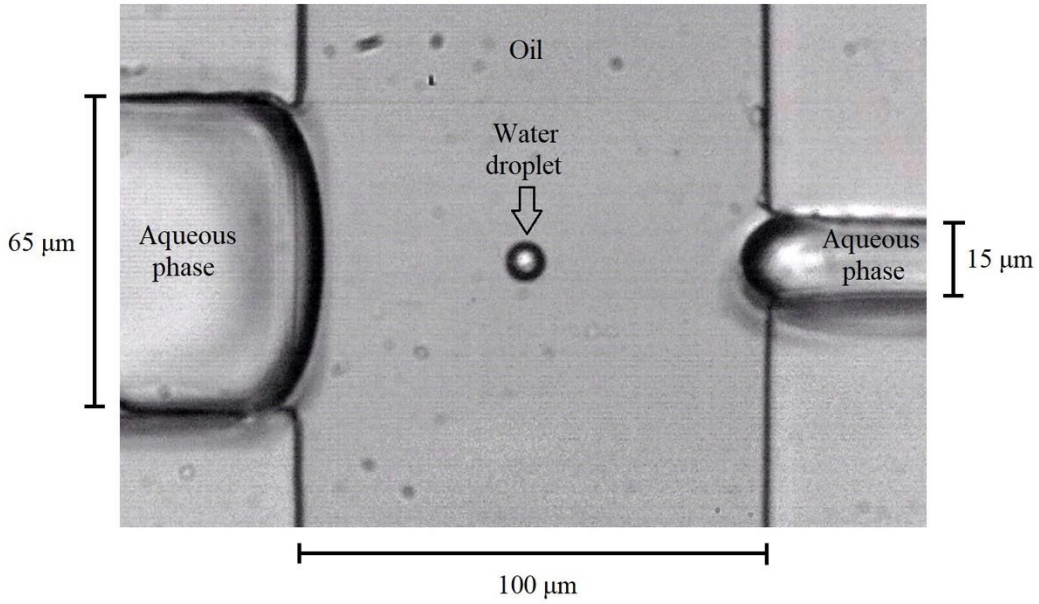

Fig. 6.4 Microchannel junction with two side branches filled with aqueous solutions. The main channel is filled with oil. The aqueous droplet is produced at the right oil-water interface by applying a short electric-field pulse. Reprinted with permission from [11].

On contact, a short-lived bridge forms between the droplet and the liquid-liquid interface through which the charge transfer takes place. The droplet having switched its charge sign reverses the direction of motion to the other reservoir with opposite charge and shows an invariantly reciprocating motion between two aqueous interfaces until the termination of the electric field. The video given in Supplemental Material of Ref. [11] shows that the reciprocating (cyclic) motion happens when a constant DC voltage above the critical value required for bouncing is applied. Since the droplet travels completely the distance between the two reservoirs, it indicates to the fact that the electrophoretic force, which is due to the interplay of droplet charge with electric field strength dominates the dielectrophoretic force and, furthermore, the charge leakage of the droplet moving in the oil medium is negligible. If there exists a severe charge leakage, the charged droplet upon contacting a reservoir (for example small reservoir) moves towards the other reservoir, but after traveling some distance without reaching the target reservoir becomes uncharged and reverses its direction of motion back to the initial reservoir, which will be due to the purely dielectrophoretic force. This type of cyclic motion has been already observed in experimental study of Mhatre and Thaokar [61] (so-called near-electrode cyclic motion) and Hase et al. [60]. The droplet presumably loses its charge within oil medium as the oil medium is not perfectly dielectric, and thereby the dielectrophoretic force becomes the driving force for the motion until droplet recharging. Nevertheless, this type of motion has not been observed in the experiments performed within this work.

Time-lapse images of such a droplet at the large reservoir are shown in Fig. 6.5(a), where the arrows denote the direction of motion. The droplet has a diameter of approximately 6 µm, a voltage of 300 V is applied, and the main channel is filled with 2000 mm^2/s silicone oil. When reaching the oil-aqueous interface, the droplet does not merge with the aqueous reservoir, but bounces back. The noncoalescence of oppositely charged microliter droplets was

studied by Ristenpart et al. [59]. They showed that a droplet bounced off from a liquid interface for sufficiently high values of the electric-field strength and oil viscosity. This behavior can be explained by considering the geometric shape of the liquid bridge forming between the droplet and the liquid interface. The liquid bridge is a result of two Taylor cones forming at the droplet surface and at the liquid interface. The two principal curvatures of the oil-aqueous interface have opposite signs at the neck of the bridge. With increasing electric field strength, the concave curvature reduces, such that the Laplace pressure inside the bridge increases, leading to a rapid breakup of the liquid bridge. Corresponding to these predictions, when the voltage is reduced to 200 V, the droplet merges with the large reservoir [cf. Fig. 6.5(b)]. After its initial discovery, the noncoalescence of droplets driven by electric fields has been studied in more detail. Among others, predictions for the critical cone angle separating the coalescence from the bouncing regime were made [186,205].

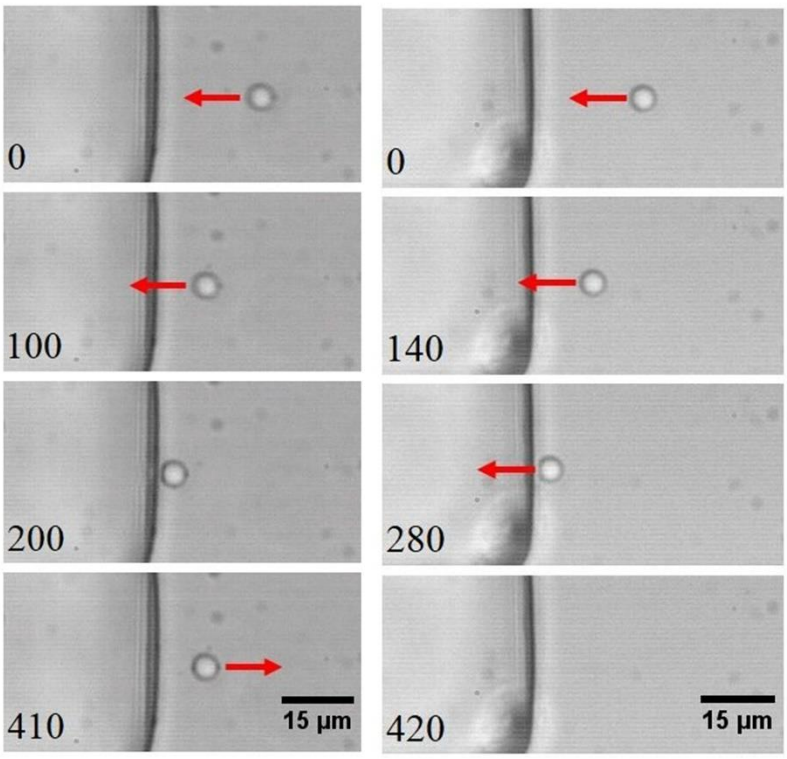

Fig 6.5 (a) Modes of droplet motion: when the voltage between the two oil-water interfaces exceeds a threshold value, a droplet only briefly touches the liquid interface, after which it reverses its direction of motion. The instantaneous direction of motion is indicated by the arrows. (b) Below the threshold voltage, a droplet coalesces with the aqueous reservoir. The numbers given in the individual frames denote the time in milliseconds. Reprinted with permission from [11].

As a rough estimation in the study of Ristenpart et al. [59], the pressure difference was obtained as a function of cone angle located at the fluid neck in the meniscus bridge, suggesting a certain transition angle of 45° above which the droplet bounces. Later, they showed a more exact solution theory based on a surface energy model

(volume-constrained area minimization), yielding a critical cone angle of 30.8 °[186]. Having performed a simulation including the effect of fluid inertia on the neck, Bartlett et al. [205] obtained a slightly different value of 25°, but consistent with their experimental transition value of 27±2° [186]. In our experiments, the droplets are orders of magnitude smaller than those studied in the original noncoalescence experiments [59], which means that the Taylor cones and liquid bridges have submicron dimensions. This makes it impossible to study the formation and dynamics of these structures based on available experimental methods. Nevertheless, experiments performed at 10000 frames/s, which is the limiting frame rate under the given illumination conditions, indicate that the liquid bridge exists only for a time span of less than 0.1 ms. For convenience, most of the experiments reported here are performed on droplets with diameters of about 9 μm for 1000 mm^2/s silicone oil AP and 6 μm for standard silicone oils. However, the same behavior with droplets as small as 2 μm has been observed.

The frequency of the reciprocating droplet motion can be tuned by varying the applied voltage and the oil viscosity. The influence of these two parameters is shown in Fig. 6.6, where the frequency, *f*, of droplet motion is displayed as a function of the oil viscosity, μ. The two lines represent fits of the form $f \propto \mu^{-1}$, which is the prediction of the Hadamard–Rybczynski equation [206], given below, in the limiting case that the viscosity of the continuous phase is much larger than that of the droplet viscosity.

The Hadamard–Rybczynski equation obtains the terminal velocity of a slowly moving fluidic object surrounded by another fluid. With viscosity of the continuous phase being much larger than that of the disperse phase viscosity, the (disperse phase) droplet velocity (and consequently respective frequency) is scaled as the inverse of viscosity of the surrounding (continuous phase) fluid. An assumption inherent in the model equation is that the droplet charge does not change with the oil viscosity. As it is apparent from Fig. 6.6, the experimental data are roughly consistent with the model equation. This indicates that, although the droplet motion is significantly slowed down at higher oil viscosities, the charge transferred from the reservoir to the droplet remains largely unaffected. It becomes apparent that the oil viscosity has a large influence on the droplet frequency. As the frequency motion of the droplet is directly proportional to the droplet velocity, one can expect the average droplet velocity in a cycle in the oil with the lowest viscosity be the largest. Another interesting expected point is that the velocity of a droplet at each half cycle (i.e. the distance between the two reservoirs) is different from its next half cycle. This is because of the fact that the electric field is non-uniform where its strength is maximal at the small reservoir and is minimal at the large reservoir. Consequently, the electrophoretic force, i.e. *qE*, acting on a droplet at the vicinity of the small reservoir should be higher than when it is close to the large reservoir, which results in a faster motion of the droplet when it moves from the small towards the large reservoir.

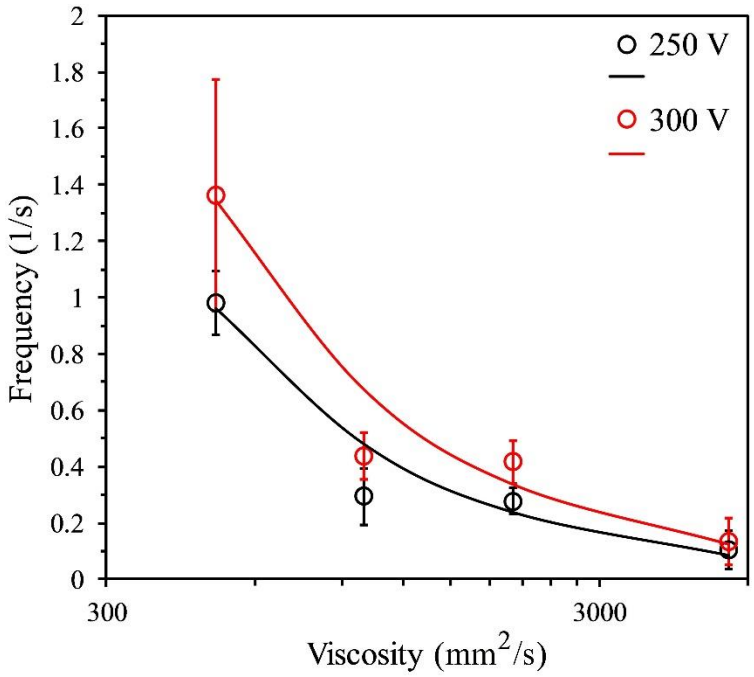

Fig. 6.6 Frequency of reciprocating motion as a function of oil viscosity for two different voltages. The symbols mark experimental data as the average of six measurements for each viscosity, with the errors bars representing the standard deviation. The curves are fits according to the prediction of the Hadamard–Rybczynski equation. Reprinted with permission from [11].

6.5.1.4 Regimes of droplet motion

As mentioned above, the ping-pong mode occurs only in a specific parameter range. For potential applications of the principle, it is reported here that it will be important to identify the different physical regimes of electrically driven droplets between two liquid interfaces. Three different regimes are identified: bouncing, coalescence and failure regimes. The bouncing regime is the regime in which a droplet bounces back and forth between the two aqueous reservoirs without merging in them, which results in a reciprocating (cyclic) motion. Accordingly, the droplet makes apparent contact with each reservoir without loss of size. Apart from the bouncing regime (corresponding to the ping-pong mode), there is a coalescence regime and a failure regime. The coalescence regime is the regime in which a droplet merges with the liquid filling the side channels. In the failure regime, the Maxwell stress acting on the liquid interface becomes so large that the aqueous phase permanently protrudes into the oil phase, i.e., the capillary-pressure barrier breaks down. In the experiments reported here, this occurs at the side channel with smaller width (more details will be given in the relevant section).

Through experimental observations, it is found that these regimes are a strong function of the electrical and fluidic parameters and therefore they define their territories according to these key parameters. Figures 6.7(a) and 6.7(b) provide maps of these three regimes, in terms of the applied voltage, the viscosity of the oil phase, and the salt concentration in the aqueous phase. The choice of these parameters is motivated by previous work [59,186,205], which gives clear indications that the electric-field strength and salt concentration are key parameters and

suggests that the properties of the continuous phase also have an influence. Each square symbol indicates a parameter combination for which experiments are performed. The black squares mark the non-coalescence regime. The colored areas approximately indicate the different regimes. In Fig. 6.7(a), the salt concentration is kept fixed at 1 M NaCl, while different silicone oils are used. In Fig. 6.7(b), 1000 mm2/s silicone oil AP is used, while the salt concentration is varied. Because of the excellent reproducibility of droplet production in silicone oil AP, this type of oil (only available with viscosities of 100 and 1000 mm2/s) is used whenever possible. Figures 6.7(a) and 6.7(b) clearly highlight the influence of the voltage. A voltage that is too low results in coalescence, whereas a voltage that is too high leads to failure. The existence of a lower boundary of the coalescence regime, in terms of voltage, is related to the fact that the electric-field strength determines the characteristic angle of the cones from which the liquid bridge is formed [59,186,205]. For field strength values that are too low, the convex curvature of the liquid bridge becomes too high, which prevents the breakup of the bridge driven by the Laplace pressure. With increasing viscosity of the oil phase, the voltage range where bouncing is observed becomes broader, extending to lower voltages. This is consistent with recent observations on the coalescence of oppositely charged drops in liquids with different viscosities [207], and thus, indicates that increasing the viscosity of the oil phase decreases the chance of coalescence. The coalescence occurs when the electric field strength is not enough large to pinch off the droplet from the meniscus after a brief contact. The upper limit of the voltage at which the coalescence happens stands at a voltage of 200 V up to the viscosity of 2000 cSt and beyond this viscosity value the coalescence seems to presumably take place at a lower voltage. However, at the largest viscosity, i.e. 5500 cSt, marked with open diamond symbol, the droplet neither merges nor bounces from the interface, it rather sticks to it.

Reducing the salt concentration shifts the voltage interval in which bouncing is observed to higher values or, in other words, can bring the system from the bouncing to the coalescence regime at fixed voltage. Similar effects of salt concentration are observed for much larger droplets [59]. Reducing the salt concentration also increases the voltage related to failure. The dependence of the interfacial tension on salt concentration offers a possible explanation in this context. It has been shown that, in combination with small amounts of ionic surfactants, NaCl significantly reduces the interfacial tension between silicone oil and water [208]. This can be explained by considering the Debye layer thickness around charged surfactant molecules. The addition of NaCl reduces the Debye layer thickness and, therefore, the repulsive force between neighboring surfactant molecules, thereby allowing more molecules to adsorb at the silicone oil-water interface. Small amounts of surface-active species often cannot be excluded from experiments. As a result, the addition of NaCl will reduce the capillary-pressure barrier and promote the protrusion of aqueous phase from the side channels into the main channel, when a voltage is applied.

The boundaries between the different regimes are partially characteristic for the specific setup used in the experiment. Naturally, it is not the voltage but the local electric-field strength at the liquid interfaces that governs the physics. Also, at which values of the local electric-field strength the transition from bouncing to failure will occur depends on a number of parameters, such as the pressure head used to introduce the aqueous phase into the side channels or the liquid-liquid contact angle at the channel walls. The intention behind Figs. 6.7(a) and 6.7(b), however, is to map different regimes in a qualitative manner and to highlight the limiting factors for the ping-pong mode.

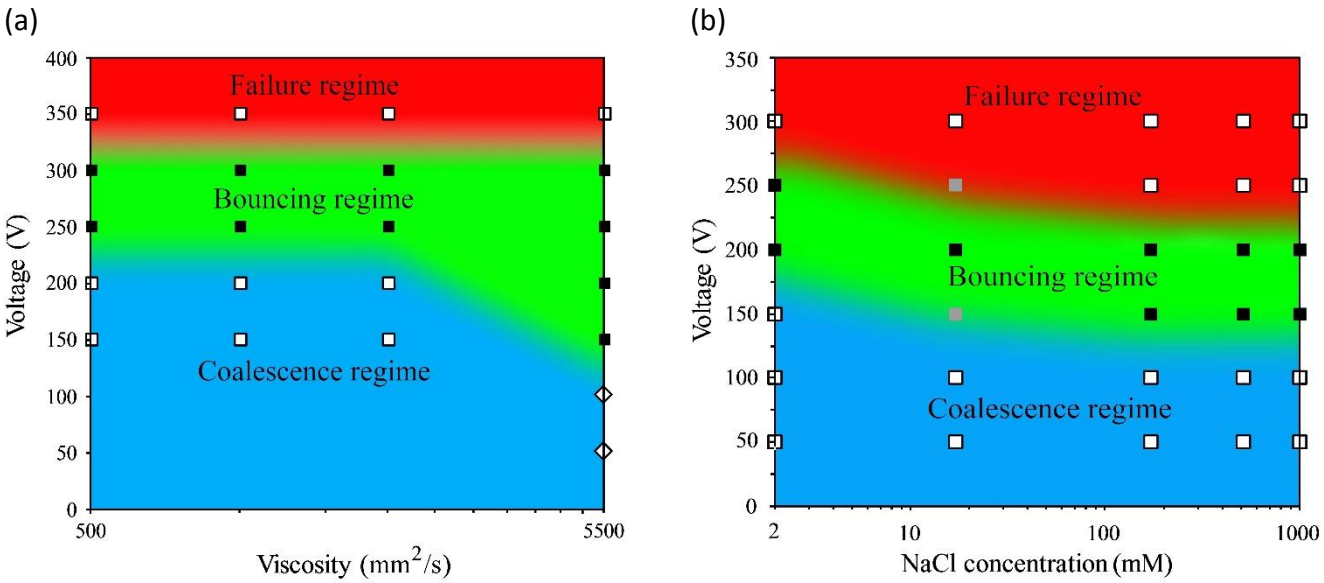

Fig. 6.7 (a) Dynamic regimes corresponding to the setup shown in Fig. 6.4 in a space spanned by viscosity and voltage. The filled symbols represent the bouncing regime, the underlying colors indicate the boundaries between the different regimes. The open square symbols are data points that belong either to the coalescence or to the failure regime. The diamond-shaped symbols represent a special situation where a droplet stays at the liquid interface after touching it, but does not merge with the aqueous reservoir. (b) The same as that in (a), but in a space spanned by NaCl concentration and voltage. The gray symbols represent data points that could not be unambiguously assigned to one of the regimes. Reprinted with permission from [11].

6.5.1.5 Time lapse images of failure

Figure 6.8 shows time-lapse of images of the electric-field induced failure of the capillary barrier at the small reservoir. The experiment is done with 1000 cSt silicone oil AP and water containing 1M NaCl, applying a voltage amplitude of 300 V. It can be seen that at the small reservoir the aqueous phase protrudes into the oil phase. Finally, a short circuit occurs at the large reservoir, resulting in the formation of a multitude of droplets.

The breakdown of the capillary barrier is a result of the Maxwell stress at the liquid interface exceeding the maximum Laplace pressure. To get a qualitative understanding of this process, for simplicity the backpressure that needs to be applied to keep the two reservoirs filled with water is neglected. In an order-of-magnitude sense, the maximum Laplace pressure that can be generated at the junction between the main channel and a side channel is given by $\Delta p_L=\gamma(w^{-1}+h^{-1})$, where w is the width of the side channel and h is the depth of the main channel. Since in the present case, h=10 µm, while w=65 µm and w=15 µm for the large and the small reservoir, respectively, the Laplace pressure is dominated by the depth of the main channel. As a result, there is no large difference between the maximum Laplace pressures at the interfaces between the main channel and the two side channels. In terms of the Maxwell stress, however, there is a large difference between the two interfaces. The aqueous NaCl solution can be viewed as a conductor, which means that both the interface between aqueous solution and oil and the interface between aqueous solution and the wall material are isopotential surfaces. As a result, the electric field lines converge between the large and the small reservoir, resulting in a higher electric field strength at the oil-

aqueous interface of the small reservoir. When converting the field strength to a stress, this disparity between the large and the small reservoir gets amplified, owing to the scaling of the Maxwell stress by E^2. Therefore, the failure is expected to occur at the small reservoir, which is confirmed by Figure 6.8.

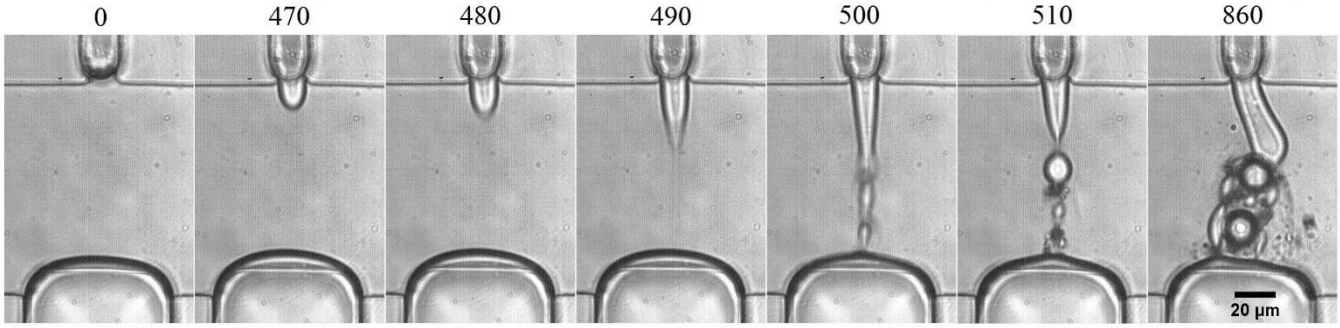

Fig. 6.8 Time-lapse images of the failure of the capillary barrier at the small reservoir. A constant voltage of 300 V is applied. The numbers above the individual frames denote the time in milliseconds. Reprinted with permission from [11].

6.5.1.6 Motion of multiple droplets

In this section, it is briefly reported the phenomena occurring when multiple droplets are located between the two reservoirs. This brief report has to be understood as an outlook to potential follow-up research rather than a detailed account of the physical phenomena. The corresponding experiments are performed with 5500 cSt silicone oil.

Multiple droplets can be produced from the small reservoir (see Fig. 6.9) by applying a voltage pulse with a duration longer than that adequate for single droplets. After applying a constant voltage of 300 V, the droplets immediately align in a chain and start bouncing back and forth in a complex pattern. In that case, charge transfer and avoided coalescence not only occurs between a droplet and a reservoir, but also between neighboring droplets. Motivated by the findings reported in the main text, it is hypothesized that also a chain of multiple droplets will mediate mass transfer between the two reservoirs.

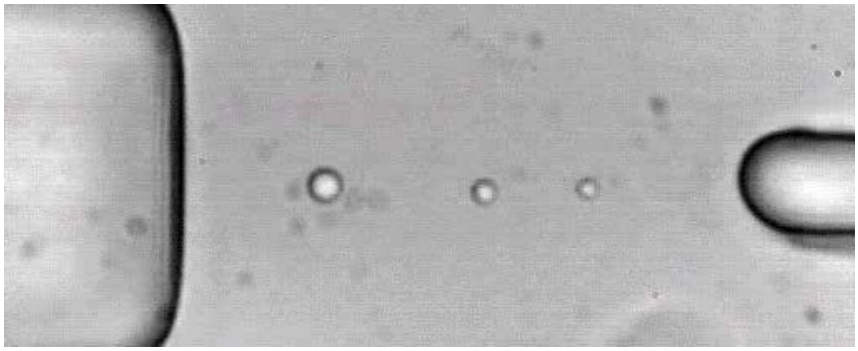

Fig 6.9 Alignment of multiple droplets in chain inside 5500 cSt silicone oil upon applying a voltage of 300 V.

6.5.1.7 Applications of droplet motion

One main objective of the work reported here is to study mass transfer from the aqueous phase filling the side channels to a droplet reciprocating between the two liquid interfaces. In an application context, mass transfer could enable (bio)chemical reactions in a tiny reaction space in semibatch mode, with educts being supplied to a droplet and products extracted from it. Alternatively, the setup shown in Fig. 6.4 could be used to transfer tiny amounts of liquid between two reservoirs.

6.5.1.7.1 Mass transfer to droplets

Both the transfer of dissolved molecular species and nanoparticles are presented in the following. Figure 6.10 shows three selected snapshots of experiments conducted with fluorescent polystyrene beads of 500 nm in diameter. The individual frames in Fig. 6.10 are obtained by superposing image sections recorded with a fluorescence microscope on bright-field images. Figure 6.10(a) shows the small reservoir filled with a nanoparticle suspension. A droplet containing nanoparticles is created by applying a voltage pulse. The droplet (diameter approximately 12 µm) is shown in Fig. 6.10(b) close to the liquid interface at the large reservoir. Remarkably, when such a droplet undergoes reciprocating motion between the two liquid interfaces, no nanoparticles are transferred between the droplet and the aqueous reservoirs. Apparently, the throat of the liquid bridge is too narrow and/or exists for a too short a time span to let 500 nm particles pass. To transfer nanoparticles from the small to the large reservoir, it is necessary to switch from the bouncing regime to the coalescence regime by reducing the voltage. Figures 6.10(b) and 6.10(c) show two subsequent images from the video recording, immediately before and after the coalescence event. The time increment between the images is 14 ms. Within this time span, the droplet merges with the aqueous reservoir. The nanoparticles are distributed over the liquid interface, as shown in Fig. 6.10(c).

When transferring a molecular dye dissolved in one of the aqueous reservoirs, a different scenario emerges. Experiments are performed with rhodamine B, which is a fluorescent dye that can be considered as uncharged [209,210]. The liquid inside the large reservoir contains the dye, while the liquid inside the small reservoir is water with 1 M NaCl. A droplet in ping-pong mode, initially containing no dye, starts to fluoresce after coming into contact with the large reservoir. The droplet picks up dye at the large reservoir and releases it at the small reservoir. The fluorescence increases during the first few cycles, after which time it takes a more or less constant value. This shows that mass transfer via femtoliter droplets in ping-pong mode is selective: dissolved molecules are transferred, while 500 nm particles are rejected. The dye concentration inside the droplet as a function of cycle number is shown in Fig. 6.11 for two different values of oil viscosity. The two different data sets in each panel represent the intensity inside the droplet after touching the interface at the large and small reservoir, respectively. The constant values reached after a few cycles represent a dynamic equilibrium state: the amount of dye taken up at the large reservoir equals the amount released at the small reservoir.

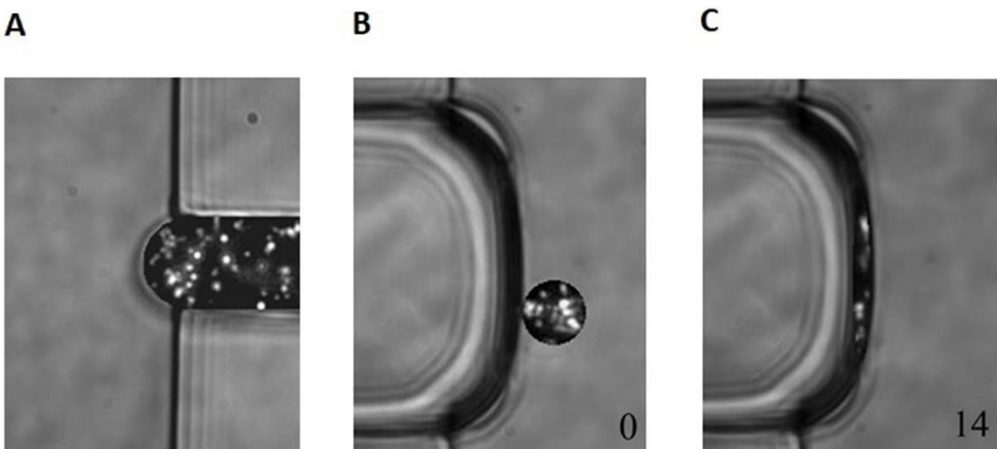

Fig. 6.10 Transfer of 500 nm particles between two aqueous reservoirs. (a) Small reservoir filled with a suspension of 500 nm particles. (b) Particle-laden droplet at the oil-aqueous interface of the large reservoir immediately before coalescence. (c) Oil-aqueous interface immediately after coalescence with the droplet. Nanoparticles are distributed over the interface. The numbers given in the individual frames in (b), (c) denote the relative time in milliseconds. Reprinted with permission from [11].

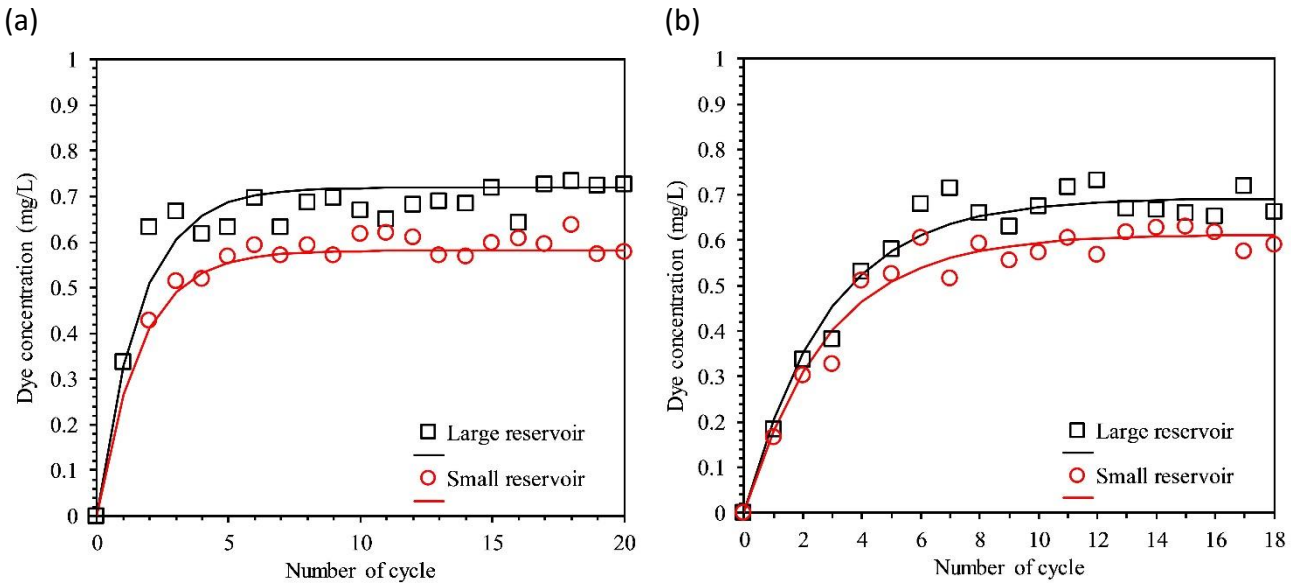

Fig. 6.11 Dye concentration inside a droplet as a function of cycle number, when transferring rhodamine B from the large to the small reservoir. (a) Data for 500 mm^2/s silicone oil filling the main channel. Dye concentrations after touching the large and small reservoirs are shown. The symbols represent experimental data; the curves are fits based on Eq. (6.1). (b) The same as that in (a), but with 1000 mm^2/s silicone oil filling the main channel. Reprinted with permission from [11].

6.5.1.7.2 Mass transfer model

The mass transfer model to be presented in the following paragraphs describes the mass transfer to/from the droplet when touching the two reservoirs, denoted large and small reservoir in the main text. The model is based on the assumption that the droplet volume does not change after each contact with a reservoir. The validity of this assumption was verified by examining the images obtained from video microscopy.

It is considered a droplet reciprocating between the large and the small reservoir, where the large reservoir contains some dissolved species, and the species concentration in the small reservoir vanishes. The droplet takes up dissolved species upon each contact with the large reservoir and subsequently delivers a fraction of it to the small reservoir. The species transfer occurs via the thin liquid bridge forming between the droplet and a reservoir. For charged species, there will be three mechanisms contributing to mass transfer. Diffusive mass transfer will occur via the difference in species concentration between the droplet and the reservoir. Upon contact between the droplet and the reservoir, the electric field results in re-charging of the droplet through which electromigrative (or electrophoretic transport of) species mass transfer. Other possible mode of transport is potentially advective. The latter is very difficult to study experimentally, since the liquid neck has submicron dimensions. In the present case, our goal is to study mass transfer in the simplest possible scenario. For this reason, an uncharged species for which electrophoretic transport does not play any role is considered. Furthermore, it is hypothesized that advective transport can be neglected. Therefore, the number of moles of the considered species transferred upon each contact between a droplet and a reservoir is given as

$$n_f = kA\Delta t\Delta c \tag{6.1}$$

where k is a mass transfer coefficient, A is the cross-sectional area of the liquid bridge, Δt is the time during which the liquid bridge exists, and Δc is the difference in species concentration between the droplet and the reservoir. For the large reservoir $\Delta c=c_l-c_{d,l}$, and for the small reservoir $\Delta c=c_{d,s}-c_s$, wherein $c_{d,l}$ and $c_{d,s}$ denote the species concentrations inside of the droplet when contacting to the large and small reservoir, respectively, and c_l and c_s are the concentrations inside the large and small reservoir, respectively. The large reservoir has a fixed concentration, that is c_l, whereas initially the concentration vanishes inside the small reservoir. Initially, the droplet (generated from the small reservoir) does not contain dissolved species. As stated in the main text, the quantity $\alpha=kA\Delta t/V_d$ will be considered as a fit parameter, wherein V_d represents the volume of the droplet. Note that $kA\Delta t$ has units of m^3, therefore α is a dimensionless parameter that has to be less than unity. It is allowed for different values at the large and the small reservoir, i.e. α_l, α_s. Based on that, the concentration inside the reciprocating droplet after touching the large reservoir (N+1) times is given by

$$c_{d,l}^{(N+1)} = c_{d,s}^{(N)} + \alpha_l \left(c_l - c_{d,s}^{(N)} \right) \tag{6.2}$$

where the superscript refers to the cycle number. Likewise, the concentration inside the droplet after touching the small reservoir (N+1) times is given by

$$c_{d,s}^{(N+1)} = c_{d,l}^{(N+1)} - \alpha_s \left(c_{d,l}^{(N+1)} - c_s \right) \tag{6.3}$$

Since initially c_s=0, and since the volume of the small reservoir is much larger than the droplet volume, it can be safely assumed that c_s stays very small during the whole process. Species that have been deposited close to the oil/aqueous interface of the small reservoir will spread over the reservoir by diffusion. Therefore, in the following it is assumed that c_s=0. Based on that, Eqs. (6.2) and (6.3) can be reformulated as recursion relations

$$c_{d,l}^{(N+1)} = \left(1 - \alpha_l - \alpha_s + \alpha_l \alpha_s\right) c_{d,l}^{(N)} + \alpha_l c_l \tag{6.4}$$

and

$$c_{d,s}^{(N+1)} = \left(1 - \alpha_l - \alpha_s + \alpha_l \alpha_s\right) c_{d,s}^{(N)} + \left(\alpha_l - \alpha_l \alpha_s\right) c_l . \tag{6.5}$$

These relations have explicit solutions of the forms

$$c_{d,l}^{(N)} = b_l \sum_{i=1}^{N} a_l^{i-1} \tag{6.6}$$

$$c_{d,s}^{(N)} = b_s \sum_{i=1}^{N} a_s^{i-1} \tag{6.7}$$

where

$$\begin{aligned} a = a_l = a_s &= 1 - \alpha_l - \alpha_s + \alpha_l \alpha_s \\ b_l &= \alpha_l c_l \\ b_s &= \left(\alpha_l - \alpha_l \alpha_s\right) c_l \end{aligned} \tag{6.8}$$

Closed-from expressions of the concentrations can be obtained by recognizing that the expressions of Eqs. (6.6) and (6.7) have the form of a geometric series:

$$c_{d,l}^{(N)} = \frac{\alpha_l \left[\left(1 - \alpha_l - \alpha_s + \alpha_l \alpha_s\right)^N - 1 \right]}{-\alpha_l - \alpha_s + \alpha_l \alpha_s} c_l \tag{6.9}$$

$$c_{d,s}^{(N)} = \frac{\left[\alpha_l - \alpha_l\alpha_s\right]\left[\left(1-\alpha_l-\alpha_s+\alpha_l\alpha_s\right)^N - 1\right]}{-\alpha_l-\alpha_s+\alpha_l\alpha_s} c_l \tag{6.10}$$

The asymptotic values of these expressions for $N \to \infty$ are given by

$$c_{d,l}^{(\infty)} = \frac{-b_l}{a-1} \tag{6.11}$$

$$c_{d,s}^{(\infty)} = \frac{-b_s}{a-1} \tag{6.12}$$

provided that $|a|<1$. Note that in this asymptotic limit, a droplet still takes up dissolved species at the large reservoir and releases species at the small reservoir. However, the concentration inside the droplet no longer changes, since the species amount taken up is equal to the amount released.

Equations (6.9) and (6.10) are used for modelling the experimental data obtained with Rhodamine B. For that purpose, a Gaussian least squares method is used to determine α_l and α_s. The solutions are computed using the Generalized Reduced Gradient (GRG) solver, a steepest descent method for solving nonlinear equations with constraints. It is ensured that the solutions are independent of the initial guess for the solution.

The curves shown in Figs. 6.11(a) and 6.11(b) represent the corresponding model fits. The resulting parameter values are = α_l 0.331 and α_s= 0.192 for Fig. 6.11(a) and α_l = 0.207 and α_s = 0.116 for Fig. 6.11(b). Increasing the oil viscosity, therefore, reduces the mass-transfer coefficients. It is hypothesized that an increase in viscosity reduces the cross-section area and/or the opening time of the liquid bridge between the droplet and the reservoir. Overall, the experimental data follow the trend predicted by the model, which suggests that the model captures the essential mass-transfer mechanism.

6.5.2 Partial coalescence

One prominent factor in studying coalescence of droplets in a liquid-liquid interface is the electrical conductivity (i.e. salt concentration) of the aqueous phase, based on which a demarcation can be drawn on the possibility of partial coalescence occurrence. Earlier, the effect of a salt concentration of 0.01w/v% NaCl (or ~2 mM) or less was investigated in details in which the coalescence and non-coalescence phenomena were observed. The question that may arise here is that what happens if the salt concentration (and its respective electrical conductivity) goes further below 0.01 w/v%? Performing experiments for such a case reveals that, interestingly, a noticeably different regime emerges: the droplet neither completely coalesces nor bounces back following contact with the liquid-liquid interface, it rather partially coalesces, a phenomenon known as partial coalescence. Using the current setup of microfluidics configuration, a sequence of partial coalescence events is observed, in contrast to other partial coalescence generators. The novelty of the present partial coalescence system studied is first implementing this type of generator in a microfluidic device, second enabling multiple partial coalescence events in sequence, and finally achieving very small size of droplets typically in submicron after performing a certain number of sequences.

In this section, therefore, the parameters governing the partial coalescence are explored. It is found that the salt concentration (as the main factor based on which the transition to partial coalescence takes place) and the electric field strength (or applied voltage) are significant parameters, similar to coalescence and non-coalescence phenomena. However, the effect of viscosity is not studied here because the silicone oil AP is commercially available only in two values of oil viscosity, being as 100 and 1000 cSt. Accordingly, all experiments are performed for the 1000 cSt silicone oil AP as the silicone oil AP with a viscosity of 100 cSt is inconsistent with to the present set-up system. This inconsistency comes from the failure in keeping the liquid-liquid interface at the junction due to breakdown of (Laplace) pressure barrier as a consequence of comparatively low interfacial tension of 100 cSt silicone oil AP-water system, which results in protrusion of the aqueous phase into the oil channel. Nevertheless, the effect of viscosity on the partial coalescence has been already and recently investigated in few studies [201,202]. In addition to the abovementioned parameters, the effects of number of cycles and initial droplet size on daughter droplet size are investigated and a scaling estimate for determination of daughter droplet size is presented.

6.5.2.1 Partial coalescence regime

Unlike coalescence and/or non-coalescence regimes in which a droplet completely coalesces and/or bounces back from a liquid-liquid interface, as described earlier, the partial coalescence regime is defined when a droplet leaves behind a fraction of its initial volume after contacting to the (each) interface. Generally, to bring a droplet in contact with an interface or other droplet, it can be driven via different driving forces such as gravitational force, electric force etc. either individually or in a combination form. Alternatively, an interface can be actuated (vibrated) rather than droplet itself [211]. In most studies earlier, gravity runs coalescence events and is used as a driving force. As such, a droplet can move towards the interface by gravity force and this can be coupled with electric actuation as well. Accordingly, a droplet may completely or partially coalesce with a liquid-liquid interface, which depends on governing parameters, and is known as cascade (partial) coalescence. Despite that gravity triggers the coalescence event, however, the gravitational effects are usually negligible and the coalescence process is indeed controlled by surface/interfacial tension through which competition in rates of collapse inward and outward is determinant. In some situations when gravity cannot be used as an external force to bring a droplet into contact with an interface, particularly in microfluidic devices, other alternative external forces such as electric force can be a solution [11]. In presence of an electric field, such a coalescence event, regardless of being complete, partial or none coalescence, is not anymore cascade coalescence, it is rather sometimes called electrocoalescence, although a combination of electric field and gravity as a driving force in bringing a droplet into contact with a liquid-liquid is possible and is found elsewhere [59,202].

The partial coalescence events are observed for salt concentrations of 10^{-3} w/v% (1.7×10^{-3} mM) or less for all applied voltages (electric fields) at any initial droplet size in the studied range. However, the occurrence of the partial coalescence is not solely due to the sufficiently low salt concentration. In other words, having salt concentrations of 10^{-3} w/v% or less is the primary and critical condition but does not guaranty the occurrence of partial coalescence. It was already found that at salt concentrations of $c>>10^{-3}$ w/v% the full coalescence and non-coalescence take place [11]. By contrast, the partial coalescence can be only observed at salt concentrations of 10^{-3} w/v% or less but in a space shared with full coalescence and non-coalescence, although its occurrence is

comparatively much prevalent. Whether which of full, none or partial coalescence wins depends on the competition of electrophoretic force acting during the events with other governing forces discussed later.
Figure 6.12 shows the time-lapse images of a partial coalescence event when a voltage of 200 V is switched on between the two liquid-liquid interfaces after generation of a droplet with a salt concentration of 1.7×10^{-3} mM from the small reservoir. In the partial coalescence in the present scheme, similar to the non-coalescence case where a droplet reciprocates between the two reservoirs, the droplet does the same way but simultaneously undergoes a size reduction upon each contact with reservoirs if suitable conditions meet. It is worth noting that the droplet size shrinkage at each contact with the reservoirs during the partial coalescence events is arbitrary, which means that a droplet may shrink in size either only with one reservoir or with both reservoirs (or a mix of them).

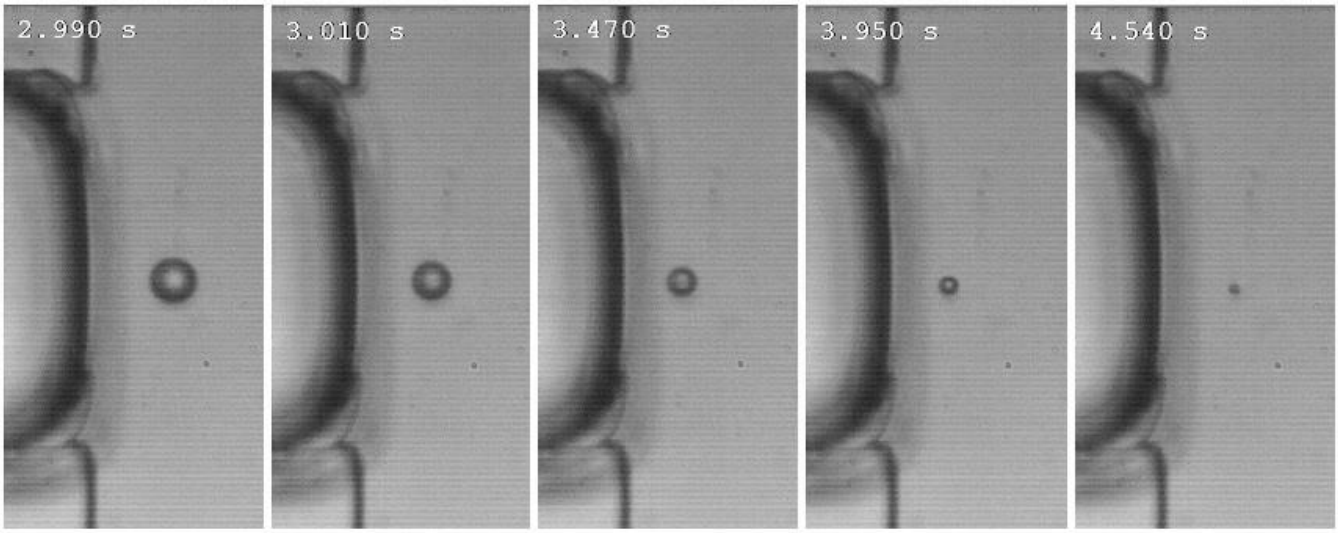

Fig. 6.12 Time-lapse images of the partial coalescence event of a water droplet in 1000 mm^2/s silicone oil AP using a voltage of 200 V. The numbers above the individual frames denote the time in seconds.

The figure depicts some specific frames of the droplet after contacts with the large reservoir in a sequence of partial coalescence events reciprocating between the two reservoirs. As seen, for a typical example here, the droplet size before contact, shown in the first frame, is 8.3 μm, which step-by-step reduces to 6.9, 5.1, 3.4 and 1.6 μm after each contact, respectively. By switching the voltage off, in a suitable time, during the process one may be left with a droplet of the reduced size. However, the size reduction ratio is not generally constant or regular due to involving various parameters in practice and, therefore, one may not expect a well-predicted size in a well-controlled manner. In most cases, the droplet size eventually reaches a very small size in nanoscale whose measurement (and detection sometimes) requires high tech methodology and high precision instrumentations. Figure 6.13 shows the trace of an exemplary non-measurable nanoscale sized droplet (marked with red circles) after its last partial coalescence to the small reservoir. The frame at 0 ms corresponds to the droplet before contact with the small reservoir whose size is still measurable. Considering the limitation of measuring devices, one could

only guess that its size should be below 400 nm. In the following section, a scaling is presented by which it will be possible to roughly estimate the size of nanoscale droplets.

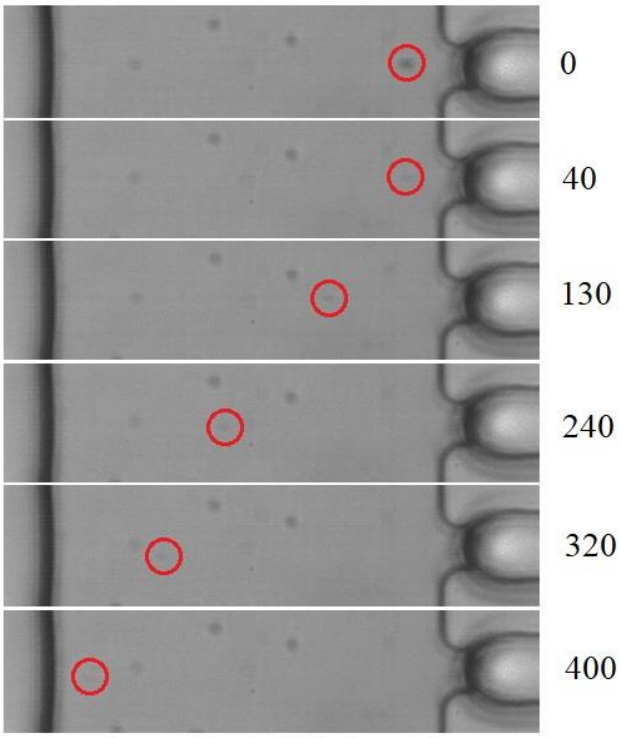

Fig. 6.13 Time-lapse images of the trace of an exemplary non-measurable nanodroplet in a partial coalescence event. The numbers next to the individual frames denote the time in miliseconds. The frame at 0 ms corresponds to the droplet before its last partial coalescence.

6.5.2.2 Scaling estimate: The effects of electric field strength and salt concentration

In the following, a scaling estimate is presented by which the ratio of daughter droplet radius to the initial radius is represented as a function of the ratio of average electrophoretic force during the event to the interfacial tension force. Since the amount of droplet charge by which the actual electrophoretic force acts during the partial coalescence process is difficult to obtain, the charge on a single droplet right before and right after the event is predicted by balancing the relevant forces involved, being as electrophoretic force and viscous (Stokes') drag while inertial and gravitational (buoyancy) forces are negligible. The balance is written as

$$4\pi\mu a_0 c\frac{dx}{dt} = qE \tag{6.13}$$

where μ is the dynamic viscosity of the oil phase, a_o is the droplet radius, $\frac{dx}{dt}$ is the local droplet velocity and $c = \frac{3\mu_r+2}{2(\mu_r+1)}$ with μ_r being as the viscosity ratio of the droplet to the oil medium. From the Eq. (6.13) it is easily figured out that the electrophoretic force, qE, can be calculated through performing droplet velocimetry without any needs to directly quantify the individual droplet charge and electric field strength. However, if the evaluation of the droplet charge is concerned, the electric field must be known or obtained.

Performing the balance for droplets passing by a fixed location very close to the (large) reservoir right before and after the partial coalescence events, with respective velocities known from the droplet velocimetry, one could roughly compute the electrophoretic forces corresponding to the early (from before contact) and the last (from after contact) stages of the partially coalescing process. Because the electric field between the liquid-liquid interfaces is non-uniform owing to the different dimensions of the reservoirs, performing the evaluation at a fixed location ensures that the electric field is constant as long as the voltage is not varied.

It is found that the averaged value of electrophoretic forces (corresponding to the right before and after contact) gives rise the best fit to the experimental data sets when we cast them in the scaling given by Hamlin et al. [202]. However, the trend of the experimental results obtained with the present scaling is different from the one given by Hamlin et al. [202] in a way that the fitted line does not intersect the x-axis at origin. It rather meets the x-axis at a certain value (of ~0.27). This indicates that a minimum charge must exist on a droplet so as to lead the full coalescence (i.e. a/a_o=0). This is consistent with the experimental results in which a droplet impacting an interface with a low velocity (i.e. low droplet charge) shows a full coalescence. Another point is that in the present system the droplets are charged upon production and, as mentioned earlier, the electrostatic force is the only driving force bringing the droplets in contact with the interface since the gravity effect is absent, which supports the necessity of existing a minimum droplet charge for running a full coalescence. Notably that recently Ananl et al. [201] found that their experimental data collapse on the scaling with the exponent value of “1.5”, in contrast to the value of “1” given by Hamlin et al. [202] and the present study.

Taking the averaged electrophoretic force not only gives the best fit to the experimental data sets, but also allows one to roughly estimate the size of nano-droplets which are not measurable (while their trace visible) with the available technique. Accordingly, for example, if the velocity and the size of last visible droplet along with the velocity of its corresponding daughter droplet whose trace is visible, but not measurable, are known, one can obtain an estimation for the size of daughter droplet. A droplet diameter of 840 nm is estimated by this prediction model as an exemplary for the droplet shown in Fig 6.13.

As earlier mentioned, the parameters investigated in this work for the partial coalescence are the electric field strength (or applied voltage), salt concentration and initial droplet size. The effects of the electric field and salt concentration on the daughter droplet size produced following contact with the reservoirs is discussed in this section and the details about the effect of initial droplet size will be given in a separate section later on. Since the droplets experience reciprocating motions between the reservoirs while undergoing shrinkage in size, it is necessary to focus on certain initial droplet sizes in order to grasp better insights about the effects of the electric field and the salt concentration in a more systematic manner. In that context, droplets having the initial sizes of 7 and 11 μm in diameter at a salt concentration of 10^{-3} w/v% and less for different applied voltages are examined and their corresponding results are cast into a scaling. Correspondingly, their ratios of daughter droplet radius to the initial radius as a function of $\left(qE_{avg}/\gamma a_0\right)^{1/2}$ for droplets contacting with the large reservoir are plotted in Fig. 6.14. The open symbols denote the droplets with a diameter of 7 μm and the closed symbols denote a diameter

of 11 μm. From the figure, it is seen that the daughter droplet size generally increases with electrophoretic force (i.e. the interplay of both electric field strength and the droplet charge). At higher electrophoretic force (i.e. *qE*), it is observed that droplets have tendency to bounce back from the interface. Furthermore, it can be reasonably stated that a clear dependency of the daughter droplet size on the salt concentration (or ionic conductivity) is not seen. Similarly, this was observed by Hamlin et al. [202] reporting insensitivity of the daughter droplet size to the ionic conductivity.

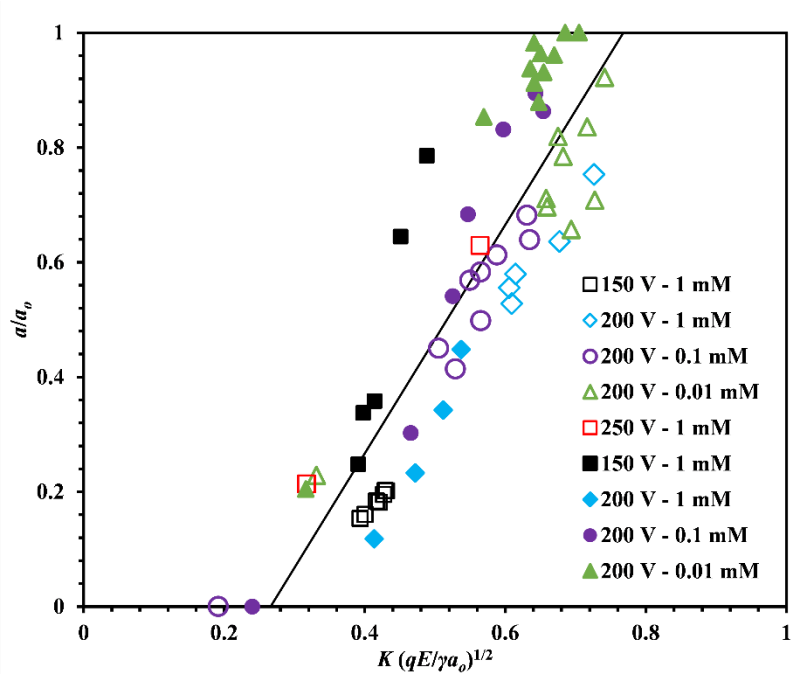

Fig. 6.14 The ratio of the daughter radius to initial radius versus the scaling prediction. Here, *K*=1.24 is a dimensionless prefactor. The open symbols denote the droplets with a diameter of 7 μm and the closed symbols denote the ones with a diameter of 11 μm.

It is known that charge is transferred in three different ways, being as convection, diffusion and conduction (or electromigration), as indicated from conservation of charge [212]

$$\frac{\partial \rho_f}{\partial t} = D\nabla^2\rho_f + \nabla\cdot(\sigma \boldsymbol{E}) - \boldsymbol{u}\cdot\nabla\rho_f \tag{6.14}$$

where the terms on the right-hand-side represent diffusion, electromigration (or conduction) and convection, respectively.

Hamlin et al. [202] reported that the charge transfer is strongly influenced by convection for which the Peclet numbers, the ratio of convection to diffusion, were roughly equal or larger than 1, indicating to the comparable or larger order-of-magnitude of the convention with respect to the diffusion. They also proved that the effect of conduction (or electromigration) is negligible and the independency of daughter drops size to the ionic conductivity additionally supports the domination of convection and diffusion over the conduction. In the current

study, since the velocity of droplets in the microfluidics channels is typical very small, the corresponding Peclet numbers are very small and therefore it implies the diffusion to play the dominant role for the charge transfer. Hamlin et al. [202] also added that the daughter drop acquired the opposite charge due to polarization of the droplets prior to contact in a way that the charge at the leading of the drops convected away to the reservoir while the residual dipolar opposite charge located at the top of droplet becomes the net charge of daughter drops. Pillai et al. [213] explained that the charge in the macrodrops in the study of Hamlin [202] mainly migrate to the interface region owing to the very small Debye length, in contrast to droplets in microscale whose Debye length are comparatively large. Accordingly, the droplet charges still occupied a significant portion of the droplet due to the charge polarization when approaching the interface. In our case, the conduction is believed to be negligible because a clear dependency of droplet size on the salt concentration has not been observed, similar to the implication drawn by Hamlin et al. [202], and the charge of micro-droplet perhaps does not instantaneously transfer to the interface. Considering all abovementioned, the implication of charge transfer by diffusion in the present study could be that the charge transfer and consequently the electrophoretic force are time-dependent during the partial coalescence process, starting from the formation of the neck all the way during the growth of the neck until eventually the pinch-off moment. Accordingly, taking the average of electrophoretic forces in the partial coalescence process into account makes sense, and the corresponding scaling results look quite consistent with experimental trends.

6.5.2.3 Mechanism of partial coalescence

Several decades ago, it was hypothesized that the formation of daughter droplets originates from a static Rayleigh-Plateau instability during the evolution of the coalescing drop with an interface into a fluidic columnar shape whose breakup generates daughter droplets [189]. Nevertheless, after many years, Blanchette and Bigioni [188] disproved that hypothesis through manipulating their numerical simulations. They alternatively suggested that the competition between the surface tension driven vertical and horizontal rates of collapse controls the process of coalescence, where the gravitational effect is negligible. As such, they argued that when the drop makes a contact with the interface, the process goes toward formation of a fluid column (a bridge) followed by necking stage. The downward pull of surface tension at top of drop (i.e. vertical collapse strength) is generally larger than the inward pull of the neck (i.e. vertical collapse strength), and therefore, the vertical collapse is dominant and full coalescence occurs unless the vertical collapse is delayed somehow under a condition. They described that such a delay could be achievable if capillary waves produced during the opening of the neck at the early stages of coalescence event successfully converge at the top of drop. The convergence of sufficiently vigorous waves could significantly stretch the drop upward and the delay in the vertical collapse avoided the complete drainage of droplet into the interface, and thereby produced daughter drops.

By contrast, a different scenario seems to be valid in this study. As coalescence process takes place in presence of an electric field, the electrophoretic force comes to play and the mechanism by which a delay in vertical collapse of droplet occurs should be the action of electrophoretic force rather than convergence of capillary waves. Accordingly, when the charged droplet approaches the reservoirs, presumably along with a formed cone angle at the leading edge of droplet, a liquid bridge creates between the droplet surface and the liquid-liquid interface upon contact, which gradually evolves into a fluid columnar shape followed by necking stage and eventually pinch-off. It is worth noting that, unlike other studies in the literature where the gravity force with/without the

electrophoretic force runs the droplets [201], here the electrophoretic force acting on the individual single charged droplet in the oil channel is the mere driving force to bring the droplet in contact with the reservoirs. Since the experiments are performed in a microfluidic device, the gravitational force is absent. Upon contact, the capillary pressure in the droplet, which is the difference in pressure between the meniscus bridge and the droplet, tends to drain the bulk fluid of the droplet into the reservoir while the viscous stress exerted by the external oil resists against it. At sufficiently large electric field strengths, the electric field effect leads the pressure in the liquid bridge to become larger than the pressure inside the droplet itself, driving the liquid to move from the bridge towards the droplet. As a result, the droplet pinches off from the interface and thus it triggers the droplet bouncing behavior. Consequently, following the droplet pinch-off, the droplet migrates away from the interface toward the other reservoir (aqueous electrode) due to switching sign of the droplet charge at contact. Repeating this behavior would lead to a reciprocating motion of droplets between two aqueous interfaces [11] or pin metallic electrode-aqueous interface [59]. It seems that in the partial coalescence case, the droplet cone angle should be small as well. More recently, Anand et al. [201] showed that the critical angle for transition from full coalescence to partial coalescence is roughly 17^{o} for an experimental set-up similar to what Hamlin et al. [202] already reported. When the electrophoretic force is sufficiently large so that it delays the complete drainage of droplet into the reservoir, the inward interfacial tension (or capillary pressure) driven horizontal collapse prevails during the necking stage, leaving behind a fraction of the initial droplet volume, that is, a daughter droplet (sometimes called secondary droplet). Therefore, this implies that the delaying mechanism by which a full drainage of droplet in the reservoir avoids would be prominently the electrophoretic force acting on the charges migrated to the summit region of the droplet rather than the converged capillary waves, as suggested by Blanchette and Bigioni [188].

The forces involved in the partial coalescence event in the present study are the interfacial tension force, electrophoretic force, and viscous force. The gravitational and the inertial forces are also negligible. Upon contact, the interfacial tension force drives the coalescence, but the viscous force by resisting against the coalescence controls the rate of drainage of the fluid bulk of droplet into the reservoir [197]. Simultaneously, the electrophoretic force interplays with the interfacial and viscous forces, deciding whether a daughter droplet form or not. Hamlin et al. [202] reported that the change in oil viscosity did not affect the daughter droplet size when Ohnesorge number (the ratio of viscous to inertial-capillary effects) was larger than 1. The Ohnesorge number related to the present work is larger than one as well. A full description of these forces is challenging because the droplet changes dynamically during the course of partial coalescence, where the electrophoretic force plays a key role in the process.

6.5.2.4 The effect of initial droplet size and cycle number

The partial coalescence process and thus the daughter droplets can be significantly affected by the initial droplet size. The point could be that how an initial droplet size can influence the pressure difference between the meniscus bridge and the droplet as a key physical element for droplet pinch-off. Ristenpart et al. [59] with a simple derivation showed that an appropriate pressure difference drives the droplet pinch-off when a liquid bridge is formed between a drop and an interface when an electric field is applied. They stated that for sufficiently steep cone angles the pressure inside the drop gets smaller than in the meniscus bridge and thus drives the fluid from meniscus back into the drop, resulting in the droplet pinch-off and accordingly the non-coalescence of the charged drop to the interface. Bird et al. [186] showed that whether two drops coalesces or recoils is dependent on the

cone angle between them, which can be controlled by varying drop size and electric field. Mousavichoubeh et al. [193,197] observed that the daughter droplet size is relatively independent of the initial droplet size at low electric field strengths while exhibiting strong dependency to it at larger field strengths. They argued the larger droplets having lower internal pressure, according to the Young-Laplace equation $\Delta p=2\gamma/a$, are more prone to deformation and thus leading to formation of a long neck (liquid bridge). They added that the polarization of larger droplets enhances the effectiveness of producing a neck and therefore all mentioned factors lead to a larger daughter droplet. The point here is that although the droplets in the studies of Mousavichoubeh et al. [193,197] were uncharged, however, for partial coalescence of charged droplets, the polarization can be significant too, as justified by Hamlin et al. [202]. When a short-lived bridge forms between a droplet and a liquid-liquid interface, the pressure difference between the droplet and the meniscus bridge is a function of the interfacial tension stress represented by a cone angle, the viscous shear stress exerted by the surrounding oil and the electrical stress [214]. The size of initial droplet together with the electric field strength can adjust the cone angle θ, as reported by Bird et al. [186]. Accordingly, daughter droplets can be influenced by the initial droplet size and it would be worthy to examine the effect of initial size of mother droplets on their offspring. The partial coalescence droplet generator employed in the present study is distinctly different from others reported in the literature from two aspects: the first is the process takes place in a microfluidic device and another is the appearance of a sequence of events originated from a single droplet. For that purpose, the ratios of daughter droplet radius to the initial radius versus cycle number for different initial droplet sizes are depicted in Fig. 6.15 for the case when the electrically produced charged droplets initially make their contacts with the small reservoir. The salt concentration is fixed at 10^{-5} w/v%, and the applied voltage varies from 150 V to 300 V (presented in Figs. 6.15 a-d). Here, one cycle number means a droplet makes contacts with both reservoirs. This figure illustrates that the size of the larger droplets decreases more slowly than that of the smaller droplets representing in the increase in the number of the partial coalescence events, which intuitively indicates that the droplet shrinkage in size decreases with the increase of the initial droplet size. At initial contacts, the droplets with larger size in a partial coalescence process undergo lower loss of volume fractions. The same effect is generally seen when the electric field is increased from 150 V (Fig. 6.15 (a)) to 300 V (Fig. 6.15(d)). The increase in the applied voltage (or equivalently the electrophoretic force) causes the increase of the droplet radius ratio, which implies the escalation in tendency of droplets to bounce at the beginning of the sequential partial coalescence events at sufficiently large electric field strength, particularly observed for larger droplets.

(a)

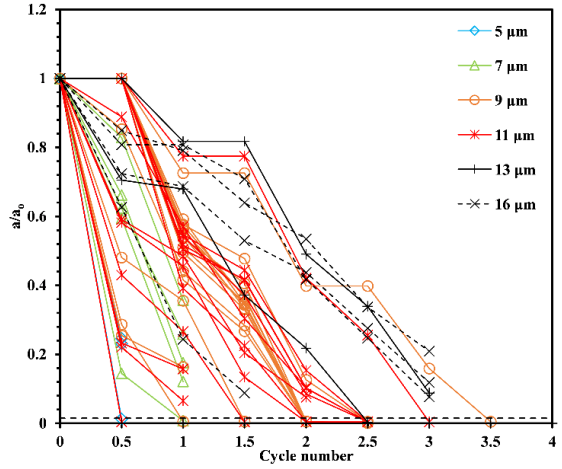

(b)

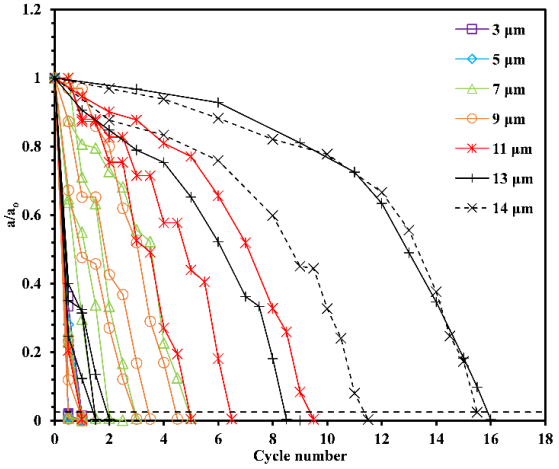

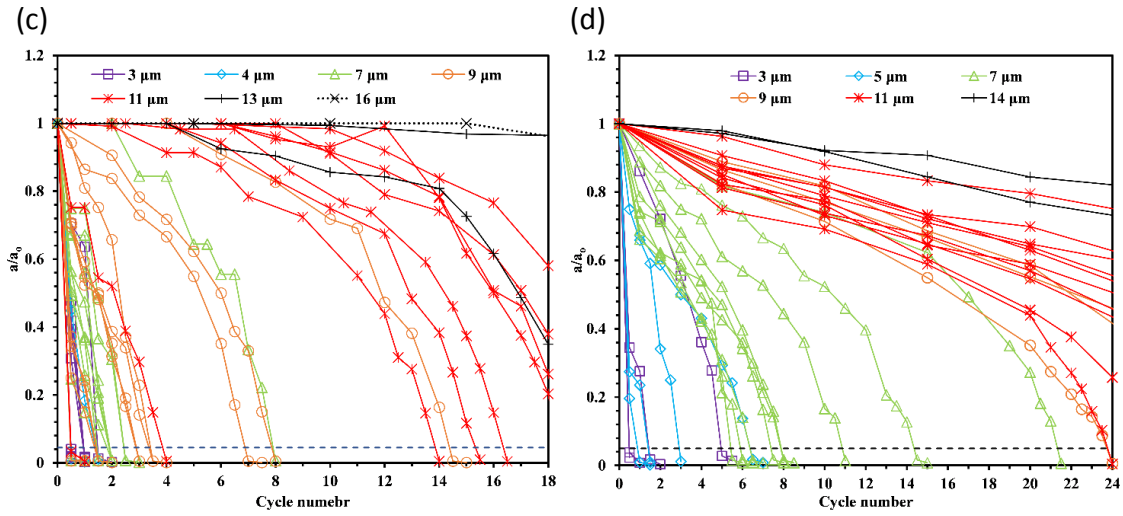

Fig. 6.15 The ratio of the daughter radius to initial radius as a function of cycle number for different droplet diameters at a fixed salt concentration of 10^{-5} w/v% and different applied voltages of a) 150 V b) 200 V c) 250 V d) 300 V.

The most intriguing behavior observed in the experiments examining the effect of initial droplet size is the existence of a critical droplet diameter at which the trend in droplet shrinkage rate remarkably changes. This critical droplet diameter is different for each salt concentration (without displaying any clear dependency to that), but is seemingly a week function of the applied voltage (or the electric field strength) such that the critical droplet diameter decreases with the applied voltage. As such, when a droplet has a diameter smaller than the corresponding critical droplet diameter, the reduction in size of successive daughter droplets is large and, as observed in Fig. 6.15 for small droplets, the slope of the plots (of the droplet diameter versus the cycle number) is steep. By contrast, when a droplet has a diameter larger than the associated critical droplet diameter, the droplet shows two distinct behaviors before and after reaching the critical droplet diameter during the course of the sequential partial coalescence events. Before reaching the critical droplet diameter, the rate of droplet shrinkage per cycle is relatively slow (or none in some cases), exhibiting a slight slope. After having reached the critical droplet diameter, there will be a sudden increase in the droplet shrinkage rate (with a steep slope) similar to the case where the initial droplet diameter is less than its critical droplet diameter. Nevertheless, there is a criterion yet to observe the trend described for initial droplets with diameter larger than the critical droplet diameter. This criterion is that the droplet diameter resulting from the first partial calescence event must be larger than the critical one. Otherwise, it behaves like the case when the initial droplet diameter is smaller than the critical one.

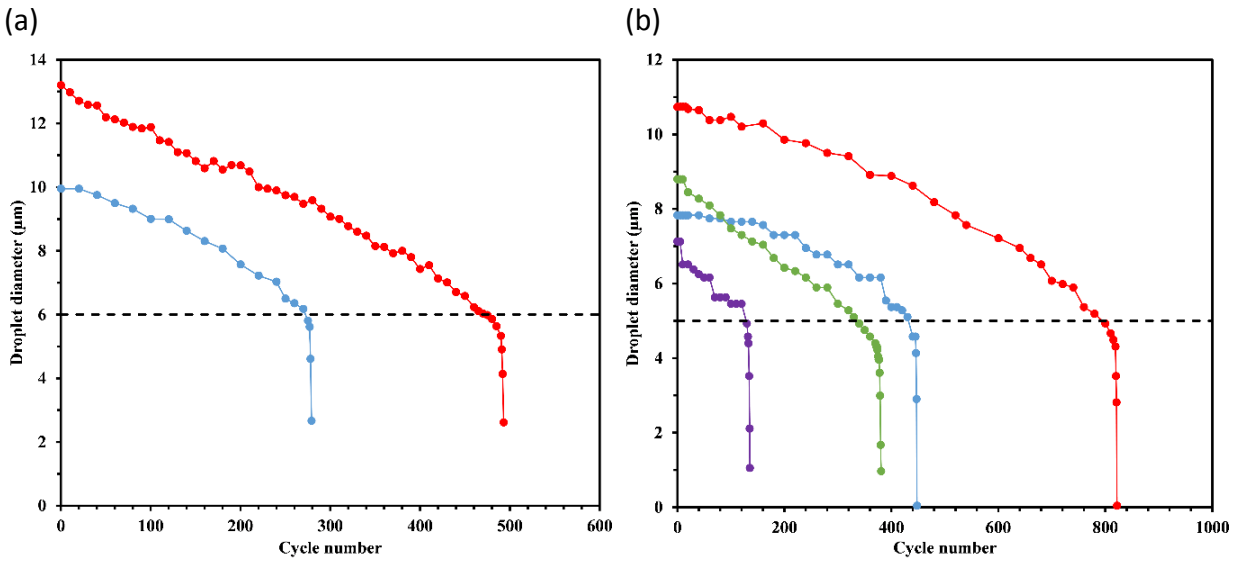

Fig. 6.16 Critical droplet diameter characterization. Droplet diameter as a function of cycle number for droplets (contacting large reservoir) having a salt concentration of 10^{-3} w/v% using a voltage of a) 250 V and b) 300 V when the conditions meet for the critical droplet diameter to occur.

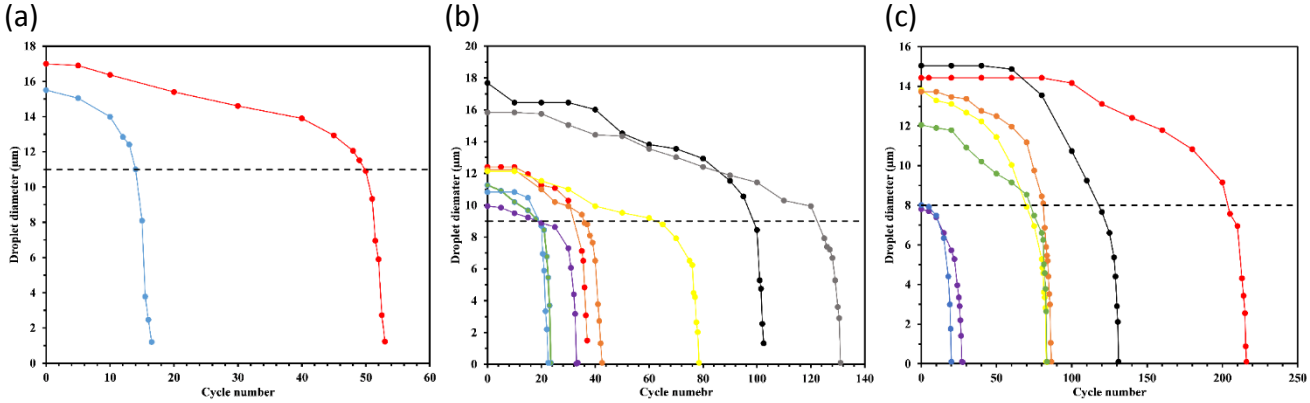

Fig. 6.17 Critical droplet diameter characterization. Droplet diameter as a function of cycle number for droplet having a salt concentration of 10^{-4} w/v% using a voltage of a) 200 V, b) 250 V and c) 300 V when the conditions meet for the critical droplet diameter to occur.

It is surprising that the value of the critical droplet diameter is independent of the initial droplet size. As long as the electric field strength and salt concentration are fixed, there will be almost a unique critical droplet diameter irrespective to the initial droplet size (see Fig. 6.16 and Fig. 6.17 for salt concentrations of 10^{-3} w/v% and 10^{-4} w/v% at different voltages). A possible qualitative explanation for observing the two different trends for the case where the droplet diameter is larger than a critical diameter might be ascribed to the deformability of a droplet due to the applied field. For a fixed applied voltage, the deformability of a droplet probably manifests itself in the formation of a cone angle at the leading edge of droplet near/connected to the liquid-liquid interface. Based on this hypothesis, the associated cone angle is higher for larger droplets and perhaps droplets more readily form the cone angles favorable to the non-coalescence (bouncing) of droplet from the interface [59]. That is why at the

very beginning of sequential partial coalescence events, the larger droplets exhibit a bouncing like behavior at sufficiently large electric fields. Nevertheless, it seems that the complete bouncing (or non-coalescence) does not sustain or occur and there will be still a slight reduction in the size of droplets as cycle goes. The size of droplets gradually diminishes per cycle until reaching the critical droplet diameter, which could be assigned to an associated critical cone angle (or a degree of deformation). Having reached the critical droplet diameter beyond which a remarkable decrease in size with the cycle number observes, the tendency for coalescing exceeds the tendency for bouncing. As a hypothesis, this could be attributed to a critical cone angle at which a transition from non-coalesce to partial coalescence occurs, analogous to the recent study of Anand et al. [201] who determined critical cone angles at which a transition from full coalescence to partial coalescence or from partial coalescence to non-coalescence regimes occurred. Another possibility could be related to the sudden decline in the ratio of droplet charge to the droplet size. Perhaps, a droplet at this point (i.e. critical diameter value) loses its charge much faster, which is reflected in lower impact velocity. When the droplet charge becomes gradually less and less, the corresponding electrophoretic force gets lower and lower, leading to gradually shifting to coalescence regime passing through partial coalescence regime. That is why the droplets are expected to coalesce with the interface at last.

6.6 Summary

The reciprocating motion of femtoliter droplets between two aqueous reservoirs under DC electric fields is studied. The regimes in which this so-called ping-pong motion occurs are identified in terms of the voltage, salt concentration, and viscosity of the surrounding oil phase. Most significantly, mass transfer between the two reservoirs and the droplet has been studied. While 500 nm polystyrene beads cannot be transferred from the reservoirs to a reciprocating droplet, a fluorescent dye is proven to be transferred. In this context, it has been shown that a diffusive mass transfer model can be obtained that describes the experimental data. Corresponding droplets with volumes in the femtoliter range may serve as tiny semi-batch reactors, allowing the addition of reagents and extraction of products. Alternatively, the method can be used to transfer tiny amounts of liquid between two reservoirs in a well-controllable way. Under certain circumstances, the reciprocating droplets exhibit simultaneously volume loss, reaching to eventually nanoscale sized where their detection and measurements become quite challenging. An interesting observation is the existence of a critical diameter in which the trend of decrease in droplet size versus cycle number (under application of a DC electric field) significantly changes.

7 Conclusions

Droplet-based microfluidics manifests itself as a potential medium for characterizing biochemical and engineering processes occurring in small scales. Microfluidic and lab-on-a-chip devices is a suitable platform for performing and analyzing these processes in a well-controlled, efficient and fast way. Low cost of fabrication along with the requirement for small amounts of samples also adds the utility of microfluidic devices much broader. Droplets as a partner of microfluidic devices enrich the versatility of microfluidics for being a suitable colony for biological and chemical entities. This PhD dissertation highlights to some extent some fundamental and application studies of femtoliter droplets as biological reaction compartments and carriers using electric fields. In the experiments, different working fluid such as water, biological samples and xanthan gum solutions, shear-thinning fluids with zero-shear viscosities up to 10^4 larger than the viscosity of water, have been used. Different amounts of NaCl salt have been dissolved with pure water, which yield different values of electrical conductivity. Besides fluorescent polystyrene beads of 500 nm in diameter and Rhodamine B are added to water for proving some applications as well as some biological entities. In this work, electric field plays a very significant role, where the pulsed and DC fields are used to produce and manipulate droplets, respectively. The oil viscosity also shows to be another parameter influencing the dynamic behavior of droplets.

In the on-stream production of droplets of water and xanthan gum solutions in sunflower oil inside a microfluidic T-junction, the DC electric field can tune the size of droplets similar to what the flow rates ratio of disperse to continuous fluids does, but comparatively in a very quicker way. It is shown that the electric field causes a significant decrease in the droplet diameter up to a certain field whereas larger electric field strengths only marginally affect the size of droplets. The sequence of pulsed electric fields with different pulse durations has also exhibited appealing droplet features, which shows the significant potential of electric field in manipulation of droplet size.

For on-demand droplet generation, the pulsed electric fields are applied on an aqueous phase-oil interface inside a microchannel to produce droplets of water and xanthan gum solutions at certain time and specific location. The effects of pulse amplitude, pulse duration and salinity on the size of droplets are investigated. It has been shown that the production of a single droplet regime (a regime in which no droplets or multiple droplets are produced) is a strong function of electric field characteristics and salt concentration. To prove the applicability of droplets as biological reaction compartments, the electrically generated droplets containing a cell-free transcription-translation system have shown to execute gene transcription synthesising green fluorescence protein in a timely and programmable fashion. Also, it has been proven that biomolecules inside the aqueous droplets such as small RNAs are activated from the outside through diffusion of ligand into droplets and binding with them.

In a different scheme of droplet generation on demand, it has been demonstrated that the droplets can be produced on demand in between two aqueous interfaces (reservoirs) of different width. The design is such that the droplets are produced from the small reservoir for better control of droplet generation process. Having

produced the droplets in silicon oil mediums of different viscosity, they show different dynamic regimes when electric fields are applied. However, the regimes (being as coalescence, non-coalescence, partial coalescence and failure regimes) are a function of salt concentration (or electrical conductivity) and oil viscosity as well as the electric field strength. Of the most interest, the non-coalescence regime is the regime in which the femtoliter droplets undergo reciprocating motion (ping-pong motion) between two aqueous reservoirs under DC electric fields. It has been observed that 500 nm polystyrene beads are not able to transfer from droplets to the reservoir in a reciprocating motion (at non-coalescence regime), whereas switching from non-coalescence to coalescence regime via sufficiently reducing the electric field strength makes the transfer possible. By contrast, it is proven that the transfer of dissolved fluorescent dye molecules becomes possible by the droplets reciprocating between the two reservoirs in the non-coalescence regime. Accordingly, the mass transfer between the two reservoirs and the droplets has been investigated and a model based on diffusive mass transfer is given, which describes the experimental data. Therefore, the method can be used to transfer tiny amounts of liquid between two reservoirs in a selective and controllable way. Interestingly, at sufficiently small salt concentrations, the droplets have shown to simultaneously lose their volume while reciprocating between the two reservoirs, a regime so-called “partial coalescence”. In this regime, the submicron droplets are eventually produced after a sequence of partial coalescence events whose sizes are sometimes challenging to identify.

References

[1] Y. Zeng, M. Shin, T. Wang, Programmable active droplet generation enabled by integrated pneumatic micropumps, Lab Chip. 13 (2013) 267–273. doi:10.1039/c2lc40906b.

[2] M. Shojaeian, F.-X. Lehr, H.U. Göringer, S. Hardt, On-demand production of femtoliter drops in microchannels and their use as biological reaction compartments, Anal. Chem. 91 (2019) 3484–3491. doi:10.1021/acs.analchem.8b05063.

[3] D.J. Collins, A. Neild, A. deMello, A.Q. Liu, Y. Ai, The Poisson distribution and beyond: Methods for microfluidic droplet production and single cell encapsulation, Lab Chip. 15 (2015) 3439–3459. doi:10.1039/c5lc00614g.

[4] T. Thorsen, R.W. Roberts, F.H. Arnold, S.R. Quake, Dynamic pattern formation in a vesicle-generating microfluidic device, Phys. Rev. Lett. 86 (2001) 4163–4166. doi:10.1103/PhysRevLett.86.4163.

[5] J.H. Xu, G.S. Luo, S.W. Li, G.G. Chen, Shear force induced monodisperse droplet formation in a microfluidic device by controlling wetting properties, Lab Chip. 6 (2006) 131–136. doi:10.1039/b509939k.

[6] L. Wang, Y. Zhang, L. Cheng, Magic microfluidic T-junctions: Valving and bubbling, Chaos, Solitons and Fractals. 39 (2009) 1530–1537. doi:10.1016/j.chaos.2007.06.020.

[7] K. Khoshmanesh, A. Almansouri, H. Albloushi, P. Yi, R. Soffe, K. Kalantar-Zadeh, A multi-functional bubble-based microfluidic system, Sci. Rep. 5 (2015). doi:10.1038/srep09942.

[8] M.L.J. Steegmans, K.G.P.H. Schroën, R.M. Boom, Characterization of emulsification at flat microchannel y junctions, Langmuir. 25 (2009) 3396–3401. doi:10.1021/la8035852.

[9] A.R. Abate, A. Poitzsch, Y. Hwang, J. Lee, J. Czerwinska, D.A. Weitz, Impact of inlet channel geometry on microfluidic drop formation, Phys. Rev. E - Stat. Nonlinear, Soft Matter Phys. 80 (2009) 1–5. doi:10.1103/PhysRevE.80.026310.

[10] B. Zheng, J.D. Tice, R.F. Ismagilov, Formation of droplets of alternating composition in microfluidic channels and applications to indexing of concentrations in droplet-based assays, Anal. Chem. 76 (2004) 4977–4982. doi:10.1021/ac0495743.

[11] M. Shojaeian, S. Hardt, Mass Transfer via Femtoliter Droplets in Ping-Pong Mode, Phys. Rev. Appl. 13 (2020) 014015. doi:10.1103/PhysRevApplied.13.014015.

[12] P.B. Umbanhowar, V. Prasad, D.A. Weitz, Monodisperse emulsion generation via drop break off in a coflowing stream, Langmuir. 16 (2000) 347–351. doi:10.1021/la990101e.

[13] A.S. Utada, A. Fernandez-Nieves, H.A. Stone, D.A. Weitz, Dripping to jetting transitions in coflowing liquid streams, Phys. Rev. Lett. 99 (2007) 1–4. doi:10.1103/PhysRevLett.99.094502.

[14] S. Takeuchi, P. Garstecki, D.B. Weibel, G.M. Whitesides, An axisymmetric flow-focusing microfluidic device, Adv. Mater. 17 (2005) 1067–1072. doi:10.1002/adma.200401738.

[15] P. Zhu, L. Wang, Passive and active droplet generation with microfluidics: a review, Lab Chip. 17 (2017) 34–75. doi:10.1039/C6LC01018K.

[16] V. Van Steijn, C.R. Kleijn, M.T. Kreutzer, Flows around confined bubbles and their importance in triggering pinch-off, Phys. Rev. Lett. 103 (2009) 1–4. doi:10.1103/PhysRevLett.103.214501.

[17] P. Garstecki, M.J. Fuerstman, H.A. Stone, G.M. Whitesides, Formation of droplets and bubbles in a microfluidic T-junction - Scaling and mechanism of break-up, Lab Chip. 6 (2006) 437–446. doi:10.1039/b510841a.

[18] J.H. Xu, S.W. Li, J. Tan, G.S. Luo, Correlations of droplet formation in T-junction microfluidic

devices: From squeezing to dripping, Microfluid. Nanofluidics. 5 (2008) 711–717. doi:10.1007/s10404-008-0306-4.
[19] D. Version, Tip-Streaming of drops insimple shear flows, (1991).
[20] J.J.M. Janssen, A. Boon, W.G.M. Agterof, Influence of Dynamic Interfacial Properties on Droplet Breakup in Plane Hyperbolic Flow, AIChE J. 43 (1997) 1436–1447. doi:10.1002/aic.690430607.
[21] W.W. Zhang, Viscous entrainment from a nozzle: Singular liquid spouts, Phys. Rev. Lett. 93 (2004) 2–5. doi:10.1103/PhysRevLett.93.184502.
[22] R. Suryo, O.A. Basaran, Tip streaming from a liquid drop forming from a tube in a co-flowing outer fluid, Phys. Fluids. 18 (2006). doi:10.1063/1.2335621.
[23] A.G. Marín, F. Campo-Cortés, J.M. Gordillo, Generation of micron-sized drops and bubbles through viscous coflows, Colloids Surfaces A Physicochem. Eng. Asp. 344 (2009) 2–7. doi:10.1016/j.colsurfa.2008.09.033.
[24] Y.H. Tseng, A. Prosperetti, Local interfacial stability near a zero vorticity point, J. Fluid Mech. 776 (2015) 5–36. doi:10.1017/jfm.2015.246.
[25] J.M. Gordillo, A. Sevilla, F. Campo-Cortés, Global stability of stretched jets: Conditions for the generation of monodisperse micro-emulsions using coflows, J. Fluid Mech. 738 (2014) 335–357. doi:10.1017/jfm.2013.600.
[26] S.H. Tan, N.T. Nguyen, Generation and manipulation of monodispersed ferrofluid emulsions: The effect of a uniform magnetic field in flow-focusing and T-junction configurations, Phys. Rev. E - Stat. Nonlinear, Soft Matter Phys. 84 (2011) 1–7. doi:10.1103/PhysRevE.84.036317.
[27] M. Shojaeian, S. Hardt, Fast electric control of the droplet size in a microfluidic T-junction droplet generator, Appl. Phys. Lett. 112 (2018) 194102. doi:10.1063/1.5025874.
[28] M. Zhang, J. Wu, X. Niu, W. Wen, P. Sheng, Manipulations of microfluidic droplets using electrorheological carrier fluid, Phys. Rev. E - Stat. Nonlinear, Soft Matter Phys. 78 (2008) 1–5. doi:10.1103/PhysRevE.78.066305.
[29] Q. Yan, S. Xuan, X. Ruan, J. Wu, X. Gong, Magnetically controllable generation of ferrofluid droplets, Microfluid. Nanofluidics. 19 (2015) 1377–1384. doi:10.1007/s10404-015-1652-7.
[30] N.T. Nguyen, T.H. Ting, Y.F. Yap, T.N. Wong, J.C.K. Chai, W.L. Ong, et al., Thermally mediated droplet formation in microchannels, Appl. Phys. Lett. 91 (2007) 89–92. doi:10.1063/1.2773948.
[31] C.A. Stan, S.K.Y. Tang, G.M. Whitesides, Independent control of drop size and velocity in microfluidic flow-focusing generators using variable temperature and flow rate, Anal. Chem. 81 (2009) 2399–2402. doi:10.1021/ac8026542.
[32] M. Robert De Saint Vincent, H. Chraïbi, J.P. Delville, Optical flow focusing: Light-induced destabilization of stable liquid threads, Phys. Rev. Appl. 4 (2015) 1–8. doi:10.1103/PhysRevApplied.4.044005.
[33] S.-Y. Tang, I.D. Joshipura, Y. Lin, K. Kalantar-Zadeh, A. Mitchell, K. Khoshmanesh, et al., Liquid-Metal Microdroplets Formed Dynamically with Electrical Control of Size and Rate, Adv. Mater. 28 (2016) 604–609. doi:10.1002/adma.201503875.
[34] D.A. Saville, Electrohydrodynamics: The Taylor-Melcher leaky dielectric model, Annu. Rev. Fluid Mech. 29 (1997) 27–64. doi:10.1146/annurev.fluid.29.1.27.
[35] J.U. Brackbill, D.B. Kothe, C. Zemach, A continuum method for modeling surface tension, J. Comput. Phys. 100 (1992) 335–354. doi:10.1016/0021-9991(92)90240-Y.
[36] M. Davanipour, H. Javanmardi, N. Goodarzi, Chaotic self-tuning PID controller based on fuzzy wavelet neural network Model, Iran. J. Sci. Technol. - Trans. Electr. Eng. 42 (2018) 357–366. doi:10.1007/s40998-018-0069-1.
[37] G. Tomar, D. Gerlach, G. Biswas, N. Alleborn, A. Sharma, F. Durst, et al., Two-phase

electrohydrodynamic simulations using a volume-of-fluid approach, J. Comput. Phys. 227 (2007) 1267–1285. doi:10.1016/j.jcp.2007.09.003.
[38] Y. Ouedraogo, E. Gjonaj, T. Weiland, H. De Gersem, C. Steinhausen, G. Lamanna, et al., Electrohydrodynamic simulation of electrically controlled droplet generation, Int. J. Heat Fluid Flow. 64 (2017) 120–128. doi:10.1016/j.ijheatfluidflow.2017.02.007.
[39] C.H. Chen, Electrohydrodynamic Stability, CISM Int. Cent. Mech. Sci. Courses Lect. 530 (2011) 177–220. doi:10.1007/978-3-7091-0900-7_6.
[40] S.F. Kistler, Hydrodynamics of wetting, in: 1993: pp. 311–430.
[41] M.M. Hohman, M. Shin, G. Rutledge, M.P. Brenner, Electrospinning and electrically forced jets. I. Stability theory, Phys. Fluids. 13 (2001) 2201–2220. doi:10.1063/1.1383791.
[42] C.H. Chen, D.A. Seville, I.A. Aksay, Scaling laws for pulsed electrohydrodynamic drop formation, Appl. Phys. Lett. 89 (2006). doi:10.1063/1.2356891.
[43] J. Fernández de la Mora, The fluid dynamics of Taylor cones, Annu. Rev. Fluid Mech. 39 (2007) 217–243. doi:10.1146/annurev.fluid.39.050905.110159.
[44] G. Taylor, Disintegration of water drops in an electric field, Proc. R. Soc. London A Math. Phys. Eng. Sci. 280 (1964) 383–397.
[45] A.M. Gañán-Calvo, On the theory of electrohydrodynamically driven capillary jets, J. Fluid Mech. 335 (1997) 165–188. doi:10.1017/S0022112096004466.
[46] N. Gawande, Y.S. Mayya, R. Thaokar, Jet and progeny formation in the Rayleigh breakup of a charged viscous drop, J. Fluid Mech. 884 (2019). doi:10.1017/jfm.2019.970.
[47] R.L. Grimm, J.L. Beauchamp, Dynamics of field-induced droplet ionization: Time-resolved studies of distortion, jetting, and progeny formation from charged and neutral methanol droplets exposed to strong electric fields, J. Phys. Chem. B. 109 (2005) 8244–8250. doi:10.1021/jp0450540.
[48] J. Zeleny, On the Conditions of Instability of Liquid Drops, with Applications to the Electrical Discharge from Liquid Point, Proc. Camb. Philol. Soc. 18 (1915) 71–93.
[49] A.M. Gañán-Calvo, Cone-jet analytical extension of Taylor's electrostatic solution and the asymptotic universal scaling laws in electrospraying, Phys. Rev. Lett. 79 (1997) 217–220. doi:10.1103/PhysRevLett.79.217.
[50] C. Chen, Electrohydrodynamic Stability, Electrokinet. Electrohydrodynamics Microsystems (Ed. A. Ramos), Springer. 220 (2011) 177–220.
[51] D.B. Bober, C.H. Chen, Pulsating electrohydrodynamic cone-jets: From choked jet to oscillating cone, J. Fluid Mech. 689 (2011) 552–563. doi:10.1017/jfm.2011.453.
[52] F. Liu, C.H. Chen, Electrohydrodynamic cone-jet bridges: Stability diagram and operating modes, J. Electrostat. 72 (2014) 330–335. doi:10.1016/j.elstat.2014.05.004.
[53] O. Yogi, T. Kawakami, M. Yamauchi, Jing Yong Ye, M. Ishikawa, On-demand droplet spotter for preparing pico- to femtoliter droplets on surfaces, Anal. Chem. 73 (2001) 1896–1902. doi:10.1021/ac0012039.
[54] M. Smoluchowski, Contribution to the theory of electro-osmosis and related phenomena, Bull. Int. Acad. Sci. Cracovie. 3 (1903) 184–199.
[55] A.Y.H. Cho, Contact charging of micron-sized particles in intense electric fields, J. Appl. Phys. 35 (1964) 2561–2564. doi:10.1063/1.1713799.
[56] A. Khayari, A.T. Pérez, Charge acquired by a spherical ball bouncing on an electrode: Comparison between theory and experiment, IEEE Trans. Dielectr. Electr. Insul. 9 (2002) 589–595. doi:10.1109/TDEI.2002.1024437.
[57] A. Khayari, A.T. Pérez, Nonlinear dynamics of a bouncing ball driven by electric forces, Int. J. Bifurcat. Chaos. 13 (2003) 2959–2975. doi:10.1142/S0218127403008314.

[58] G. Quincke, Über die Fortführung materieller Teilchen durch strömende Elektrizität, Ann. Der Phys. Und Chemie. 113 (1861) 513–598.
[59] W.D. Ristenpart, J.C. Bird, A. Belmonte, F. Dollar, H.A. Stone, Non-coalescence of oppositely charged drops, Nature. 461 (2009) 377–380. doi:10.1038/nature08294.
[60] M. Hase, S.N. Watanabe, K. Yoshikawa, Rhythmic motion of a droplet under a dc electric field, Phys. Rev. E. 74 (2006) 3–6. doi:10.1103/PhysRevE.74.046301.
[61] S. Mhatre, R.M. Thaokar, Drop motion, deformation, and cyclic motion in a non-uniform electric field in the viscous limit, Phys. Fluids. 25 (2013). doi:10.1063/1.4813236.
[62] D.J. Im, J. Noh, D. Moon, I.S. Kang, Electrophoresis of a charged droplet in a dielectric liquid for droplet actuation, Anal. Chem. 83 (2011) 5168–5174. doi:10.1021/ac200248x.
[63] D.J. Im, M.M. Ahn, B.S. Yoo, D. Moon, D.W. Lee, I.S. Kang, Discrete electrostatic charge transfer by the electrophoresis of a charged droplet in a dielectric liquid, Langmuir. 28 (2012) 11656–11661. doi:10.1021/la3014392.
[64] H.A. Pohl, Some effects of nonuniform fields on dielectrics, J. Appl. Phys. 29 (1958) 1182–1188. doi:10.1063/1.1723398.
[65] B.H. Lapizco-Encinas, M. Rito-Palomares, Dielectrophoresis for the manipulation of nanobioparticles, Electrophoresis. 28 (2007) 4521–4538. doi:10.1002/elps.200700303.
[66] M. Washizu, O. Kurosawa, Electrostatic Manipulation of DNA in Microfabricated Structures, IEEE Trans. Ind. Appl. 26 (1990) 1165–1172. doi:10.1109/28.62403.
[67] M. Washizu, S. Suzuki, O. Kurosawa, I. Arai, N. Shimamoto, Applications of Electrostatic Stretch-and-Positioning of DNA, IEEE Trans. Ind. Appl. 31 (1995) 447–456. doi:10.1109/28.382102.
[68] M. Washizu, DNA manipulation in electrostatic fields, 7th Int. Conf. Miniaturized Chem. Biochem. Anal. Syst. 2 (2003) 869–873.
[69] T. Kawabata, M. Washizu, Dielectrophoretic detection of molecular bindings, IEEE Trans. Ind. Appl. 37 (2001) 1625–1633. doi:10.1109/28.968170.
[70] M. Viefhues, R. Eichhorn, DNA dielectrophoresis: Theory and applications a review, Electrophoresis. 38 (2017) 1483–1506. doi:10.1002/elps.201600482.
[71] F. Camacho-Alanis, L. Gan, A. Ros, Transitioning streaming to trapping in DC insulator-based dielectrophoresis for biomolecules, Sensors Actuators, B Chem. 173 (2012) 668–675. doi:10.1016/j.snb.2012.07.080.
[72] C. Zhang, K. Khoshmanesh, A. Mitchell, K. Kalantar-Zadeh, Dielectrophoresis for manipulation of micro/nano particles in microfluidic systems, Anal. Bioanal. Chem. 396 (2010) 401–420. doi:10.1007/s00216-009-2922-6.
[73] S. Tuukkanen, J.J. Toppari, A. Kuzyk, L. Hirviniemi, V.P. Hytönen, T. Ihalainen, et al., Carbon nanotubes as electrodes for dielectrophoresis of DNA, Nano Lett. 6 (2006) 1339–1343. doi:10.1021/nl060771m.
[74] Z. Zhu, J.J. Lu, S. Liu, Protein separation by capillary gel electrophoresis: A review, Anal. Chim. Acta. 709 (2012) 21–31. doi:10.1016/j.aca.2011.10.022.
[75] C. Lin, F. Cotton, C. Boutique, D. Dhermy, F. Vertongen, B. Gulbis, Capillary gel electrophoresis: Separation of major erythrocyte membrane proteins, J. Chromatogr. B Biomed. Sci. Appl. 742 (2000) 411–419. doi:10.1016/S0378-4347(00)00205-X.
[76] C.G. Sotelo, C. Piñeiro, R.I. Pérez-Martín, J.M. Gallardo, Analysis of fish and squid myofibrillar proteins by capillary sodium dodecyl sulfate gel electrophoresis: Actin and myosin quantification, Eur. Food Res. Technol. 211 (2000) 443–448. doi:10.1007/s002170000176.
[77] G. Hunt, W. Nashabeh, Capillary electrophoresis sodium dodecyl sulfate nongel sieving analysis of a therapeutic recombinant monoclonal antibody: A biotechnology perspective, Anal. Chem. 71

(1999) 2390–2397. doi:10.1021/ac981209m.
[78] A.T. Woolley, R.A. Mathies, Ultra-high-speed DNA sequencing using capillary electrophoresis chips, Anal. Chem. 67 (1995) 3676–3680. doi:10.1021/ac00116a010.
[79] A.T. Woolley, R.A. Mathies, Ultra-high-speed DNA fragment separations using microfabricated capillary array electrophoresis chips, Proc. Natl. Acad. Sci. U. S. A. 91 (1994) 11348–11352. doi:10.1073/pnas.91.24.11348.
[80] Y.W. Park, S.-L. Tan, M.G. Katze, Rapid Genetic Screeningfor Hemochromatosis Using Automated SSCP-Based Capillary Electrophoresis (SSCP-CE), 234 (1998) 230–234.
[81] F. Rousseau, R. Réhel, P. Rouillard, P. DeGranpré, E.W. Khandjian, High throughput and economical mutation detection and RFLP analysis using a minimethod for DNA preparation from whole blood and acrylamide gel electrophoresis, Hum. Mutat. 4 (1994) 51–54. doi:10.1002/humu.1380040107.
[82] R. Ahmed, T.B. Jones, Dispensing picoliter droplets on substrates using dielectrophoresis, J. Electrostat. 64 (2006) 543–549. doi:10.1016/j.elstat.2005.10.008.
[83] S. Mhatre, Dielectrophoretic motion and deformation of a liquid drop in an axisymmetric non-uniform AC electric field, Sensors Actuators, B Chem. 239 (2017) 1098–1108. doi:10.1016/j.snb.2016.08.059.
[84] T.P. Hunt, D. Issadore, R.M. Westervelt, Integrated circuit/microfluidic chip to programmably trap and move cells and droplets with dielectrophoresis, Lab Chip. 8 (2007) 81–87. doi:10.1039/b710928h.
[85] M.T. Guo, A. Rotem, J.A. Heyman, D.A. Weitz, Droplet microfluidics for high-throughput biological assays, Lab Chip. 12 (2012) 2146. doi:10.1039/c2lc21147e.
[86] K.S. Elvira, X.C. i Solvas, R.C.R. Wootton, A.J. DeMello, The past, present and potential for microfluidic reactor technology in chemical synthesis, Nat. Chem. 5 (2013) 905–915.
[87] C.-X. Zhao, Multiphase flow microfluidics for the production of single or multiple emulsions for drug delivery, Adv. Drug Deliv. Rev. 65 (2013) 1420–1446. doi:10.1016/j.addr.2013.05.009.
[88] O. Skurtys, J.M. Aguilera, Applications of Microfluidic Devices in Food Engineering, Food Biophys. 3 (2008) 1–15. doi:10.1007/s11483-007-9043-6.
[89] K.-S. Huang, K. Lu, C.-S. Yeh, S.-R. Chung, C.-H. Lin, C.-H. Yang, et al., Microfluidic controlling monodisperse microdroplet for 5-fluorouracil loaded genipin-gelatin microcapsules, J. Control. Release. 137 (2009) 15–19. doi:10.1016/j.jconrel.2009.02.019.
[90] H. Wu, T.W. Odom, D.T. Chiu, G.M. Whitesides, Fabrication of complex three-dimensional microchannel systems in PDMS, J. Am. Chem. Soc. 125 (2003) 554–559. doi:10.1021/ja021045y.
[91] M. Abdelgawad, S.L.S. Freire, H. Yang, A.R. Wheeler, All-terrain droplet actuation, Lab Chip. 8 (2008) 672–677. doi:10.1039/b801516c.
[92] D. Porter, J.R. Savage, I. Cohen, P. Spicer, M. Caggioni, Temperature dependence of droplet breakup in 8CB and 5CB liquid crystals, Phys. Rev. E. 85 (2012) 041701. doi:10.1103/PhysRevE.85.041701.
[93] Y.N. Cheung, H. Qiu, Acoustic microstreaming for droplet breakup in a microflow-focusing device, Appl. Phys. Lett. 97 (2010) 133111. doi:10.1063/1.3495986.
[94] S.-H. Tan, N.-T. Nguyen, L. Yobas, T.G. Kang, Formation and manipulation of ferrofluid droplets at a microfluidic *T* -junction, J. Micromechanics Microengineering. 20 (2010) 045004. doi:10.1088/0960-1317/20/4/045004.
[95] D.R. Link, E. Grasland-Mongrain, A. Duri, F. Sarrazin, Z. Cheng, G. Cristobal, et al., Electric control of droplets in microfluidic devices, Angew. Chemie - Int. Ed. 45 (2006) 2556–2560. doi:10.1002/anie.200503540.

[96] H. Kim, D. Luo, D. Link, D.A. Weitz, M. Marquez, Z. Cheng, Controlled production of emulsion drops using an electric field in a flow-focusing microfluidic device, Appl. Phys. Lett. 91 (2007) 133106. doi:10.1063/1.2790785.
[97] P. He, H. Kim, D. Luo, M. Marquez, Z. Cheng, Low-frequency ac electro-flow-focusing microfluidic emulsification, Appl. Phys. Lett. 96 (2010) 174103. doi:10.1063/1.3424791.
[98] S.H. Tan, B. Semin, J.-C. Baret, Microfluidic flow-focusing in ac electric fields, Lab Chip. 14 (2014) 1099. doi:10.1039/c3lc51143j.
[99] H. Gu, F. Malloggi, S.A. Vanapalli, F. Mugele, Electrowetting-enhanced microfluidic device for drop generation, Appl. Phys. Lett. 93 (2008) 183507. doi:10.1063/1.3013567.
[100] H. Gu, M.H.G. Duits, F. Mugele, A hybrid microfluidic chip with electrowetting functionality using ultraviolet (UV)-curable polymer., Lab Chip. 10 (2010) 1550–6. doi:10.1039/c001524e.
[101] E. Castro-Hernández, P. García-Sánchez, S.H. Tan, A.M. Gañán-Calvo, J.C. Baret, A. Ramos, Breakup length of AC electrified jets in a microfluidic flow-focusing junction, Microfluid. Nanofluidics. 19 (2015) 787–794. doi:10.1007/s10404-015-1603-3.
[102] E. Castro-Hernández, P. García-Sánchez, J. Alzaga-Gimeno, S.H. Tan, J.C. Baret, A. Ramos, AC electrified jets in a flow-focusing device: Jet length scaling, Biomicrofluidics. 10 (2016). doi:10.1063/1.4954194.
[103] M. Shojaeian, M. Karimzadehkhouei, A. Koşar, Experimental investigation on convective heat transfer of non-Newtonian flows of Xanthan gum solutions in microtubes, Exp. Therm. Fluid Sci. 85 (2017). doi:10.1016/j.expthermflusci.2017.02.025.
[104] M. Shojaeian, A. Koşar, Convective heat transfer and entropy generation analysis on Newtonian and non-Newtonian fluid flows between parallel-plates under slip boundary conditions, Int. J. Heat Mass Transf. 70 (2014) 664–673. doi:10.1016/j.ijheatmasstransfer.2013.11.020.
[105] T. Fu, O. Carrier, D. Funfschilling, Y. Ma, H.Z. Li, Newtonian and Non-Newtonian Flows in Microchannels: Inline Rheological Characterization, Chem. Eng. Technol. 39 (2016) 987–992. doi:10.1002/ceat.201500620.
[106] Y.B. Lu, G.H. Tang, W.Q. Tao, Experimental study of microchannel flow for non-Newtonian fluid in the presence of salt, Exp. Therm. Fluid Sci. 74 (2016) 91–99. doi:10.1016/j.expthermflusci.2015.11.021.
[107] E. Roumpea, M. Chinaud, P. Angeli, Experimental investigations of non-Newtonian/Newtonian liquid-liquid flows in microchannels, AIChE J. 63 (2017) 3599–3609. doi:10.1002/aic.15704.
[108] Z. Gu, J. Liow, Microdroplet formation in a t-junction with xanthan gum solutions, Chemeca 2011 Eng. a Better World …. (2011) 1–10.
[109] D. Qiu, L. Silva, A.L. Tonkovich, R. Arora, Micro-droplet formation in non-Newtonian fluid in a microchannel, Microfluid. Nanofluidics. 8 (2010) 531–548. doi:10.1007/s10404-009-0487-5.
[110] E. Chiarello, L. Derzsi, M. Pierno, G. Mistura, E. Piccin, Generation of oil droplets in a non-Newtonian liquid using a microfluidic T-junction, Micromachines. 6 (2015) 1825–1835. doi:10.3390/mi6121458.
[111] T. Fu, Y. Ma, D. Funfschilling, H.Z. Li, Gas–liquid flow stability and bubble formation in non-Newtonian fluids in microfluidic flow-focusing devices, Microfluid. Nanofluidics. 10 (2011) 1135–1140. doi:10.1007/s10404-010-0741-x.
[112] Y. Huang, Y.L. Wang, T.N. Wong, AC electric field controlled non-Newtonian filament thinning and droplet formation on the microscale, Lab Chip. 17 (2017) 2969–2981. doi:10.1039/c7lc00420f.
[113] K.W. Song, Y.S. Kim, G.S. Chang, Rheology of concentrated xanthan gum solutions: Steady shear flow behavior, Fibers Polym. 7 (2006) 129–138. doi:10.1007/BF02908257.
[114] L. Xu, G. Xu, T. Liu, Y. Chen, H. Gong, The comparison of rheological properties of aqueous

welan gum and xanthan gum solutions, Carbohydr. Polym. 92 (2013) 516–522. doi:10.1016/j.carbpol.2012.09.082.
[115] K.C. Tam, C. Tiu, Steady and Dynamic Shear Properties of Aqueous Polymer Solutions, J. Rheol. (N. Y. N. Y). 33 (1989) 257–280. doi:10.1122/1.550015.
[116] K. Muthamizhi, P. Kalaichelvi, S.T. Powar, R. Jaishree, Investigation and modelling of surface tension of power-law fluids, Rsc Adv. 4 (2014) 9771–9776. doi:Doi 10.1039/C3ra46555a.
[117] J. Fernández De La Mora, I.G. Loscertales, The current emitted by highly conducting Taylor cones, J. Fluid Mech. 260 (1994) 155–184.
[118] R. Seemann, M. Brinkmann, T. Pfohl, S. Herminghaus, Droplet based microfluidics, Reports Prog. Phys. 75 (2012) 016601. doi:10.1088/0034-4885/75/1/016601.
[119] T. Glawdel, C. Elbuken, C.L. Ren, Droplet formation in microfluidic T-junction generators operating in the transitional regime. II. Modeling, Phys. Rev. E -. 85 (2012) 016323. doi:10.1103/PhysRevE.86.026308.
[120] M. Spohner, Study of the dielectric properties of vegetable oils and their constituents, Diagnostic Electr. Mach. Insul. Syst. Electr. Eng. 451 (2016) 16–19. doi:10.1109/DEMISEE.2016.7530478.
[121] G.F. Christopher, N.N. Noharuddin, J.A. Taylor, S.L. Anna, Experimental observations of the squeezing-to-dripping transition in T-shaped microfluidic junctions, Phys. Rev. E - Stat. Nonlinear, Soft Matter Phys. 78 (2008) 1–12. doi:10.1103/PhysRevE.78.036317.
[122] J.-C. Galas, D. Bartolo, V. Studer, Active connectors for microfluidic drops on demand, New J. Phys. 11 (2009) 075027. doi:10.1088/1367-2630/11/7/075027.
[123] S. Zeng, B. Li, X. Su, J. Qin, B. Lin, Microvalve-actuated precise control of individual droplets in microfluidic devices, Lab Chip. 9 (2009) 1340. doi:10.1039/b821803j.
[124] S.Y. Tang, K. Wang, K. Fan, Z. Feng, Y. Zhang, Q. Zhao, et al., High-Throughput, off-chip microdroplet generator enabled by a spinning conical frustum, Anal. Chem. 91 (2019) 3725–3732. doi:10.1021/acs.analchem.9b00093.
[125] A.S.A. Keyon, R.M. Guijt, C.J. Bolch, M.C. Breadmore, Droplet microfluidics for postcolumn reactions in capillary electrophoresis, Anal. Chem. 86 (2014) 11811–11818. doi:10.1021/ac5033963.
[126] A. Birchler, M. Berger, V. Jäggin, T. Lopes, M. Etzrodt, P.M. Misun, et al., Seamless Combination of Fluorescence-Activated Cell Sorting and Hanging-Drop Networks for Individual Handling and Culturing of Stem Cells and Microtissue Spheroids, Anal. Chem. 88 (2016) 1222–1229. doi:10.1021/acs.analchem.5b03513.
[127] R.M. Lorenz, J.S. Edgar, G.D.M. Jeffries, D.T. Chiu, Microfluidic and optical systems for the on-demand generation and manipulation of single femtoliter-volume aqueous droplets, Anal. Chem. 78 (2006) 6433–6439. doi:10.1021/ac060748l.
[128] M. He, J.S. Edgar, G.D.M. Jeffries, R.M. Lorenz, J.P. Shelby, D.T. Chiu, Selective encapsulation of single cells and subcellular organelles into picoliter- and femtoliter-volume droplets, Anal. Chem. 77 (2005) 1539–1544. doi:10.1021/ac0480850.
[129] S.-Y. Jung, S.T. Retterer, C.P. Collier, On-demand generation of monodisperse femtolitre droplets by shape-induced shear, Lab Chip. 10 (2010) 2688. doi:10.1039/c0lc00120a.
[130] H. Zhou, S. Yao, A facile on-demand droplet microfluidic system for lab-on-a-chip applications, Microfluid. Nanofluidics. 16 (2014) 667–675. doi:10.1007/s10404-013-1268-8.
[131] M. Yu, Y. Hou, H. Zhou, S. Yao, An on-demand nanofluidic concentrator, Lab Chip. 15 (2015) 1524–1532. doi:10.1039/C4LC01480D.
[132] B.-C. Lin, Y.-C. Su, On-demand liquid-in-liquid droplet metering and fusion utilizing pneumatically actuated membrane valves, J. Micromechanics Microengineering. 18 (2008)

115005. doi:10.1088/0960-1317/18/11/115005.
[133] F. Guo, K. Liu, X.-H. Ji, H.-J. Ding, M. Zhang, Q. Zeng, et al., Valve-based microfluidic device for droplet on-demand operation and static assay, Appl. Phys. Lett. 97 (2010) 233701. doi:10.1063/1.3521283.
[134] J. Xu, D. Attinger, Drop on demand in a microfluidic chip, J. Micromechanics Microengineering. 18 (2008) 065020. doi:10.1088/0960-1317/18/6/065020.
[135] Sung Kwon Cho, Hyejin Moon, Chang-Jin Kim, Creating, transporting, cutting, and merging liquid droplets by electrowetting-based actuation for digital microfluidic circuits, J. Microelectromechanical Syst. 12 (2003) 70–80. doi:10.1109/JMEMS.2002.807467.
[136] V. Srinivasan, V.K. Pamula, R.B. Fair, An integrated digital microfluidic lab-on-a-chip for clinical diagnostics on human physiological fluids., Lab Chip. 4 (2004) 310–315. doi:10.1039/b403341h.
[137] H. Gu, C.U. Murade, M.H.G. Duits, F. Mugele, A microfluidic platform for on-demand formation and merging of microdroplets using electric control, Biomicrofluidics. 5 (2011) 011101. doi:10.1063/1.3570666.
[138] M. He, J.S. Kuo, D.T. Chiu, Electro-generation of single femtoliter- and picoliter-volume aqueous droplets in microfluidic systems, Appl. Phys. Lett. 87 (2005) 031916. doi:10.1063/1.1997280.
[139] M. He, J.S. Kuo, D.T. Chiu, Effects of Ultrasmall Orifices on the Electrogeneration of Femtoliter-Volume Aqueous Droplets, Langmuir. 22 (2006) 6408–6413. doi:10.1021/LA060259G.
[140] I. Chen, H. Tsai, C. Chang, G. Zheng, Y. Su, Sensors and Actuators B : Chemical Electric-field triggered , on-demand formation of sub-femtoliter droplets, Sensors Actuators B. Chem. 260 (2018) 541–553. doi:10.1016/j.snb.2017.12.152.
[141] S.-Y. Park, T.-H. Wu, Y. Chen, M.A. Teitell, P.-Y. Chiou, High-speed droplet generation on demand driven by pulse laser-induced cavitation, Lab Chip. 11 (2011) 1010. doi:10.1039/c0lc00555j.
[142] U. Demirci, Acoustic Picoliter Droplets for Emerging Applications in Semiconductor Industry and Biotechnology, J. Microelectromechanical Syst. 15 (2006) 957–966. doi:10.1109/JMEMS.2006.878879.
[143] D.J. Collins, T. Alan, K. Helmerson, A. Neild, Surface acoustic waves for on-demand production of picoliter droplets and particle encapsulation, Lab Chip. 13 (2013) 3225. doi:10.1039/c3lc50372k.
[144] V. Taly, B.T. Kelly, A.D. Griffiths, Droplets as Microreactors for High-Throughput Biology, ChemBioChem. 8 (2007) 263–272. doi:10.1002/cbic.200600425.
[145] T.S. Kaminski, O. Scheler, P. Garstecki, Droplet microfluidics for microbiology: techniques, applications and challenges, Lab Chip. 16 (2016) 2168–2187. doi:10.1039/C6LC00367B.
[146] Y. Schaerli, F. Hollfelder, The potential of microfluidic water-in-oil droplets in experimental biology, Mol. Biosyst. 5 (2009) 1392. doi:10.1039/b907578j.
[147] J. Shim, R.T. Ranasinghe, C.A. Smith, S.M. Ibrahim, F. Hollfelder, W.T.S. Huck, et al., Ultrarapid Generation of Femtoliter Microfluidic Droplets for Single-Molecule-Counting Immunoassays, ACS Nano. 7 (2013) 5955–5964. doi:10.1021/nn401661d.
[148] F. Wang, M.A. Burns, Performance of nanoliter-sized droplet-based microfluidic PCR, Biomed. Microdevices. 11 (2009) 1071–1080. doi:10.1007/s10544-009-9324-6.
[149] N. Shembekar, H. Hu, D. Eustace, C.A. Merten, Single-Cell Droplet Microfluidic Screening for Antibodies Specifically Binding to Target Cells, Cell Rep. 22 (2018) 2206–2215. doi:10.1016/J.CELREP.2018.01.071.
[150] E. Fradet, C. Bayer, F. Hollfelder, C.N. Baroud, Measuring Fast and Slow Enzyme Kinetics in Stationary Droplets, Anal. Chem. 87 (2015) 11915–11922. doi:10.1021/acs.analchem.5b03567.
[151] R. Williams, S.G. Peisajovich, O.J. Miller, S. Magdassi, D.S. Tawfik, A.D. Griffiths, Amplification

of complex gene libraries by emulsion PCR, Nat. Methods. 3 (2006) 545–550. doi:10.1038/nmeth896.
[152] M. Margulies, M. Egholm, W.E. Altman, S. Attiya, J.S. Bader, L.A. Bemben, et al., Genome sequencing in microfabricated high-density picolitre reactors, Nature. 437 (2005) 376–380. doi:10.1038/nature03959.
[153] Y. Marcy, T. Ishoey, R.S. Lasken, T.B. Stockwell, B.P. Walenz, A.L. Halpern, et al., Nanoliter Reactors Improve Multiple Displacement Amplification of Genomes from Single Cells, PLoS Genet. 3 (2007) e155. doi:10.1371/journal.pgen.0030155.
[154] H. Leemhuis, V. Stein, A.D. Griffiths, F. Hollfelder, New genotype–phenotype linkages for directed evolution of functional proteins, Curr. Opin. Struct. Biol. 15 (2005) 472–478. doi:10.1016/J.SBI.2005.07.006.
[155] M. Srisa-Art, A.J. DeMello, J.B. Edel, High-Throughput DNA Droplet Assays Using Picoliter Reactor Volumes, Anal. Chem. 79 (2007) 6682–6689. doi:10.1021/AC070987O.
[156] A. Huebner, L.F. Olguin, D. Bratton, G. Whyte, W.T.S. Huck, A.J. de Mello, et al., Development of Quantitative Cell-Based Enzyme Assays in Microdroplets, Anal. Chem. 80 (2008) 3890–3896. doi:10.1021/ac800338z.
[157] M.J. Booth, V.R. Schild, A.D. Graham, S.N. Olof, H. Bayley, Light-activated communication in synthetic tissues, Sci. Adv. 2 (2016) e1600056–e1600056. doi:10.1126/sciadv.1600056.
[158] M. Shojaeian, F.-X. Lehr, H.U. Göringer, S. Hardt, On-Demand Production of Femtoliter Drops in Microchannels and Their Use as Biological Reaction Compartments, Anal. Chem. 91 (2019) 3484–3491. doi:10.1021/acs.analchem.8b05063.
[159] N.B. Wyatt, M.W. Liberatore, Rheology and Viscosity Scaling of the Polyelectrolyte Xanthan Gum, J. OfAppliedPolymer Sci. 114 (2009) 4076–4084. doi:10.1002/app.
[160] S.L. Anna, N. Bontoux, H.A. Stone, Formation of dispersions using "flow focusing" in microchannels, Appl. Phys. Lett. 82 (2003) 364–366. doi:10.1063/1.1537519.
[161] J. Zeleny, The electrical discharge from liquid points , and a hydrostatic method of measuring the electric intensity at their surfaces, Phys. Rev. 3 (1914) 69–91. doi:10.1103/PhysRev.3.69.
[162] J. Shin, V. Noireaux, Efficient cell-free expression with the endogenous E. Coli RNA polymerase and sigma factor 70, J. Biol. Eng. 4 (2010) 8. doi:10.1186/1754-1611-4-8.
[163] J. Garamella, R. Marshall, M. Rustad, V. Noireaux, The all E. coli TX-TL toolbox 2.0: A platform for cell-free synthetic biology, ACS Synth. Biol. 5 (2016) 344–355. doi:10.1021/acssynbio.5b00296.
[164] A. Kato, M. Yanagisawa, Y.T. Sato, K. Fujiwara, K. Yoshikawa, Cell-Sized confinement in microspheres accelerates the reaction of gene expression, Sci. Rep. 2 (2012) 283. doi:10.1038/srep00283.
[165] B. Sharma, Y. Takamura, T. Shimoda, M. Biyani, A bulk sub-femtoliter in vitro compartmentalization system using super-fine electrosprays, Sci. Rep. 6 (2016) 26257. doi:10.1038/srep26257.
[166] D.K. Karig, S.-Y. Jung, B. Srijanto, C.P. Collier, M.L. Simpson, Probing Cell-Free Gene Expression Noise in Femtoliter Volumes, ACS Synth. Biol. 2 (2013) 497–505. doi:10.1021/sb400028c.
[167] A. V. Pietrini, P.L. Luisi, Cell-free Protein Synthesis through Solubilisate Exchange in Water/Oil Emulsion Compartments, ChemBioChem. 5 (2004) 1055–1062. doi:10.1002/cbic.200400014.
[168] A. Autour, E. Westhof, M. Ryckelynck, iSpinach: a fluorogenic RNA aptamer optimized for *in vitro* applications, Nucleic Acids Res. 44 (2016) 2491–2500. doi:10.1093/nar/gkw083.
[169] E. Schäffer, T. Thurn-Albrecht, T.P. Russell, U. Steiner, Electrically induced structure formation

and pattern transfer, Nature. 403 (2000) 874–877. doi:10.1038/35002540.
[170] O.D. Velev, B.G. Prevo, K.H. Bhatt, On-chip manipulation of free droplets, Nature. 426 (2003) 515–516. doi:10.1038/426515a.
[171] M. Singh, H.M. Haverinen, P. Dhagat, G.E. Jabbour, Inkjet Printing-Process and Its Applications, Adv. Mater. 22 (2010) 673–685. doi:10.1002/adma.200901141.
[172] J. Kameoka, R. Orth, B. Ilic, D. Czaplewski, T. Wachs, H. G. Craighead, An Electrospray Ionization Source for Integration with Microfluidics, Anal. Chem. 74 (2002) 5897–5901. doi:10.1021/AC020396S.
[173] M.G. Pollack, A.D. Shenderov, R.B. Fair, Electrowetting-based actuation of droplets for integrated microfluidics, Lab Chip. 2 (2002) 96. doi:10.1039/b110474h.
[174] S. Mhatre, S. Deshmukh, R.M. Thaokar, Electrocoalescence of a drop pair, Phys. Fluids. 27 (2015) 092106. doi:10.1063/1.4931592.
[175] J.-D. Chen, Effects of London—van der Waals and electric double layer forces on the thinning of a dimpled film between a small drop or bubble and a horizontal solid plane, J. Colloid Interface Sci. 98 (1984) 329–341. doi:10.1016/0021-9797(84)90158-9.
[176] J.S. Eow, M. Ghadiri, Drop-drop coalescence in an electric field: The effects of applied electric field and electrode geometry, Colloids Surfaces A Physicochem. Eng. Asp. 219 (2003) 253–279. doi:10.1016/S0927-7757(03)00051-7.
[177] M. Chabert, K.D. Dorfman, J.-L. Viovy, Droplet fusion by alternating current (AC) field electrocoalescence in microchannels, Electrophoresis. 26 (2005) 3706–3715. doi:10.1002/elps.200500109.
[178] D.R. Link, E. Grasland-Mongrain, A. Duri, F. Sarrazin, Z. Cheng, G. Cristobal, et al., Electric Control of Droplets in Microfluidic Devices, Angew. Chemie Int. Ed. 45 (2006) 2556–2560. doi:10.1002/anie.200503540.
[179] C.S. Minardi, M. Taghioskoui, S.J. Jang, K. Jorabchi, Reagent delivery by partial coalescence and noncoalescence of aqueous microdroplets in oil, Anal. Chem. 85 (2013) 6491–6496. doi:10.1021/ac4010524.
[180] C. Priest, S. Herminghaus, R. Seemann, Controlled electrocoalescence in microfluidics: Targeting a single lamella, Appl. Phys. Lett. 89 (2006) 134101. doi:10.1063/1.2357039.
[181] P. Kebarle, U.H. Verkerk, Electrospray: From ions in solution to ions in the gas phase, what we know now, Mass Spectrom. Rev. 28 (2009) 898–917. doi:10.1002/mas.20247.
[182] F. Mugele, J. Baret, Electrowetting : from Basics to Applications, J. Phys. Condens. Matter. 17 (2005) R705–R774.
[183] S.H. Yang, D.J. Im, Electrostatic origins of the positive and negative charging difference in the contact charge electrophoresis of a water droplet, Langmuir. 33 (2017) 13740–13748. doi:10.1021/acs.langmuir.7b03281.
[184] T. Kurimura, M. Ichikawa, M. Takinoue, K. Yoshikawa, Back-and-forth micromotion of aqueous droplets in a dc electric field, Phys. Rev. E. 88 (2013) 1–5. doi:10.1103/PhysRevE.88.042918.
[185] J.G. Kim, D.J. Im, Y.M. Jung, I.S. Kang, Deformation and motion of a charged conducting drop in a dielectric liquid under a nonuniform electric field, J. Colloid Interface Sci. 310 (2007) 599–606. doi:10.1016/j.jcis.2007.02.007.
[186] J.C. Bird, W.D. Ristenpart, A. Belmonte, H.A. Stone, Critical angle for electrically driven coalescence of two conical droplets, Phys. Rev. Lett. 103 (2009) 1–4. doi:10.1103/PhysRevLett.103.164502.
[187] E.M. Honey, H.P. Kavehpour, Astonishing life of a coalescing drop on a free surface, Phys. Rev. E - Stat. Nonlinear, Soft Matter Phys. 73 (2006) 1–4. doi:10.1103/PhysRevE.73.027301.

[188] F. Blanchette, T.P. Bigioni, Partial coalescence of drops at liquid interfaces, Nat. Phys. 2 (2006) 254–257. doi:10.1038/nphys268.
[189] G.. Charles, S.. Mason, The mechanism of partial coalescence of liquid drops at liquid/liquid interfaces, J. Colloid Sci. 15 (1960) 105–122. doi:10.1016/0095-8522(60)90012-X.
[190] G.. Charles, S.. Mason, The coalescence of liquid drops with flat liquid/liquid interfaces, J. Colloid Sci. 15 (1960) 236–267.
[191] T. Hatakeyama, Y. Kagawa, Effects of electric fields on the ultrasonic attenuation in liquid crystals, J. Chem. Phys. 65 (1976) 4128–4135. doi:10.1063/1.432869.
[192] H. Aryafar, H.P. Kavehpour, Electrocoalescence: Effects of DC electric fields on coalescence of drops at planar interfaces, Langmuir. 25 (2009) 12460–12465. doi:10.1021/la902758u.
[193] M. Mousavichoubeh, M. Ghadiri, M. Shariaty-Niassar, Electro-coalescence of an aqueous droplet at an oil-water interface, Chem. Eng. Process. Process Intensif. 50 (2011) 338–344. doi:10.1016/j.cep.2010.09.017.
[194] S.H. Mousavi, M. Ghadiri, M. Buckley, Electro-coalescence of water drops in oils under pulsatile electric fields, Chem. Eng. Sci. 120 (2014) 130–142. doi:10.1016/j.ces.2014.08.055.
[195] B. Ray, G. Biswas, A. Sharma, Generation of secondary droplets in coalescence of a drop at a liquid-liquid interface, J. Fluid Mech. 655 (2010) 72–104. doi:10.1017/S0022112010000662.
[196] R.S. Allan, S.G. Mason, Effects of electric fields on coalescence in liquid-liquid systems, J. Chem. Phys. (1961) 2027–2040. doi:10.1063/1.432869.
[197] M. Mousavichoubeh, M. Shariaty-Niassar, M. Ghadiri, The effect of interfacial tension on secondary drop formation in electro-coalescence of water droplets in oil, Chem. Eng. Sci. 66 (2011) 5330–5337. doi:10.1016/J.CES.2011.07.019.
[198] D. Yang, M. Ghadiri, Y. Sun, L. He, X. Luo, Y. Lü, Critical electric field strength for partial coalescence of droplets on oil–water interface under DC electric field, Chem. Eng. Res. Des. 136 (2018) 83–93. doi:10.1016/j.cherd.2018.05.004.
[199] D. Yang, Y. Sun, L. He, X. Luo, Y. Lü, Q. Gao, Partial coalescence of droplets at oil–water interface subjected to different electric waveforms: Effects of non-ionic surfactant on critical electric field strength, Chem. Eng. Res. Des. 142 (2019) 214–224. doi:10.1016/j.cherd.2018.12.019.
[200] Y. Sun, D. Yang, L. He, X. Luo, Y. Lü, Influence of alkali concentration, electric waveform, and frequency on the critical electric field strength of droplet–interface partial coalescence, Chem. Eng. Sci. 208 (2019) 115136. doi:10.1016/j.ces.2019.07.054.
[201] V. Anand, V.A. Juvekar, R.M. Thaokar, Coalescence, partial coalescence, and noncoalescence of an aqueous drop at an oil-water interface under an electric field, Langmuir. 36 (2020) 6051–6060. doi:10.1021/acs.langmuir.9b03969.
[202] B.S. Hamlin, J.C. Creasey, W.D. Ristenpart, Electrically tunable partial coalescence of oppositely charged drops, Phys. Rev. Lett. 109 (2012) 1–5. doi:10.1103/PhysRevLett.109.094501.
[203] S. Mhatre, V. Vivacqua, M. Ghadiri, A.M. Abdullah, M.J. Al-Marri, A. Hassanpour, et al., Electrostatic phase separation: A review, Chem. Eng. Res. Des. 96 (2015) 177–195. doi:10.1016/j.cherd.2015.02.012.
[204] A.H.A. Razak, A.L. Skov, Silicone elastomers with covalently incorporated aromatic voltage stabilisers, RSC Adv. 7 (2017) 468–477. doi:10.1039/C6RA25878F.
[205] C.T. Bartlett, G.A. Généro, J.C. Bird, Coalescence and break-up of nearly inviscid conical droplets, J. Fluid Mech. 763 (2015) 369–385. doi:10.1017/jfm.2014.664.
[206] L.G. Leal, Advanced Transport Phenomena, Cambridge University Press, Cambridge, 2007.
[207] H.M. Sadeghi, B. Sadri, M.A. Kazemi, M. Jafari, Coalescence of charged droplets in outer fluids, J. Colloid Interface Sci. 532 (2018) 363–374. doi:10.1016/j.jcis.2018.08.001.

[208] K. Sainath, P. Ghosh, Stabilization of silicone oil-in-water emulsions by ionic surfactant and electrolytes: The role of adsorption and electric charge at the interface, Ind. Eng. Chem. Res. 52 (2013) 15808–15816. doi:10.1021/ie401490c.
[209] F. Lacharme, M.A.M. Gijs, Single potential electrophoresis microchip with reduced bias using pressure pulse injection, Electrophoresis. 27 (2006) 2924–2932. doi:10.1002/elps.200500723.
[210] P.H. Chiu, C.C. Chang, R.J. Yang, Electrokinetic micromixing of charged and non-charged samples near nano-microchannel junction, Microfluid. Nanofluid. 14 (2013) 839–844. doi:10.1007/s10404-012-1116-2.
[211] N. Vandewalle, D. Terwagne, K. Mulleners, T. Gilet, S. Dorbolo, Dancing droplets onto liquid surfaces, Phys. Fluids. 18 (2006) 2004–2005. doi:10.1063/1.2335905.
[212] H. Lin, B.D. Storey, M.H. Oddy, C.H. Chen, J.G. Santiago, Instability of electrokinetic microchannel flows with conductivity gradients, Phys. Fluids. 16 (2004) 1922–1935. doi:10.1063/1.1710898.
[213] R. Pillai, J.D. Berry, D.J.E. Harvie, M.R. Davidson, Electrophoretically mediated partial coalescence of a charged microdrop, Chem. Eng. Sci. 169 (2017) 273–283. doi:10.1016/j.ces.2016.07.022.
[214] X. Chen, P. Liu, C. Qi, T. Wang, Z. Liu, T. Kong, Non-coalescence of oppositely charged droplets in viscous oils, Appl. Phys. Lett. 115 (2019). doi:10.1063/1.5109181.

Appendix

Table A1 (a) Plasmid sequence of P70-deGFP-T500. The promoter highlighted in blue, the deGFP-coding sequence in green, and the terminator in grey. (b) Primer sequences for the PCR-assembly of T7-iSpinach construct. The sequence of the T7-promoter is displayed in red, the iSpinach-RNA aptamer sequence is displayed in green, and the 5' spacer in yellow.

Pbest-OR2-OR1-Pr-UTR1-deGFP-T500	tgagctaacaccgtgcgtgttgacaattttacctctggcggtgataatggttgcagctagcaataattttgtttaact ttaagaaggagatataccatggagcttttcactggcgttgttcccatcctggtcgagctggacggcgacgtaaacg gccacaagttcagcgtgtccggcgagggcgagggcgatgccacctacggcaagctgaccctgaagttcatctgc accaccggcaagctgcccgtgccctggcccaccctcgtgaccaccctgacctacggcgtgcagtgcttcagccgct accccgaccacatgaagcagcacgacttcttcaagtccgccatgcccgaaggctacgtccaggagcgcaccatct tcttcaaggacgacggcaactacaagacccgcgccgaggtgaagttcgagggcgacaccctggtgaaccgcatc gagctgaagggcatcgacttcaaggaggacggcaacatcctggggcacaagctggagtacaactacaacagcc acaacgtctatatcatggccgacaagcagaagaacggcatcaaggtgaacttcaagatccgccacaacatcgag gacggcagcgtgcagctcgccgaccactaccagcagaacaccccatcggcgacggccccgtgctgctgcccga caaccactacctgagcacccagtccgccctgagcaaagaccccaacgagaagcgcgatcacatggtcctgctgg agttcgtgaccgccgccgggatctaatcgagcaaagcccgccgaaaggcgggcttttctgtgtcgaccgatgcc cttgagagccttcaacccagtcagctccttccggtgggcgcggggcatgactatcgtcgccgcacttatgactgtct tctttatcatgcaactcgtaggacaggtgccggcagcgctcttccgcttcctcgctcactgactcgctgcgctcggtc gt

Primer Forward	tccaggaaattaatacgactcactataggcgactacggtgagggtcgggtccagtagcttcggctactgt
Primer Reverse	gcgactacggagcccacactctactcaacagtagccgaagctactggacccgaccctcaccg

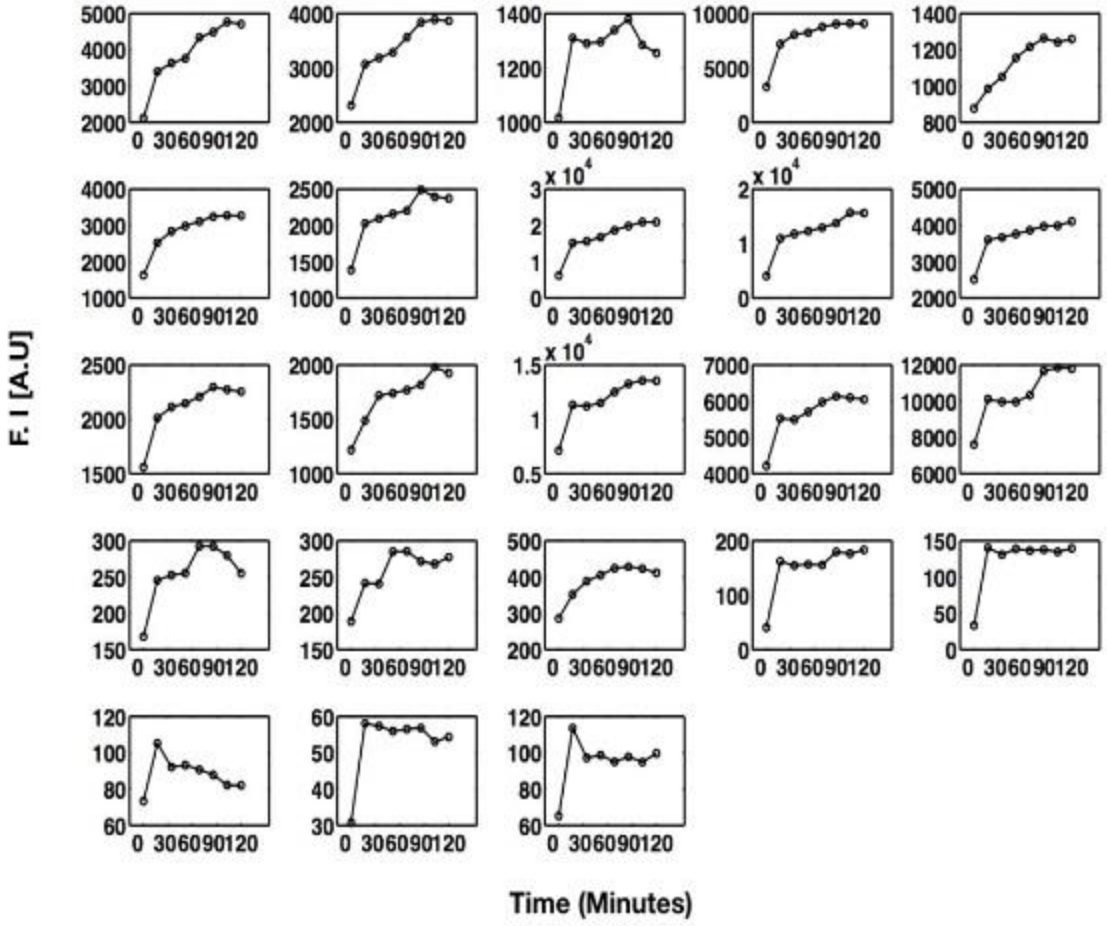

Fig. A1 Individual fluorescent traces of water-in-oil droplets for a total duration of two hours (n=23 droplets). The traces were used to generate the fluorescence curve of Fig. 5.7.

List of Figures

List of Tables